Subunit Exchange in Spinach Short-Form Rubisco Activase

by

Dayna S. Forbrook

A Dissertation Presented in Partial Fulfillment
of the Requirements for the Degree
Doctor of Philosophy

Approved April 2017 by the
Graduate Supervisory Committee:

Rebekka Wachter, Chair
Xu Wang
James Allen

ARIZONA STATE UNIVERSITY

May 2017

ABSTRACT

The primary carbon fixing enzyme Rubisco maintains its activity through release of trapped inhibitors by Rubisco activase (Rca). Very little is known about the interaction, but binding has been proposed to be weak and transient. Extensive effort was made to develop Förster resonance energy transfer (FRET) based assays to understand the physical interaction between Rubisco and Rca, as well as understand subunit exchange in Rca.

Preparations of labeled Rubisco and Rca were utilized in a FRET-based binding assay. Although initial data looked promising, this approach was not fruitful, as no true FRET signal was observed. One possibility is that under the conditions tested, Rca is not able to undergo the structural reorganizations necessary to achieve binding-competent conformations. Rca may also be asymmetric, leading to less stable binding of an already weak interaction.

To better understand the structural adjustments of Rca, subunit exchange between different oligomeric species was examined. It was discovered that subunit exchange is nucleotide dependent, with ADP giving the fastest exchange, ATP giving slower exchange and ATPγS inhibiting exchange. Manganese, like ADP, destabilizes subunit-subunit interactions for rapid and facile exchange between oligomers. Three different types of assemblies were deduced from the rates of subunit exchange: rigid types with extremely slow dissociation of individual protomers, tight assemblies with the physiological substrate ATP, and loose assemblies that provide fast exchange due to high ADP.

Information gained about Rca subunit exchange can be used to reexamine the physical interaction between Rubisco and Rca using the FRET-binding assay. These binding assays will provide insight into Rca states able to interact with Rubisco, as well as define conditions to generate bound states for structural analysis. In combination with assembly assays, subunit exchange assays and reactivation studies will provide critical information about the structure/function relationship of Rca in the presence of different nucleotides. Together, these FRET-based assays will help to characterize the Rca regulation mechanism and provide valuable insight into the Rubisco reactivation mechanism.

DEDICATION

To my husband and my family, I could not have done this without your unconditional love and encouragement.

ACKNOWLEDGMENTS

I would like to thank my advisor, Dr. Rebekka Wachter, for the opportunity to work on such impactful projects, and for her support and guidance over the years. To Dr. Suratna Hazra and Dr. Agnieszka Kuriata for their support and encouragement in and out of lab, and the rest of the past and present members of the Wachter Lab.

TABLE OF CONTENTS

CHAPTER Page

CHAPTER Page

LIST OF TABLES

LIST OF FIGURES

Figure Page

Figure Page

CHAPTER 1

INTRODUCTION

Photosynthesis

Exponential population growth is expected to yield a global population exceeding 9 billion by 2050. The Food and Agriculture Organization of the United Nations states food production needs to increase by 70% to accommodate humanity. However, by 2100, temperatures are predicted to increase between 0.5 and 8.6 °F, with a likely increase of at least 2.7 °F [1]. This increase in temperature will cause agricultural difficulties. While the increasing global population is demanding more food, rising global temperatures will reduce photosynthetic efficiency, creating a crisis point. Understanding the mechanism of Rubisco activase regulation in Rubisco during photosynthesis may lead to more efficient carbon fixation in plants.

Photosynthesis, made up of the light reactions and the dark reactions, is a process used by plants and other organisms to convert light energy into chemical energy. Photosynthesis maintains atmospheric oxygen levels while supplying all the organic compounds and most of the energy necessary for life on Earth. The overall reaction of photosynthesis uses six molecules of carbon dioxide, six molecules of water, and light energy to produce one molecule of glucose and six molecules of molecular oxygen.

$$6CO_2 + 6H_2O \xrightarrow{light} C_6H_{12}O_6 + 6O_2$$

The light reactions take place in the thylakoid membrane, and use light energy and water to produce adenosine triphosphate (ATP) and NADPH. In photosystem II, light energy is used to oxidize water and the electrons released travel down the electron transport chain. The process of the electron transport chain releases energy used to pump

protons from the stroma into the thylakoid lumen, building a H+ concentration gradient. This concentration gradient can then be used to fuel production of ATP by ATP synthase. In photosystem I, a photon excites an electron, and movement of the electron to a lower energy state is used to reduce NADP+ into NADPH.

Calvin Cycle

In the dark reactions, or Calvin Cycle, CO_2 gets incorporated into energy-rich molecules in the chloroplast stroma. The Calvin Cycle is fueled by, and dependent on, the ATP and NADPH from the light reactions, along with CO_2 from the atmosphere. The first step of the Calvin Cycle is carbon fixation, where ribulose-1,5-bisphosphate carboxylase/oxygenase (Rubisco) catalyzes the joining of CO_2 molecules and ribulose-1,5-bisphosphate (RuBP) to form 2 molecules of 3-phosphoglycerate (3-PGA). In the second step, reduction, energy from ATP and NADPH are used to convert 3-PGA into glyceraldehyde-3-phosphate (G-3-P). A few of the G-3-P molecules leave the cycle to synthesize glucose, but most of the G-3-P produced is regenerated into RuBP to continue the cycle.

Rubisco

Rubisco is the most abundant enzyme on Earth and represents the primary entry point of CO_2 into the biosphere. Rubisco is found in almost all autotrophic organisms and has been estimated to make up around 50% of the total soluble protein in the organism [2]. Rubisco's very slow carboxylation rate of RuBP and its propensity to inhibition make it a notoriously inefficient enzyme.

There is considerable sequence conservation seen in all Rubisco enzymes, leading to very similar three-dimensional structures [3], in which 19 conserved residues line the

active site [4]. Form II Rubisco is present in some prokaryotes and dinoflagellates, and forms a dimer of large subunits. Form III Rubisco is from archaea, and is unique in that it is comprised of five large subunit dimers to form a decamer [5]. The most common type of Rubisco, Form I, is found in plants, eukaryotic algae and cyanobacteria. The ~52 kDa large subunits arrange as a tetramer of antiparallel dimers, with the 12-14 kDa small subunits flanking the top and bottom of the assembly (figure 1). At the interface between

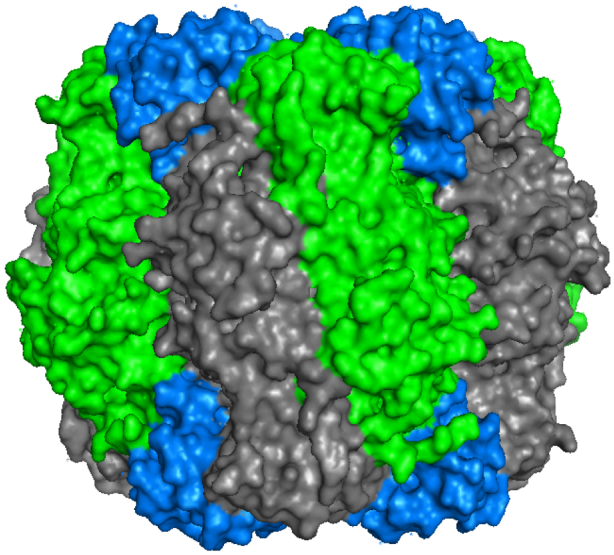

Figure 1. Structure of Form I Rubisco from Spinach. Large subunits are shown in gray and green, while small subunits are in blue. PDB ID: 1RCX.

subunits within each dimer are two active sites, where the C-terminal of one chain is in close proximity to the N-terminal domain of the other. The small subunits are not in direct contact with the active sites and are not needed for reactivation [6], but do have critical accessory functions [7]. Within Form I Rubiscos, there are red-type, present in some proteobacteria and eukaryotes of the red-plastid lineage, and green-type enzymes, present in other proteobacteria, green algae, cyanobacteria, and higher plants [8, 9]. In Form I green algae, the large subunit is encoded in the chloroplast and the small subunit in the nucleus, however, in non-green algae, the large and small subunit genes are both

encoded in the chloroplast [8]. In red-type Form I Rubisco, there is a β-hairpin extension in the small subunit that is critical for assembly, and absent in green-type Rubisco [10]. On both ends of the complex, an eight-stranded β-barrel is formed by the β-hairpins of four small subunits coming together. The β-barrels protrude into the central channel formed by the large subunits and stabilize the complex through several interactions with the large subunits [10]. Red-type Rubiscos are responsible for most of the CO_2 uptake in oceans [11]. Multiple red-type enzymes show a greater than two-fold higher specificity for CO_2 over green-type, and efforts have been made to introduce this higher CO_2 to O_2 specificity into higher plants by expressing red-type Rubisco in tobacco [12]. It was speculated that introducing Rubisco from the red algae *Griffithsia monilis* into C3 plant chloroplasts would increase biomass accumulation up to 30% by improving the efficiency of nitrogen, light and water usage without increasing the amount of Rubisco [13]. The Rubisco operon from a diatom or a red alga were inserted into the tobacco genome and were expressed abundantly. However, red-type Rubisco was unable to assemble properly in tobacco chloroplasts [12].

Open and Closed Conformations of Rubisco

Structurally, there are two main forms of Rubisco: open and closed [14]. Binding of a substrate in the active site induces the closed state formation, where mobile elements go through a conformational change to shield the active site from solvents [15]. These mobile elements include an amino-terminal loop, consisting of residues 63-69 of the large subunit N-domain, and loop 6, consisting of residues 331-340 of the large subunit C-domain (figure 2). The large subunit C-terminal tail also retracts in the closed formation to lie directly over the active site. Loop 6 interacts with bound sugar phosphates to help

stabilize the closed conformation. Other subtle N-domain motions play a role as well, and correlate with geometric changes in the substrate binding site.

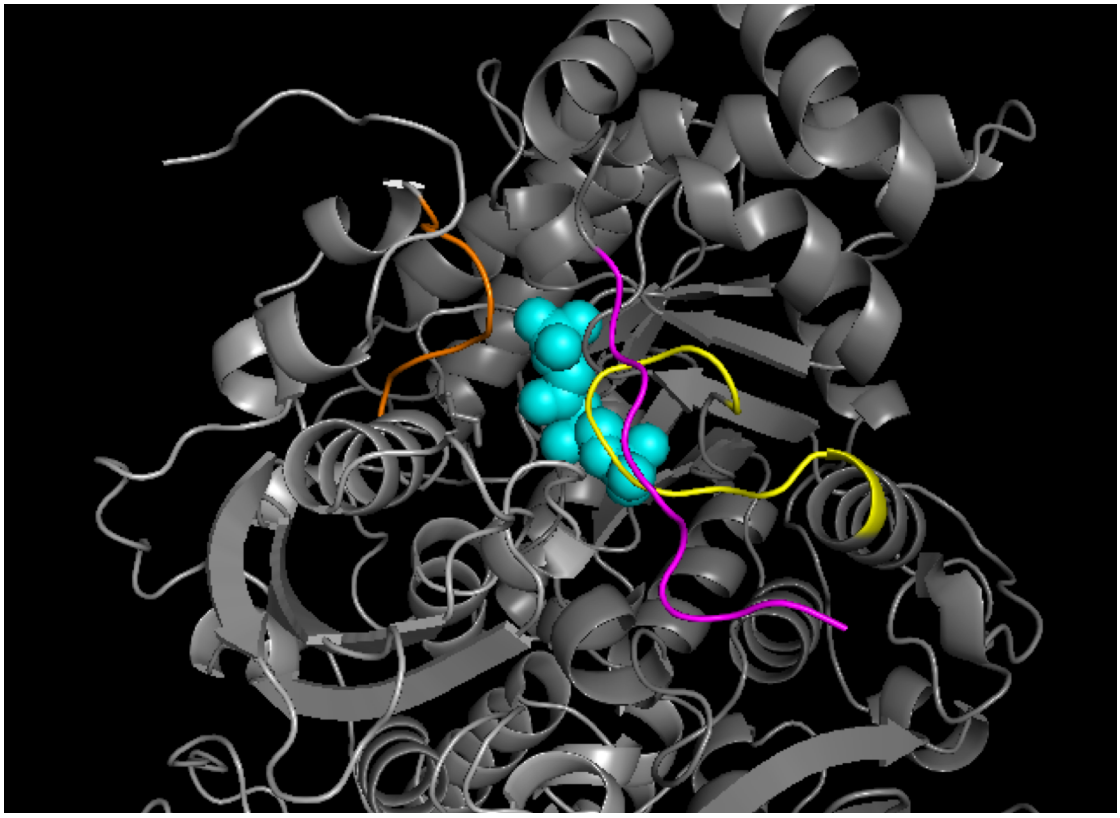

Figure 2. The closed, inhibited conformation of decarbamylated spinach Rubisco. The mobile elements retract to close the active site. The amino-terminal loop (residues 63-69) is shown in orange; loop 6 (residues 331-340) in yellow; C-terminal tail (residues 465-475) in magenta. The substrate, RuBP, shown in cyan, has become the trapped inhibitor. PDB ID: 1RCX.

Efficiency of Rubisco

The catalytic efficiency of Rubisco is reliant on several factors. First, for activation of Rubisco's active site, carbamylation of large subunit residue Lys-201 and coordination of a Mg^{2+} ion are required [16]. Without carbamylation at this site, RuBP can tightly bind and render the active site useless for enzymatic activity [17]. Catalytic efficiency can also be affected by the competition of the oxygenation reaction of RuBP by Rubisco instead of the desired carboxylation reaction of RuBP. In mild temperatures,

Rubisco's affinity for CO_2 is about 80 times higher than its affinity for O_2 [18], despite O_2 being 25 times more prevalent than CO_2 at 25 °C [19]. However, in hot conditions, plants close their stomata to preserve water, but CO_2 cannot diffuse in and O_2 cannot diffuse out, therefore the ratio of O_2 to CO_2 increases. Also in hot conditions, the relative solubility of O_2 increases compared to CO_2 and the specificity of Rubisco decreases [17]. Photorespiration leads to the loss of fixed carbon as CO_2, wastes energy and decreases sugar synthesis. Oxygenation of RuBP leads to one molecule of 3-phosphoglycerate and one molecule of 2-phosphoglycolate, which does not require CO_2 from the atmosphere to produce. 2-phosphoglycolate is not used by plants to create biomass and must be converted to a usable molecule through a process that requires energy from ATP. Photorespiration uses O_2 and produces CO_2. As global temperatures rise, Rubisco specificity decreases and, in turn, photosynthetic efficiency decreases.

Inhibition of Rubisco

Apo Rubisco is unable to catalyze the carboxylation or oxygenation reactions; therefore, when RuBP binds to decarbamylated apo enzyme, it results in inhibited complexes [20] (figure 2). This tight binding of RuBP to decarbamylated sites may have developed during evolution as a consequence of increased specificity for CO_2, as binding of RuBP to decarbamylated sites is much weaker in photosynthetic bacteria [20].

Even when Rubisco is carbamylated, sugar phosphate inhibitors that mimic RuBP can bind to and obstruct its active site. CA1P, 2-carboxy-D-arabinitol 1-phosphate, is a naturally occurring nocturnal inhibitor found only in the chloroplast, and is synthesized during periods of low irradiance or darkness [21]. Catalytic misfire can occur during both carboxylation and oxygenation, and these products can become tight binding inhibitors.

XuBP, D-xylulose-1,5-bisphosphate, is formed by misprotonation of the initial enediol intermediate. XuBP has the same structure as RuBP, except for the opposite stereochemistry at C3. It can be slowly carboxylated by carbamylated Rubisco to form 3-PGA, but acts as a tight binding inhibitor of decarbamylated Rubisco [22]. PDBP, D-glycero-2,3-pentodiulose-1,5-bisphosphate, is a daytime inhibitor and can also be induced by stress [23]. PDBP is formed about once every 260 turnovers by the elimination of H_2O_2 from a peroxyketone intermediate of the oxygenation reaction [24, 25]. It is proposed that PDBP accumulates at the catalytic site, causing progressive inhibition. Any conditions that favor the oxygenase reaction, such as high temperatures, will encourage PDBP production [17, 25]. CTBP, 2-carboxytetritol-1,4-bisphosphate, is formed by a benzylic acid rearrangement of enzyme bound PDBP and is proposed to be a tighter binding inhibitor than PDBP [24]. KABP, 3-ketoarabinitol-1,5-bisphosphate, forms from the breakdown of an unstable peroxy intermediate of the oxygenation reaction [22].

Rubisco can be inhibited in numerous ways, therefore, Rubisco activase (Rca) is essential in maintaining Rubisco activity by utilizing energy from ATP hydrolysis as the driving force behind a conformational motion, which is responsible for removing tightly binding inhibitors from the active site of Rubisco [26].

AAA+ Protein Family

Rca is a member of the AAA+ (ATPases associated with various cellular activities) protein family. AAA+ proteins go through cycles of ATP binding, hydrolysis and ADP release, which result in conformational changes and, in turn, exert force on their

macromolecular substrates. These proteins are found in broadly varying functional contexts, but frequently function as hexameric ring structures.

There are many conserved regions in AAA+ proteins, mainly located near the binding site. The N-terminal AAA+ domain/nucleotide binding domain contains an α/β Rossman fold and signature Walker A and B motifs, while the C-terminal AAA+ domain contains the arginine finger (figure 3). Within the AAA+ module, the Walker A, Box IV and Sensor I regions have been implicated in binding of the nucleotide phosphates [27]. Because the nucleotide binding sites are positioned between the two subdomains, their conformation is often nucleotide dependent.

Figure 3. AAA+ ATP binding module. The N-terminal αβ domain contains conserved Walker A and B motifs and the C-terminal α domain constains the conserved arginine finger.

The Walker A, or P-loop, motif contains the characteristic sequence GXXXXGK[T/S], which contains a lysine that coordinates a magnesium ion and directly interacts with the β-phosphate of the nucleotide. The Walker A motif also contains a conserved aspartate residue that is involved in coordination of the γ-phosphate of ATP [28]. Within the Walker B motif is a conserved aspartic acid or glutamic acid serves as a catalytic base during ATP hydrolysis. The arginine finger projects into the ATP binding site of the adjacent subunit and forms intermolecular interactions with the γ-phosphate. The arginine finger may also stabilize the negative charge from the pentacovalent transition state [29].

The Box and Sensor regions are less conserved within the AAA+ protein family than the Walker motifs, but are still important for functionality. The Sensor I domain is located between the Walker A and B motifs, and functions with the Walker B glutamic/aspartic acid to orient the water molecule for nucleophilic attack on the γ-phosphate. Within Sensor I, there is also a conserved aspartate residue that is involved in coordinating the γ-phosphate of ATP [28]. The Sensor 2 domain mediates conformational changes associated with ATP binding and hydrolysis by interacting with the α-phosphate, as well as containing two specific residues critical for species specificity recognition site of Rca [30]. Box II is located near the nucleotide binding site [31].

Class of Rubisco Activases

Within the kingdom of life, three types of activases are present: CbbQO, CbbX and Rca. These three formed by convergent evolution, as there is no direct ancestor. The AAA+ domain sequence identity to Rca in higher plants is 18% for CbbQ and 20% for CbbX. CbbQO is found in chemoautotrophic proteobacteria, and is present as a heterooligomeric complex of two proteins: ~260 residue CbbQ, and ~770 residue CbbO [32]. In anoxygenic photosynthesis, sulfur or other inorganics are oxidized instead of H_2O, and elemental sulfur is produced as a byproduct rather than molecular oxygen. Proteobacteria possess either Form I or Form II Rubisco, and there are separate forms of CbbQO for each: Q1O1 for Form I Rubisco (L8S8) and Q2O2 for Form II (L2). This newest type of activase has just recently been characterized, and shows the mechanism of QO-mediated Rubisco activation is conserved [32].

CbbX, the red-type Rubisco activase, is significantly smaller than Rca, consisting of only the AAA+ domain and a shortened N-terminal extension. While green-type Rca is

constitutively ATPase active, CbbX requires synergistic stimulation by RuBP and Rubisco to become ATPase active [33]. Similarly, RuBP and ATP must bind to convert CbbX into functionally active, hexameric rings [34]. CbbX shows a maximum ATPase rate of 8.0 ± 0.2 min^{-1} in the presence of RuBP [34], 20% of the activity reported for Rca [35]. In CbbX, the central pore is ~25 Å and is centered over the Rubisco active site, and bound at an angle. The C-terminal tail of Rubisco, important for substrate recognition, is 10 residues longer in red-type Rubisco and is threaded into the pore of the CbbX hexamer, acting as an anchor. Both CbbX and CbbQO function through manipulation of the C-terminal tail of the Rubisco large subunit, with CbbX having a less specific interaction [32, 34].

Rubisco Activase Isoforms

In some plants, such as spinach and cotton, there are two isoforms of Rca: α and β (figure 4). The ~45 kDa α-isoform sequence contains an additional ~30 C-terminal residues over the ~42 kDa β-isoform. In some species, the two isoforms arise from a single nuclear gene via alternative splicing, while in cotton, the two isoforms are encoded

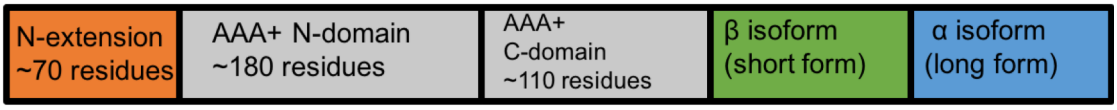

Figure 4. Rca domain organization. The AAA+ domains are conserved throughout AAA+ proteins. Some plants have both α and β isoforms.

on separate genes [15, 36, 37]. Both forms are active in ATP hydrolysis and Rubisco reactivation, but they differ in their kinetic properties and thermostability [38, 39]. The α-isoform is more sensitive to inhibition by ADP due to redox regulation by disulfide bond formation on the C-terminal tail. Oxidation of the disulfide bond (Cys392 and Cys411 in

Arabidopsis) causes a conformational change in the C-terminal extension that allows docking near or into the binding site, thereby hindering ATP binding [40, 41]. Replacement of conserved, negatively charged residues with alanine reduced sensitivity of the mutants to ADP inhibition, suggesting involvement of electrostatic interactions between those residues and the nucleotide binding pocket [41]. The sensitivity of Rca to inhibition by ADP can regulate Rca by adjusting activity based on light intensity, thereby regulating Rca by its redox state [15].

Structural Information of Rca

Rca is known to be polydisperse in its quaternary structure, which leads to difficulty in crystallization for structural determination. In 2011, a 1.9 Å structure of the creosote AAA+ C-domain (residues 250-351) was published [42]. The C-domain forms a four-helix bundle, as expected since this is conserved throughout the AAA+ protein family, but in this structure, shows an elongated helix 3 (figure 5) [42]. The two residues involved with Rubisco recognition specificity (Lys-313 and Val-316) [30] are located at the tip of the extended helix 3. Also examined in this structure was Arg-293, proposed to be equivalent to the Sensor 2 arginine that is known to interact directly with the bound nucleotide. However, in this structure, Arg-293 is approximately 22 Å from the phosphate tail of the nucleotide, and unlikely to make direct contact [42].

Also in 2011, the structure of the AAA+ domain of tobacco Rca (residues 68-360) was solved by x-ray crystallography (figures 5, 7) [43]. This 2.95 Å crystal structure was fit into a model of a closed ring hexamer, found by negative stain electron microscopy (figure 6) [43]. Both N- and C-domains of the AAA+ module were characterized, where the C-domain of one subunit interacts with the N-domain of the next. Like other AAA+

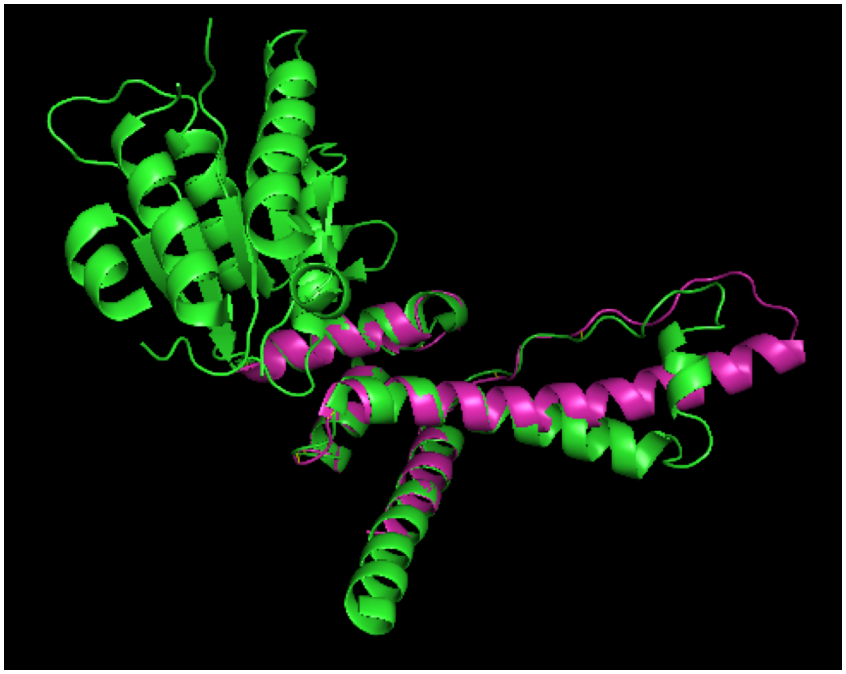

Figure 5. Overlay of creosote recognition domain (magenta, PDB ID: 3THG) and tobacco AAA+ domain (green, PDB ID: 3T15).

proteins, the N-domain Rossman fold is conserved and consists of a parallel β-sheet flanked by α-helices. Between the AAA+ N- and C- domains, near the nucleotide binding site, is a peptide linker that acts as a hinge, the angle dependent on the identity of the bound nucleotide [44]. Although the construct crystallized was comprised of residues 68-360, various loops throughout the AAA+ domain were disordered: only residues 68-176, 191-207, 219-234 and 237-360 were visible. The C-terminal domain was not consistent with that determined in the creosote structure, but instead showed an additional small, fifth helix that contained the species specificity recognition residues (figure 5). They found that, in the crystal lattice, the Rca chains formed a helix with six subunits per turn, consistent with other hexameric AAA+ proteins. This truncated variant provided quaternary structure, while the creosote variant did not, suggesting specific residues within the AAA+ N-domain are important for intermolecular interactions necessary for

oligomerization. Given that the central pore in the tobacco Rca model (figure 6) is approximately 36 Å in diameter, substantially wider than that in CbbX, it is proposed that reactivation of Rubisco involves partial threading of a more complex secondary structure, rather than only the C-terminal tail [33].

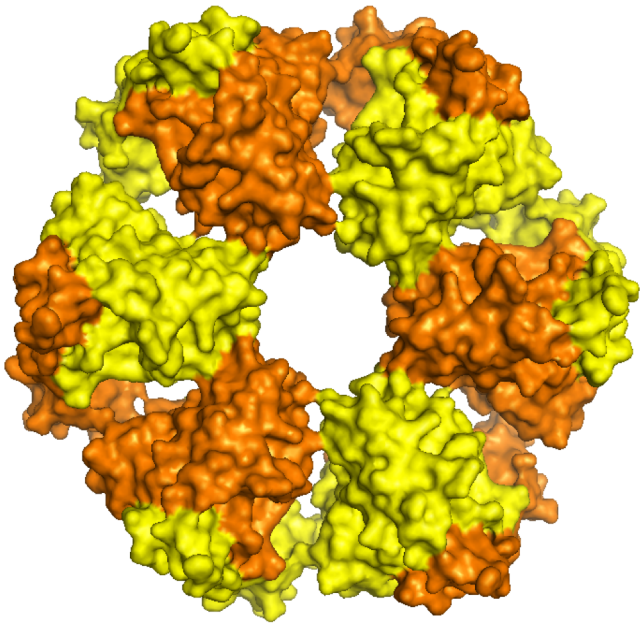

Figure 6. Hexameric model of tobacco Rca AAA+ domain. The proposed model of Rca is based on negative-stain electron microscopy and a partial x-ray structure. PDB ID: 3ZW6

In 2015, Hasse, *et al,* successfully crystallized full length *Arabidopsis*-β Rca in the apo form [45]. The structure was solved to 2.9 Å, but the N- and C-extensions are completely disordered, as are various loops in the AAA+ domain: residues 65-134, 144-172, 182-202 and 214-362 are visible. There are two sulfate ions bound in the structure, with one located in the nucleotide binding pocket that alters the hinge bending angle (figure 7).

Polydispersity of Rca in Higher Plants

The assembly mechanism of Rca is unknown but the self-association state is predicted to be primarily hexameric under certain conditions [43, 46]. Size-exclusion

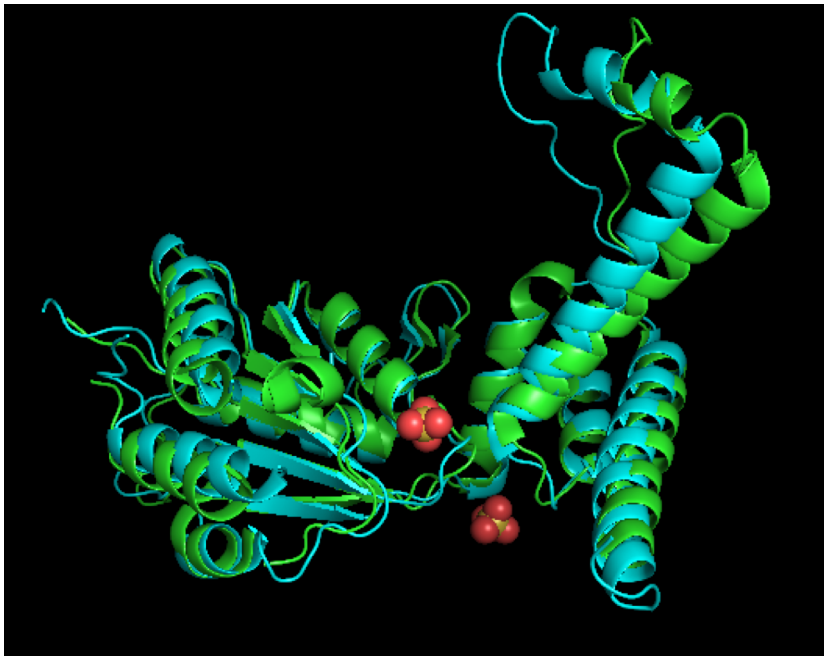

Figure 7. Overlay of AAA+ domains from tobacco (green, PDB ID: 3T15) and *Arabidopsis* (cyan, PDB ID: 4W5W). Two sulfates are present in the *Arabidopsis* structure and alter the hinge bending angle.

HPLC elution profiles of Rca consist of broad, non-Gaussian bands with long, trailing downslopes, consistent with a large range of subunit stoichiometries [36, 47]. At a single concentration, Rca is present in a variety of assembly states, dependent on species and nucleotide conditions. At 5 μM cotton-β Rca in ADP, there are equal concentrations of monomer, dimer, tetramer and hexamer. At 30 μM cotton-β Rca in ATP, 70-80% is in the hexameric state [48]. Spinach-β Rca has proven to be too polydisperse for size determination using FCS, even over a large range of concentrations and conditions (unpublished work).

Thermal Stability of Rca

Along with the issue of polydispersity, Rca is thermolabile and has been implicated in heat related limitations in photosynthesis [49]. There is a direct connection

between the heat tolerance of photosynthesis and thermostability of Rca [50]: at increased temperatures, Rca is not able to keep up with the significantly increased rate of Rubisco inhibition, which limits photosynthesis [51]. Rca activity is extremely sensitive *in vitro* [50, 52]. If ATP decreases or the temperature increases, Rca activity decreases and Rubisco is stuck in inhibited states, causing carbon fixation to stop. Thermal denaturation is irreversible, and substantial aggregation is observed upon cooling, which may be explained by non-specific interactions of newly exposed hydrophobic regions creating disordered aggregates [47]. As anticipated, species native to a temperate climate show lower apparent T_m values than those native to more tropical habitats: Arabidopsis-β: ~40°C; cotton-β: ~45°C; tobacco: ~45°C; creosote-β: ~46-47°C. In spinach-α, heating to 35°C showed heavily aggregated protein, suggesting even at room temperature, there is significant protein aggregation [47]. Apparent T_m values were used to measure the effect of nucleotides and divalents on the stability of cotton-β Rca. ATP was found to stabilize the apo protein by 5°C, ADP stabilized by 10°C, while Mg^{2+} destabilizes the ADP-bound Rca by 6°C, and stabilizes the ATP-bound Rca by 1°C. These alterations in stability may be explained by electrostatic balancing of the binding pocket upon Mg^{2+} complexation to ATP, a step necessary for catalytic ATP hydrolysis [47].

Homologs of Rca

Even though the Rca AAA+ domain has a low percentage of sequence identity with other AAA+ proteins, mechanistic and structural information is still of great relevance. One of the more closely related homologs, ClpX (10% sequence identity with the AAA+ domain), forms a rigid-body unit through interactions of the N-terminal AAA+ domain of one subunit with the C-terminal AAA+ domain of the next [53]. Even

at saturating ATP concentrations, at least two subunits in the hexamer were free of nucleotide [54]. Alternating free and bound sites may be required for activity and allosteric behavior [55]. In the bacterial protease HslU, it was determined that four sites out of the hexamer were bound to nucleotide, while two were free, and the two states had different conformations [55]. This nucleotide binding causes a rotation of the AAA+ C-domain of up to 20° in those four subunits within the hexamer [55-57]. With a drastic conformational change with nucleotide binding of four subunits, the hinge bending angle on the two empty sites can get distorted, thereby blocking any nucleotide from entering. In ClpX, three states were found: low affinity, high affinity and free [58]. Similarly, three conformational states are present in tobacco Rca in assemblies with about 6 subunits: ADP-bound, ATP-bound and free [59]. The rate limiting step in some of these AAA+ protein machines is the tight binding of nucleotide because it requires a conformational change.

Rubisco Reactivation by Rca

Species specificity is critical because Rca from the *Solanaceae* family, such as tobacco, cannot reactivate Rubisco from the non-*Solanaceae* family (spinach, Chlamy, cotton), and vice versa [60]. There are also species dependent variations in reactivation: in some cases, Rca reactivates Rubisco from a different species more effectively than Rubisco from its own species. For example, cotton Rca can reactivate Chlamy Rubisco more effectively than it can cotton Rubisco.

Interaction Between Rubisco and Rca

When Rca binds to Rubisco, a conformational change occurs, which moves these elements away from the active site and the trapped inhibitor can escape. A bound

complex of Rubisco-Rca has not yet been isolated, but the interaction has been proposed to be weak and transient. The apparent K_d is kinetically estimated to be 0.34 – 5 μM [61]. In leaves, the concentration of Rubisco holoenzyme is around 500 μM, and the concentration of Rca is estimated to be between 160 and 480 μM, therefore, it is estimated that most Rca is bound [62]. If Rca is primarily hexameric, there is approximately 1 Rca_6 per Rubisco holoenzyme.

The structure and enzymatic mechanism of Rubisco is well defined, and there have been long standing efforts to engineer Rubisco for improved crop yields. However, success is unlikely without parallel engineering of Rca. Information about the physical interaction of Rca and Rubisco and understanding the Rca regulation mechanism will assist in deconstructing the Rubisco reactivation mechanism and may lead to a more efficient enzyme and therefore, increase the efficiency of carbon fixation in plants.

CHAPTER 2

PHYSICAL INTERACTION OF RUBISCO AND RCA: DEVELOPMENT OF A FRET-BINDING ASSAY

INTRODUCTION

Rubisco's extremely slow carboxylation rate of ribulose-1,5-bisphosphate and its propensity toward inhibition make it a notoriously inefficient enzyme. Rubisco activase (Rca) is essential in maintaining Rubisco activity by catalyzing the rapid release of trapped inhibitors to reactivate Rubisco for CO_2 fixation. Because Rca is critical to maintaining active Rubisco, Rca is an important area to investigate in order to increase the carbon fixation efficiency in plants. It has been estimated that approximately 3% of all stromal proteins is Rca, whereas Rubisco makes up about 40% [36, 59].

The minimal efficiency of Rca ATPase activity is at least 1 site activated per 20 ATP hydrolyzed. However, it is likely that the efficiency is much greater as Rca operates with lower ATPase activity at physiological ATP:ADP ratios [36]. Molecular crowding and extensive binding to Rubisco could slow turnover in the stroma, but *in vitro*, the ATPase activity of Rca is not affected in the presence or absence of Rubisco [36].

It is likely that six subunit rings are required to form a reactivation-competent state, as evidenced by a hexamer being the minimum required assembly for Rubisco reactivation [43]. ATPase activity requires smaller assemblies (trimer at minimum) [43, 63], likely due to the interface of two subunits forming the active sites functional in hydrolysis [59]. It is possible additional subunits are necessary for reactivation because Rca must couple ATP hydrolysis to mechanical work. The pore loop regions in Rca were found to be important for both ATPase and reactivation [43]. The tobacco R294V mutant

forms stable closed-ring hexamers in ATP. This mutation disrupts certain subunit-subunit interactions causing inhibited aggregation, but maintains ATPase and reactivation activity [43]. Another mutation at this residue, R294A, gave hexameric structures in ATPγS, but reduced activity [64, 65]. Deletion of the N-extension in tobacco Rca was found to nearly abolish reactivation activity, but it maintained self-association and ATPase activity [66].

Interaction of Rubisco and Rubisco Activase

Rca must interact with Rubisco in order to reactivate it, but the binding of the two has not yet been observed. The binding has been proposed to be weak and transient, with a kinetically estimated apparent K_d of 0.34 – 5 μM [61]. When Rca binds to Rubisco, a conformational change occurs, which moves the mobile elements away from the Rubisco active site so the trapped inhibitor can escape (figure 8).

There are two proposed models for the physical interaction between Rca and Rubisco: side on and top on (figure 9). The side on model is more likely since there is evidence the small subunit does not play a role in Rubisco reactivation. Hybrid Rubisco studies were performed using *Chlamydomonas* large subunits and tobacco small subunits [6]. Since tobacco Rca cannot reactivate *Chlamydomonas* Rubisco, any reactivation of the hybrid Rubisco would indicate the small subunit is necessary for reactivation. Tobacco Rca was unable to reactivate hybrid Rubisco, meaning the introduction of tobacco small subunits did not interrupt the species-specific interactions between Rubisco and Rca [6]. The association is not dominated by the small subunits; therefore, the top-on model is unlikely.

The Rubisco holoenzyme (L8S8) has a diameter of about 120 Å, whereas the diameter of the hexameric Rca ring is about 135 Å. In the hexameric model of tobacco

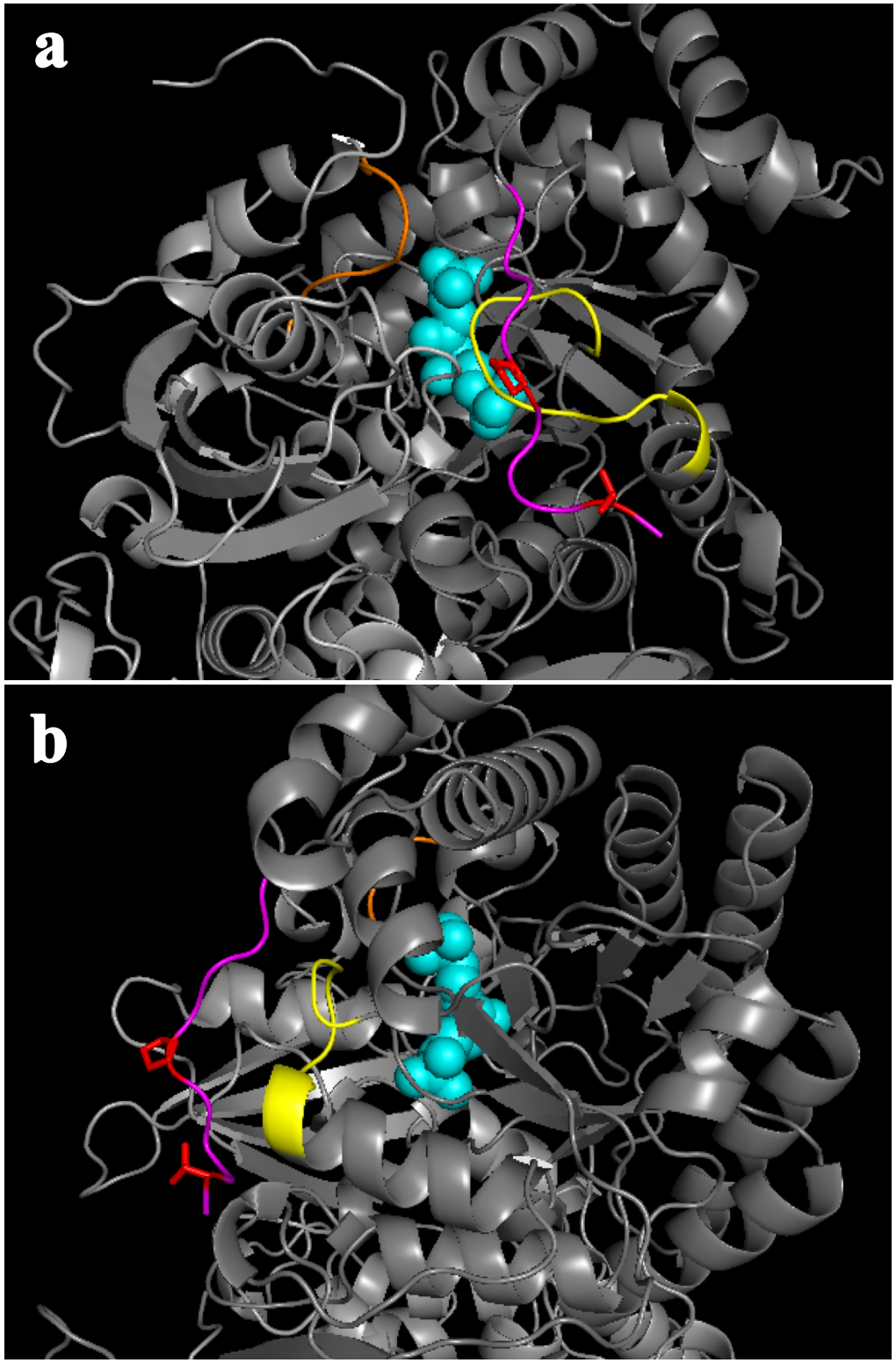

Figure 8. Structure of Rubisco active site. (a) front view, (b) side view. The mobile elements are colored: orange: amino-terminal loop; yellow: loop 6; magenta: C-terminal tail; red: residues 470 and 474; cyan: RuBP. PDB ID: 1RCX.

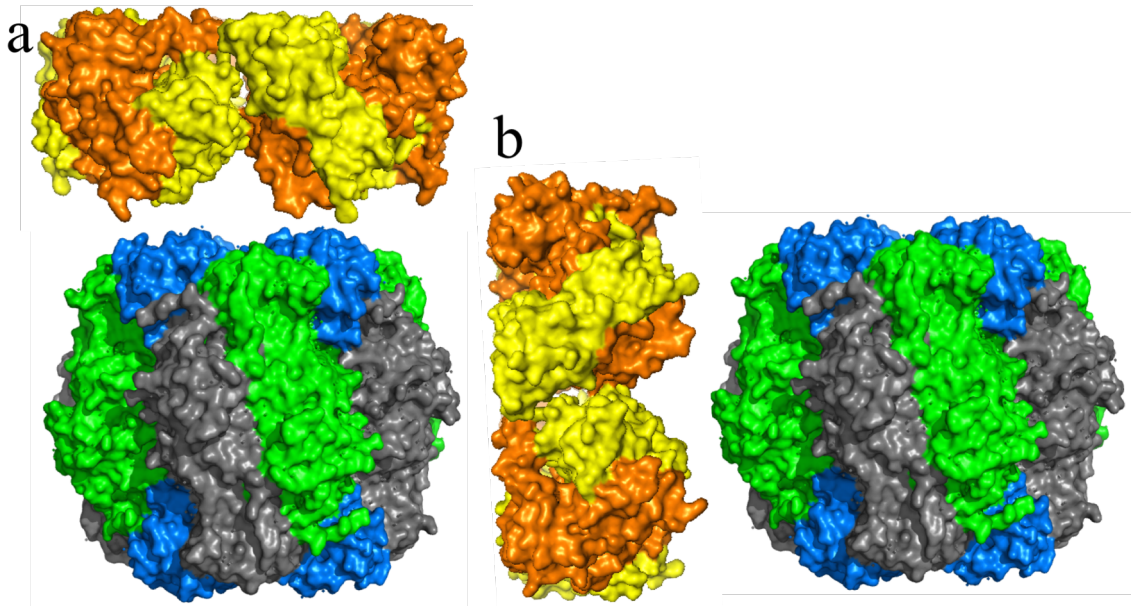

Figure 9. Models of the Rubisco-Rca interaction. (a) The top-on model shows the proteins stacked, with significant contact between Rca and the Rubisco small subunit. (b) The side on model shows contact between Rca and the large subunits of Rubisco.

Rca, the center pore is about 30 Å in diameter. If bound to Rubisco with the pore centered over the interface of two large subunits, the circumference of the pore would be in close proximity to 2 recognition domains and 2 active sites [6].

The unicellular, green alga *Chlamydomonas reinhardtii* was utilized since it can be produced on a shorter time scale than higher plants and large subunit mutations could be introduced into the chloroplast genome. There are 12 cysteine residues in the large subunit of Rubisco and four in the small subunit. All except two, C449 and C459, are buried in the protein's interior. Mutating the residues at 449 and 459 to serine residues and introducing a cysteine residue at a specific location can achieve site-specific labeling by a Michael addition between the maleimide of the dye with the thiol of the exposed cysteine residue. Mutations to serines at these locations were shown to exhibit unmodified catalytic activity [67].

The C-terminal tail was chosen as the target for the label because it is flexible, the tail is in close proximity to the active site, and the tail is solvent exposed (figures 8a, 10). To get to the disordered open form, the C-terminal tail must be loosened up to be removed from the active site. Side chains of residues 470 and 474 point away from the protein (figure 8b), which is ideal for adding a fluorophore tag, especially those approximately 1 kDa in size. C-terminal tail mutants are expected to retain near wild-type catalytic properties [15].

The hexameric tobacco Rca model is approximately 70% of full length, by sequence, and does not include the N- or C-terminal extensions [43], therefore, we do not know exactly where the labels will be on the Rca assemblies. The C-terminal tail is proposed to be disordered, and may be in a slightly different conformation on each subunit. Even though the last residue in the model (residue 360) is approximately 28 Å from the same residue on the adjacent subunit (figure 11), the C-termini of Rca dimers was shown by chemical cross-linking to be within 8 Å of each other [68].

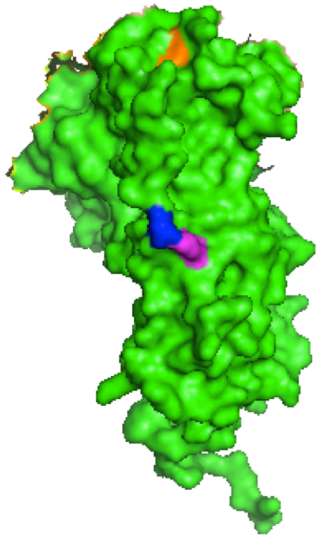

Figure 10. Mutations on the large subunit of Rubisco. One large subunit of *Chlamydomonas* Rubisco showing locations of mutated residues C449S and C459S (orange), D470C (blue) and K474C (magenta). PDB ID: 1GK8.

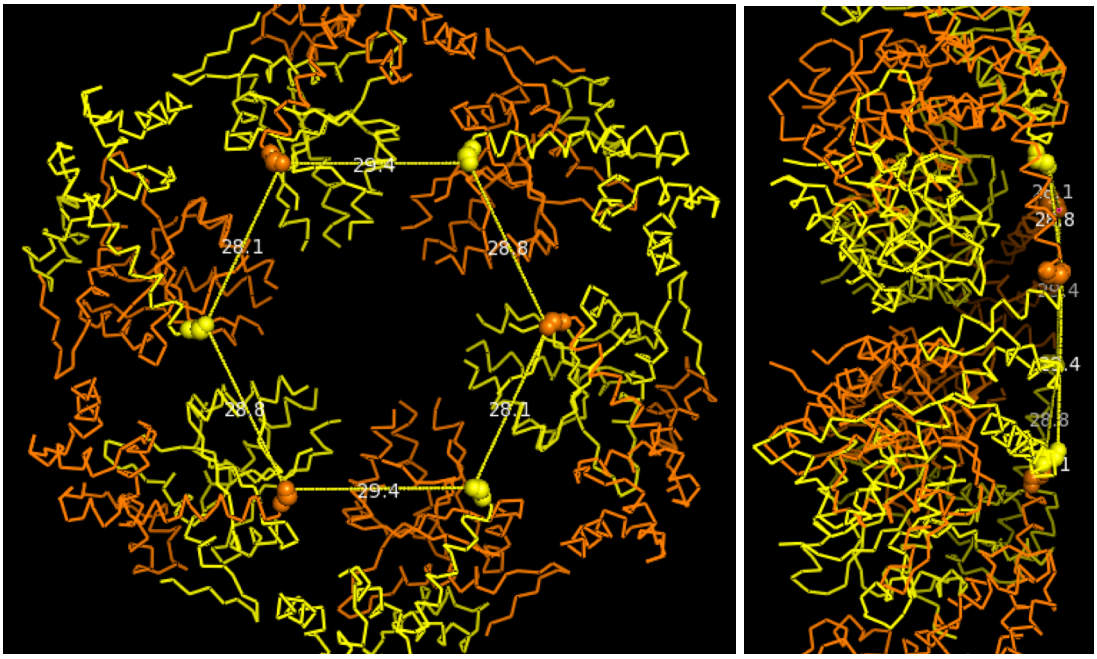

Figure 11. Model of tobacco Rca highlighting residue 360. Back and side views of Rca showing distances (28.1 – 29.4 Å) between the last ordered residues on each subunit. PDB ID: 3ZW6

The mechanism by which Rca alters the active site of Rubisco from a closed to an open form is not known, therefore, information about the interaction between Rubisco and Rca could provide important insight into the Rubisco reactivation mechanism.

By using Förster resonance energy transfer (FRET) based binding assays, information about the physical interaction between Rubisco and Rca can be obtained. Under ideal conditions, binding will be visible by FRET and equilibrium binding constants can be determined. However, the distances between the donor and acceptor cannot be accurately measured by this assay because the orientation and position of the dyes are unknown, and multiple FRET events may occur simultaneously. Two binding events could occur within 30 – 80 Å, skewing the FRET intensity.

There is a lack of knowledge of relevant Rca states and stoichiometries of Rubisco-bound species. The FRET-based binding assay will measure the strength of the

Rca-Rubisco interaction as a function of Rca assembly and Rubisco activation state. This binding assay will provide insight into Rca states able to interact with Rubisco, as well as define conditions to generate bound states for structural analysis.

METHODS

Rubisco Expression in *Chlamydomonas reinhardtii*

Rubisco strains with large subunit mutations were transformed into *Chlamydomonas reinhardtii* by Robert Spreitzer's group (U. Nebraska) and supplied to the Wachter lab. The following strains were used: CSCS, with C449S/C459S mutations; D470C with C449S/C459S/D470C mutations; and K474C with C449S/C459S/K474C mutations. Each experimental technique was performed on all three mutant strains, unless otherwise noted.

Using sterile technique in the laminar flow hood, one colony was picked and inoculated into a starter culture of acetate media (7.5 mM NH_4Cl, 0.35 mM $CaCl_2$•$2H_2O$, 0.4 mM $MgSO_4$•$7H_2O$, 40 mM Tris, 16.5 mM acetic acid, 0.103 mM K_2HPO_4, 0.067 mM KH_2PO_4, 369 μM H_3BO_3, 153 μM $ZnSO_4$•$7H_2O$, 19 μM $MnCl_2$•H_2O, 36 μM $FeSO_4$•$7H_2O$, 14 μM $CoCl_2$•$6H_2O$, 13 μM $CuSO_4$•$5H_2O$ and 2 μM $(NH_4)_6Mo_7O_{24}$•$4H_2O$) and grown, with shaking, covered at room temperature until culture is fully green, approximately seven days when grown in the dark. The starter culture was used to inoculate 1.5 L of acetate media, which was grown covered, with stirring and 0.2 μm filtered compressed air bubbled in, and monitored until fully green, approximately seven days. 24 hours before harvesting, 1.5 L of fresh acetate media was added to the culture and growth continued. The wet cell paste for a 3 L culture (mass typically around 5 g) was pelleted and stored at -80°C.

Rubisco Purification from *Chlamydomonas*

The cell paste was suspended in 50 mL of Rubisco Isolation Buffer (RIB) (50 mM Tris-HCl pH 7.5, 10 mM $NaHCO_3$, 10 mM $MgCl_2$, 1 mM EDTA) and disrupted by sonication. The lysate was ultra-centrifuged at 50,000 RPM and the supernatant was subjected to ammonium sulfate precipitations, where Rubisco precipitated out in the 45% or 50% fraction, determined by sodium dodecyl sulfate polyacrylamide gel electrophoresis (SDS-PAGE). The sample was dialyzed overnight at 4°C against 500 mL of RIB. The dialysate was applied to an anion exchange column and Rubisco was collected in the 205mM or 280mM NaCl fractions, determined by SDS-PAGE. Protein was concentrated and buffer-exchanged into 50 mM HEPES pH 7.2. The protein concentration was determined by UV absorbance and the Bradford method, with typical yields of 0.75 mg/L cell culture. All Rubisco preparations were flash-frozen and stored at -80°C.

Rca Expression and Purification

The pET151/dTOPO vector carrying the gene for cotton-β-Rca-378AC, a short-form Rca with a C-terminal Ala-Cys insert [46, 68], was transformed into *E. coli* strain BL21*(DE3) (Invitrogen). Bacterial cells were cultured in 3 L LB broth with 100 mg/L carbenicillin at 37°C until the OD_{600} reached 0.6, then induced by addition of 1 mM IPTG and grown at 25°C with shaking at 200 rpm for 8 hours. After centrifugation, the cells were frozen at -80°C.

Cell paste was suspended in 40 ml of 25 mM Tris-HCl pH 8.0, 10 mM Imidazole pH 8.0, 10% glycerol, 2 mM DTT, 0.1 mM ADP, 0.1 mM EDTA pH 8.0, 1 mM PMSF and 20 mg hen egg white lysozyme and then disrupted by 5 rounds of sonication (60

seconds on, 30 seconds off). 5 M NaCl and 1 M DTT were added to final concentrations of 0.5 M and 2 mM, respectively. The lysate was centrifuged at 15K rpm (17,600xg) and 4°C for 30 minutes, and the supernatant was passed through a 0.22 μm syringe filter before loading onto a nickel-nitrilotriacetic acid column (Qiagen). His-tagged protein was purified using an imidazole step gradient from 10 to 500 mM in 25 mM Tris-HCl pH 8.0, 500 mM NaCl, 2 mM DTT and 0.05 mM ADP. Fractions containing the His-tagged protein were pooled, EDTA was added to 1 mM, ADP to 0.5 mM and DTT to 2 mM. After addition of 1.2 mg of tobacco etch virus (TEV) protease, the sample was dialyzed overnight at 4°C against 1 L of 25 mM Tris-HCl pH 8.0, 40 mM NaCl, 1 mM EDTA pH 8.0, 0.05 mM ADP and 2 mM DTT. The next morning, the dialysis buffer was replaced with fresh buffer that contained 0.1 mM EDTA (instead of 1 mM), and dialysis continued at 4°C for 3 hours. The dialysate was reapplied to a Ni-NTA column, and Gh-β-Rca was collected in the early fractions. Protein fractions were concentrated and buffer-exchanged into 25 mM HEPES pH 7.2, 250 mM KCl, 5 mM $MgCl_2$, 10% glycerol, and 2 mM ATPγS (adenosine 5′-[γ-thio]triphosphate). Aliquots were flash-frozen in liquid N_2 and stored at -80°C. Rca preparations were quantitated utilizing the Bradford method (n=9) with BSA as a standard.

Dye Conjugation Methodology

Rubisco mutants (CSCS, D470C, K474C) were covalently labeled with the Alexa-647 C5-maleimide fluorophore (Molecular Probes). A typical reaction consisted of 100 μL of 82 μM Rubisco, buffer stock, and 11 μL of 1.91 mM Alexa dye stock (prepared in 50 mM HEPES pH 7.2), giving a 3:1 molar ratio of Alexa dye to Rubisco large subunit, and final reaction components of 50 mM HEPES pH 7.2, 125 mM KCl.

Reactions were incubated overnight at 4°C. To remove excess free dye, 400 µL of saturated ammonium sulfate was added drop-wise, followed by 30 min incubation at 4°C. The pellets were collected by microcentrifugation in an eppendorf tube, suspended in 25 mM HEPES pH 7.5, 250 mM KCl and 10% glycerol, and desalted by two passes through a gel filtration spin column equilibrated in the same buffer (Sephadex G50-fine, 2 mL bed volume, 400x*g* centrifugation for 2 min). Aliquots were flash-frozen and stored at -80°C.

Wild-type cotton Rubisco was a generous gift from Dr. Mike Salvucci (USDA), and was labeled using the same method, with a 4:1 molar ratio of Alexa dye to Rubisco large subunit and higher pH to label non-specifically. Cotton-β-Rca-378AC was labeled in a similar manner with Alexa-488, at pH 7.2 and a 3.5:1 molar ratio of Alexa dye to Rca subunit, and in the presence of 5 mM ATPγS.

RP-HPLC and Spectrophotometric Analysis of Labeled Protein

Alexa-labeled Chlamy Rubisco samples were analyzed by reverse-phase high pressure liquid chromatography **(**RP-HPLC) (Waters 600 HPLC system, Waters 996 photodiode array detector) on a C18 analytical column (Vydac) using a linear water/acetonitrile (ACN) gradient with 0.1% trifluoroacetic acid (TFA). Alexa-labeled cotton Rubisco and cotton-β Rca samples were analyzed by reverse-phase HPLC (Agilent Technologies 1260 Infinity Quaternary LC system, Agilent Technologies 1100 Series Diode-Array detector) on a C18 analytical column (Phenomenex Prodigy, 5 mm ODS-3, 100 Å pore size, 250 x 4.6 mm) using a linear water/acetonitrile gradient with 0.1% TFA. The eluent was monitored for protein and Alexa dye absorbance by OD_{220}, OD_{280}, OD_{490} and OD_{650}. Free dye was not observed in any of the Rca-488 or Rubisco-647 samples.

Protein-containing fractions were collected, and the absorbance was measured from 800 - 250 nm using 50% acetonitrile, 50% water, 0.1% TFA as a solvent blank (Shimadzu UV2401-PC Spectrophotometer).

The degree of labeling was calculated from the absorbance of each species, using the published (Molecular Probes, Inc.) extinction coefficients of each dye (Alexa-488: ε_{494} = 71,000 $M^{-1}cm^{-1}$; Alexa-647: ε_{650} = 239,000 $M^{-1}cm^{-1}$) (equations 1, 2). The protein concentration was determined by OD_{280}, using an extinction coefficient calculated from the amino acid sequence (Chlamy Rubisco: ε_{280} = 837,920 $M^{-1}cm^{-1}$; cotton Rubisco: ε_{280} = 826,000 $M^{-1}cm^{-1}$; cotton Rca: ε_{280} = 44,350 $M^{-1}cm^{-1}$). To correct for Alexa-488 contributions to the $OD_{280,}$ the OD_{494} was multiplied by the correction factor 0.11, then subtracted from the OD_{280} (equation 1). To correct for Alexa-647 contributions to the $OD_{280,}$ the OD_{650} was multiplied by the correction factor 0.03, then subtracted from the OD_{280} (Molecular Probes, Inc.). To verify the correct molecular weight of labeled protein, MALDI spectra were collected on a Voyager DE STR mass spectrometer using a matrix of sinapinic acid.

$$\text{Protein concentration (M)} = \frac{[A_{280}-(A_{494}\times 0.11)]\times DilutionFactor}{\varepsilon_{protein}} \qquad \text{Equation 1 [69]}$$

$$\text{Dye to protein ratio} = \frac{A_{494}\times DilutionFactor}{\varepsilon_{dye}\times M_{protein}} \qquad \text{Equation 2 [69]}$$

Rubisco Activation Assay

Rubisco preparations were assayed for percent activation by an enzyme-linked assay measuring NAD+ production by decreasing A_{340} and comparing to activity of ECM samples. Assay concentrations were 100 mM Tricine-NaOH pH 8.0, 10 mM $MgCl_2$, 10 mM $NaHCO_3$, 20 mM KCl, 5 mM DTT, 0.5 mM NADH, 1.85 U pyruvate kinase,

2.33 U lactic dehydrogenase, 0.5 U enolase, 0.5 U diphosphoglyceromutase, 0.2 mM 2,3-diphosphoglycerate, 2 mM ADP, 0.5 mM RuBP, and 26 μg/mL Rubisco. For the ECM samples, Rubisco was incubated for 3 minutes in the assay mix to allow for carbamylation and binding of Mg^{2+}, then RuBP was added, the sample was mixed manually and the scan was started. To test percent activation, Rubisco was added to the assay mix and RuBP, mixed manually and scanned. The percent activation was determined by comparing the slope of 3-PGA production of the Rubisco samples to those of the ECM Rubisco samples of the same strain.

Continuous ATPase Assays Based on Phosphate Production

This assay was carried out to compare the activity of label-free Gh-β-Rca-CA with the activity of the same variant conjugated to Alexa-488 (Rca-488). The rate of inorganic phosphate release upon ATP hydrolysis was monitored by an enzyme-coupled spectrophotometric assay [59, 70]. To assay phosphate production in a continuous fashion, the absorbance difference between the reactant and product species was monitored by absorbance at 360 nm as a function of time. To monitor residual phosphate in assay components, baseline scans were collected in the absence of Rca with and without ATP. To monitor ATP turnover by Rca, 704 μL working solution was added to the sample and reference cuvettes and the absorbance set to zero. 200 μL MESG stock, 30 μL PNP stock, 8 μL 0.5 M $MgCl_2$ stock and 50 μL Rca (in 25 mM HEPES pH 7.5, 250 mM KCl, 5 mM $MgCl_2$, 10% glycerol) were added to the cuvette, and the time scan was started. After 60 seconds, 8 μL ATP stock (500 mM) was added, the solution was mixed using a manual cuvette mixer, and the A_{360} was monitored for 300 seconds. The final composition of the sample in the cuvette was 55 mM HEPES pH 8.0, 50 mM Tris-

HCl pH 7.5, 0.8 mM DTT, 200 μM MESG, 0.1 mM Sodium Azide, 3 units PNP, 9 mM $MgCl_2$, 4 mM ATP, 5.3-8.5 μM Rca, 0.5% glycerol, 12.5 mM KCl, 1.25 mM HEPES pH 7.5 and 0.1 mM ATPγS. The baseline scan was subtracted from the response curve, and the slope was determined between 70 and 90 seconds, consistently the steepest part of the curve. Using a phosphate standard curve, the Rca turnover velocity was calculated (μM phosphate produced per second) and normalized with respect to Rca subunit concentration. Each reaction was carried out in triplicate, using independently prepared protein pools.

Control Experiments to Examine Dye-Dye Interactions

For urea-based denaturation experiments, 300 μL of 8 M urea was added to 100 μL of the assay samples to obtain a final concentration of 6 M urea. The samples were incubated for 15 minutes at 70°C. Samples consisted of 33.6 μM Rubisco with 17 dyes per holoenzyme, 30 μM Rca with 1.4 dyes per subunit in 25 mM HEPES pH 7.5, 250 mM KCl, 5 mM $MgCl_2$, and 10% glycerol, with or without 20% Ficoll. Excitation and emission scans were compared to those before denaturation.

To rule out any ionic effects with the dye, a series of free dye tests were performed in the presence and absence of all buffer components. All samples contained 25 mM HEPES pH 7.5, Alexa-488 and Alexa-647. Final concentrations of additives were 250 mM KCl, 5 mM $MgCl_2$, and 10% glycerol. A free dye experiment was performed to examine concentration dependence on the peak shift observed in Alexa-647. A series of serial dilutions of Alexa-647 were made starting from 26.2 μM to 0.82 μM, and diluted in 25 mM HEPES pH 7.5.

For all control experiments, instrumental parameters were identical to those in the binding assay. Fluorescence was monitored in 1.0 nm increments with an integration time of 0.4 seconds. Excitation scans were collected from 400 nm to 660 nm with emission monitored at 672 nm, and an excitation and emission slit widths of 1.0 nm. Emission spectra were collected from 500 nm to 800 nm with excitation at 420 nm, 440 nm or 490 nm and a slit width of 1.0 nm for both excitation and emission.

Testing Crowding Agents with Free Dye

To determine whether the inert carbohydrate polymer crowding agent, Ficoll, was suitable to use in FRET-based binding assays, a free dye test was performed to examine any effect on the excitation and emission of the free dyes. At 10% Ficoll, the experimental volume fraction of Ficoll 70 is ~7%, and there is a 5-fold increase in enzyme activity of phosphoglycerokinase [71]. The samples contained 37.5 μM Alexa-488, 300 μM Alexa-647, 25 mM HEPES pH 7.5, 5 mM $MgCl_2$, 250 mM KCl, 10% glycerol, and 0-20% Ficoll 70 or 0-18% BSA, in a final volume of 110 μL.

Fluorescence excitation and emission scans were collected using a Jobin Yvon Fluoromax-3 fluorimeter and a quartz microcuvette. Fluorescence was monitored in 1.0 nm increments with an integration time of 0.4 seconds. Excitation scans were collected from 400 nm to 660 nm with emission monitored at 672 nm, and an excitation and emission slit widths of 1.0 nm. Emission spectra were collected from 500 nm to 800 nm with excitation at 420 nm, 440 nm or 490 nm and slit widths of 1.0 nm.

Rubisco-Rca FRET Binding Assay

A variety of conditions were tested in the assay. Chlamy or cotton Rubisco was at a concentration between 4 and 30 μM, with 1 – 25 dyes per L8S8. Cotton Rca was

between 25 – 50 μM (typically 30 μM), with 1 – 1.5 dyes per subunit. For most of the assays, ATPγS was used, but ATP was present occasionally. The buffer was consistent and contained 25 mM HEPES pH 7.5, 250 mM KCl, 5mM $MgCl_2$ and 10% glycerol. Typically, only one time measurement was taken and compared to controls, but during the last few experiments, a 15 – 20 minute time course was performed.

Rubisco and Rca were mixed in an eppendorf tube, then transferred to the cuvette. An aliquot of nucleotide/Mg^{2+} mix was added, and excitation and emission scans were immediately taken. Controls were also prepared and scanned in an identical fashion, and consisted of: Alexa-488 + Alexa-647, Rca-488 + Alexa-647, Rca-488 only, Rubisco-647 only, Rubisco-647 + Alexa-488, Alexa-488 only, and Alexa-647 only.

Fluorescence excitation and emission scans were collected using a Jobin Yvon Fluoromax-3 fluorimeter and a quartz microcuvette. Fluorescence was monitored in 1.0 nm increments with an integration time of 0.4 seconds. Excitation scans were collected from 400 nm to 660 nm with emission monitored at 672 nm, and an excitation and emission slit widths of 1.0 nm. Emission spectra were collected from 500 nm to 800 nm with excitation at 420 nm, 440 nm or 490 nm and a slit width of 1.0 nm for both excitation and emission.

The last conditions tried (and most promising for future experiments) consisted of 26.5 μM Rubisco-647 (cotton, 1 dye per L8S8), 30 μM Rca-488 (mixed with unlabeled for 0.21 dye per subunit), 100 μM ADP, 5 mM ATP, 10 mM $MgCl_2$, 2 mM RuBP, 25 mM HEPES pH 7.5, 250 mM KCl and 10% glycerol.

RESULTS

Analytical Data on Alexa Derivatized Rubisco and Rca Preparations

Alexa-488 and Alexa-647 dyes were chosen due to their spectral overlap (figure 12) and FRET efficiency. R_o, the distance at 50% FRET efficiency, is ~56 Å for the Alexa-488 and Alexa-647 pair. FRET using these specific dyes is most sensitive to changes in distance when the donor and acceptor are separated by 35 – 75 Å.

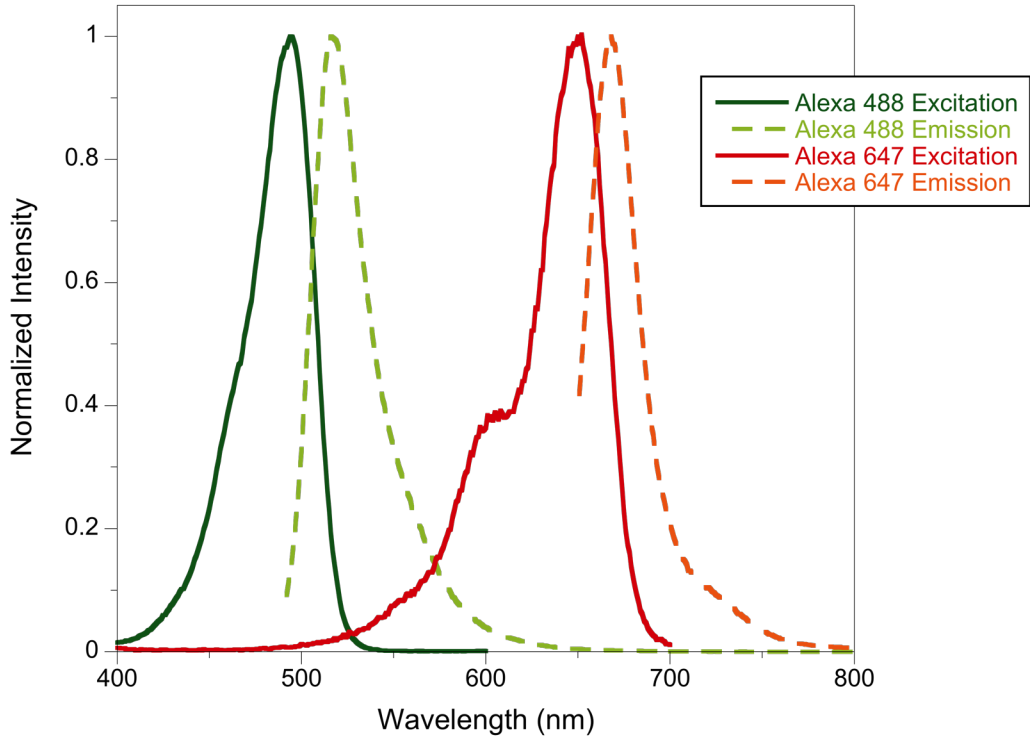

Figure 12. Normalized fluorescence spectra of Alexa-488 and Alexa-647. For the Alexa 488 excitation scan (solid green), the emission was monitored at 519 nm. For the Alexa 488 emission scan (dashed light green), the excitation wavelength was set to 495 nm. For the Alexa-647 excitation scan (solid red), the emission was monitored at 672 nm. For the Alexa-488 emission scan (dashed orange), the excitation wavelength was set to 651 nm. For Alexa-488, λ_{ex} = 494 nm and λ_{em} = 519 nm. For Alexa-647, λ_{ex} = 651 nm and λ_{em} = 672 nm.

At the start of assay development, the goal was to label every large subunit of Rubisco and every subunit of Rca with one dye each. Labeling was quite efficient in

Chlamydomonas (table 1), but the background mutant (CSCS) with no solvent exposed cysteines, was getting the same degree of labeling as those with an introduced C-terminal cysteine (figure 13).

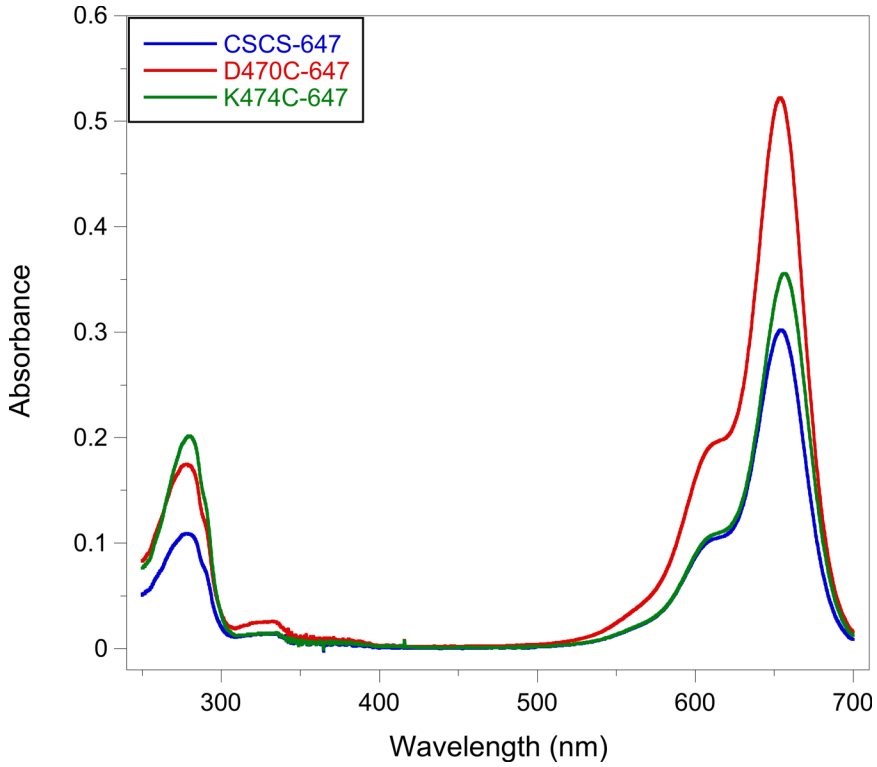

Figure 13. Absorbance spectra of Alexa-647 labeled Chlamy Rubisco mutants CSCS (blue), D470C (red) and K474C (green). The molar ratio of Alexa:Rubisco in covalently labeled preparations was determined by absorbance at 280 nm and 650 nm following equations 1 and 2. Labeling results gave Alexa-647:Rubisco L8S8 of 10.2:1 for the CSCS mutant, 11:1 for the D470C mutant and 5.8:1 for the K474C mutant.

Table 1. *Chlamydomonas* Rubisco Labeling Results.

Strain	Labeling Reaction Ratio (L8S8:dye)	pH	Labeling Efficiency
CSCS	20:1	7.2	4.4 mol Alexa/mol L8S8
CSCS	24:1	7.2	10.2 mol Alexa/mol L8S8
CSCS	24:1	8.0	20 mol Alexa/mol L8S8
D470C	20:1	7.2	3.1 mol Alexa/mol L8S8
D470C	24:1	7.2	11.1 mol Alexa/mol L8S8
D470C	24:1	8.0	26 mol Alexa/mol L8S8
K474C	20:1	7.2	3.4 mol Alexa/mol L8S8
K474C	24:1	7.2	5.8 mol Alexa/mol L8S8
K474C	24:1	8.0	18 mol Alexa/mol L8S8

Rubisco activation assays showed Chlamy Rubisco was active without incubation in CO_2 and Mg^{2+}. CSCS was 83.3 ± 4.17 % active, K474C: 91.8 ± 4.37 %, and D470C: 89.9 ± 2.43 %. However, purification of *Chlamydomonas* led to extremely low yields of Rubisco. Extensive effort was put into optimizing purification conditions, to no avail. Around 10 FRET assays were carried out with Chlamy Rubisco and cotton Rca, but the desired Rubisco concentration was much higher than our production of *Chlamydomonas* Rubisco allowed for. We had access to wild-type cotton Rubisco purified from leaves and decided to proceed with that.

Since wild type cotton Rubisco did not have a C-terminal cysteine to site-specifically label, additional dye was added to the reactions. Although the reactions were successful in non-specific labeling, they were not very reproducible, as the same conditions often gave drastically different labeling efficiencies, or different conditions resulted in the same degree of labeling (table 2). Labeling of cotton Rca was reproducible and gave results near the desired 1 dye per Rca subunit (table 3).

Table 2. Cotton Rubisco Labeling Results.

Labeling Reaction Ratio (L8S8:dye)	pH	Labeling Efficiency
17:1	7.2	0.55 mol Alexa/mol L8S8
24:1	7.2	10.3 mol Alexa/mol L8S8
32:1	7.2	0.5 mol Alexa/mol L8S8
32:1	7.5	1.1 mol Alexa/mol L8S8
32:1	7.5	3.5 mol Alexa/mol L8S8
32:1	8.0	19.6 mol Alexa/mol L8S8
40:1	8.0	13.9 mol Alexa/mol L8S8

Table 3. Cotton Rca Labeling Results.

Labeling Reaction Ratio (Rca:dye)	pH	Labeling Efficiency
3.25:1	7.2	0.84 mol Alexa/mol Rca
3.5:1	7.2	1.42 mol Alexa/mol Rca
3.5:1	7.2	1.28 mol Alexa/mol Rca

To verify the identity of Alexa-derivatized Rubisco, protein preparations were analyzed by reverse phase HPLC. All Chlamy labeled Rubisco eluted between 43 and 50.5 min, corresponding to 53-60.5% ACN (C449S/C459S at 43 min and 53% ACN, D470C at 49 min and 59% ACN, K474C at 50.5 min and 60.5% ACN) (figure 14), whereas free Alexa 647 eluted at 14.5 min and 24.5% ACN. In the HPLC chromatograms for CSCS and D470C, the peaks were slightly broader than those of K474C and had additional minor peaks.

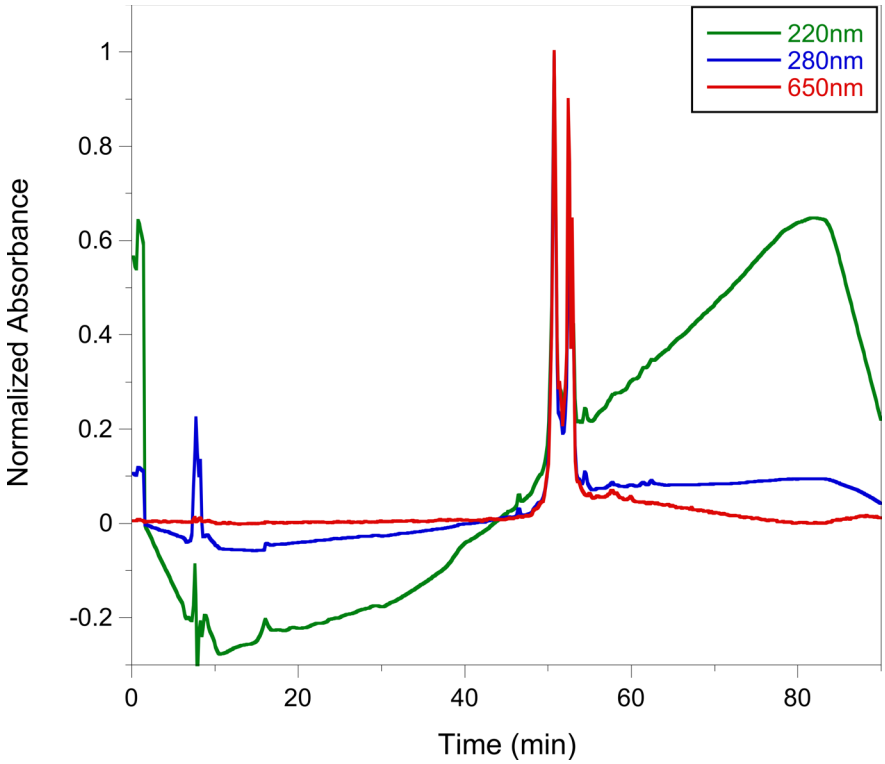

Figure 14. HPLC chromatogram. Reverse-phase HPLC chromatograms of Alexa-labeled Chlamy K474C Rubisco monitored at 220 nm (green), 280 nm (blue) and 650 nm (red). The chromatograms indicate that labeled Rubisco preparations do not contain any traces of free Alexa dye.

It was expected that if labeled correctly, each large subunit of D470C or K474C Rubisco would contain one Alexa-647 molecule attached at the mutated cysteine residue, giving an 8:1 ratio of dye:L8S8, and the CSCS mutant with no exposed cysteine residues would result in very little labeling. From figure 13, however, the ratio of dye to protein in

the CSCS mutant is much higher than expected. It is seen, though, that there is more than one Alexa label per Rubisco large subunit. It may also be possible that the small subunit is labeled as well as the large subunit. Optimization of labeling conditions such as pH and ratio of Alexa 647 concentration to Rubisco concentration will be performed in hopes of more precise labeling. Optimization may also lead to more distinct, narrow peaks on the HPLC spectrum.

Labeled cotton Rubisco also showed multiple peaks on the HPLC, often with shoulders before and after the main peaks. Likely these multiple peaks were due to heterogeneous non-specific labeling. Absorbance spectra of labeled cotton Rubisco and Rca eluted from RP-HPLC were used to determine the molar ratio of dye to protein in each labeling reaction (figure 15). We were hopeful that performing matrix-assisted laser desorption/ionization (MALDI) on the labeled Rubisco to determine molecular weight and degree of labeling by weight would assist in identification of species present in the samples. MALDI was attempted on multiple preparations of Rubisco from both Chlamy and cotton, however, none of the samples provided decent spectra of both the large and small subunits (figure 16). MALDI was successful on labeled and unlabeled Rca samples, and confirmed a labeling efficiency of about 1 dye per protein chain.

The C-terminal Label Does Not Interfere with the ATPase Activity of Cotton Rca

ATPase assays based on MESG (phosphate production measurements) were carried out on cotton β-Rca using preparations that contain 0, 25, 50, 75 and 100% Alexa-488 labeled subunits, and found the variations of observed activity are within error typically seen in the lab (table 4). Turnover rates were approximately 5-fold lower than previously determined [48], and standard deviation was high. Although this Rca

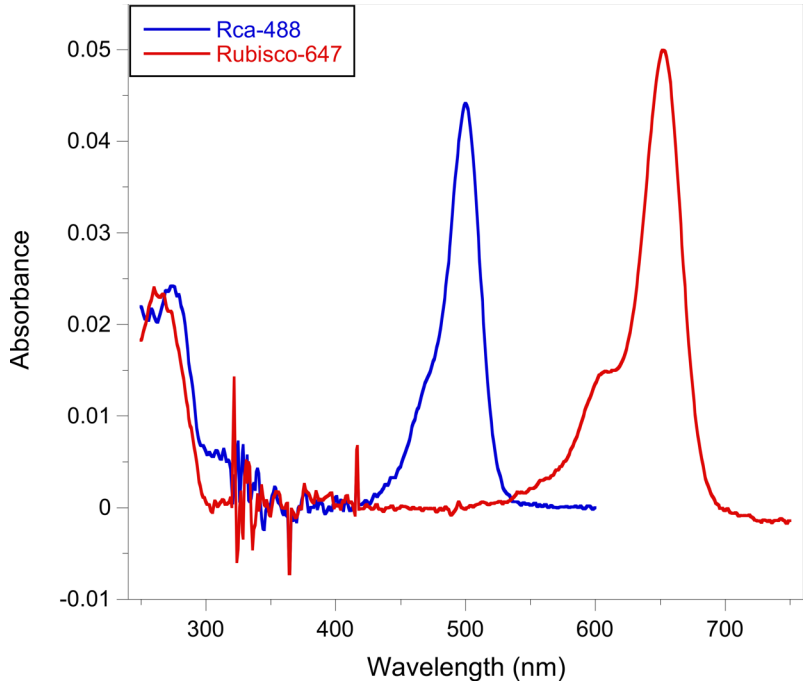

Figure 15. Absorbance spectra of labeled cotton Rubisco and Rca. The peak eluting from the HPLC column of each labeled protein (Rca-488: blue; Rubisco-647: red) was collected and analyzed by absorbance. The molar ratio of dye to protein in covalently labeled preparations was determined by absorbance as described in the Methods section.

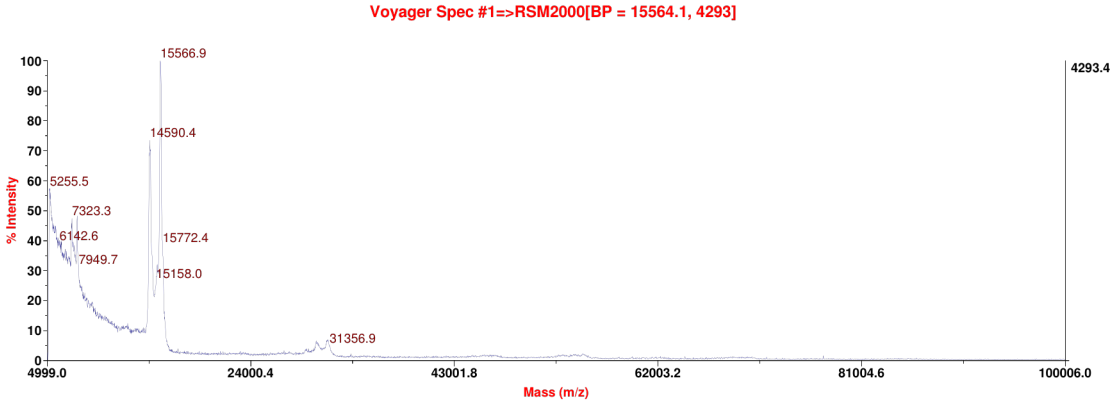

Figure 16. MALDI spectra of cotton Rubisco. Spectra were collected on the labeled cotton Rubisco preparation corresponding to the absorbance spectra in figure 14. The large subunit of Rubisco (53282 Da) was not seen in any spectra. The small subunit shows two distinct peaks with at 14590.4 and 15566.9. The theoretical mass for the unlabeled small subunit is 14559 Da, and for the small subunit with one label is 15809 Da. The error of this instrument is estimated to be about 100 Da for a protein of this size.

preparation was very sluggish in its turnover of ATP, covalently bound Alexa-488 does not affect the ATPase activity of cotton β-Rca.

Table 4. Turnover rates of cotton Rca with varying degrees of labeling.

% labeled	Average turnover (min^{-1})	Standard deviation
0	0.842	0.317
25	0.746	0.157
50	0.722	0.139
75	0.815	0.139
100	0.629	0.267

Control Experiments to Address Dye-Dye Interactions

Experiments with up to 30 μM Rubisco were performed, but optical effects were seen. A drastic decrease in overall intensity, along with a blue-shifted peak for Alexa 647 was observed. To see if this signal loss was reversible, the sample was denatured with 6 M urea and the fluorescence increased, suggesting dye dimers were self-quenching. While the denaturation experiment solved the intensity issue, the dramatically shifted peak (from 650 to 575 nm) was still a problem. To rule out any ionic effects with the dye, a series of free dye tests were performed in the presence and absence of buffer components (250 mM KCl, 5 mM $MgCl_2$ and 10% glycerol), which showed the fluorescence was not affected. A free dye experiment examined concentrations between 0.82 and 26.2 μM and found the peak shift appears at concentrations above 6 μM Alexa-647. 100 μM free dye was also tested and the overall intensity dropped to around 20% of the intensity seen in the 3 μM sample. As concentration increased to 26 μM, the main peak (650 nm) decreased, while the shoulder (575 nm) increased. It was concluded that all cuvette Alexa-647 dye concentrations should stay below 6 μM.

Preliminary Results

In an effort to get the most Rca in the best conditions for Rubisco reactivation, a concentration of 30 μM cotton Rca was used, at which 70-80% is in the hexameric state in ATP [48]. It was assumed all Rca assembled into hexamers in the assay, to determine the ratios of L8S8 to Rca_6 in solution. The four independent trials in figures 17 and 18 represent four different ratios of Rubisco to Rca, however, the fluorescence signal stays constant. In trial 1, there was a 1:1 ratio of L8S8:Rca_6; in trial 2, 1.2:1; in trial 3, the Rubisco concentration was increased drastically to 3.9:1; and in trial 4, 5.9:1. A very slight increase in the red dye emission upon green dye excitation is seen in the excitation scan in trial 4 (figure 17b), however, a corresponding change in the emission scan is not seen, suggesting this increase was not due to FRET.

Figures 17 and 18 show a distinct peak where you would expect FRET to occur: an increase in the 672 nm emission upon 495 nm excitation in the samples with both Rubisco and Rca. As expected at this wavelength, Rubisco only samples showed a small signal from the direct excitation of Alexa-647 by green light. Rca only samples had a small peak, from Alexa-488 emission leakage into the red channel. While these experiments did show promising results, no changes were seen in the spectra with increasing Rubisco concentrations.

One kinetic time scan was performed using 2.26 μM Chlamy D470C Rubisco-647 (20 dye per L8S8) with 50 μM cotton Rca-488 (1 dye per subunit). The scan was run for approximately 30 minutes, with excitation wavelength of 440 nm and emission wavelength of 672 nm. It was spiked with 2 mM ATP, incubated for 4 minutes on ice, then measured for 2000 seconds. There was no significant signal change, over noise.

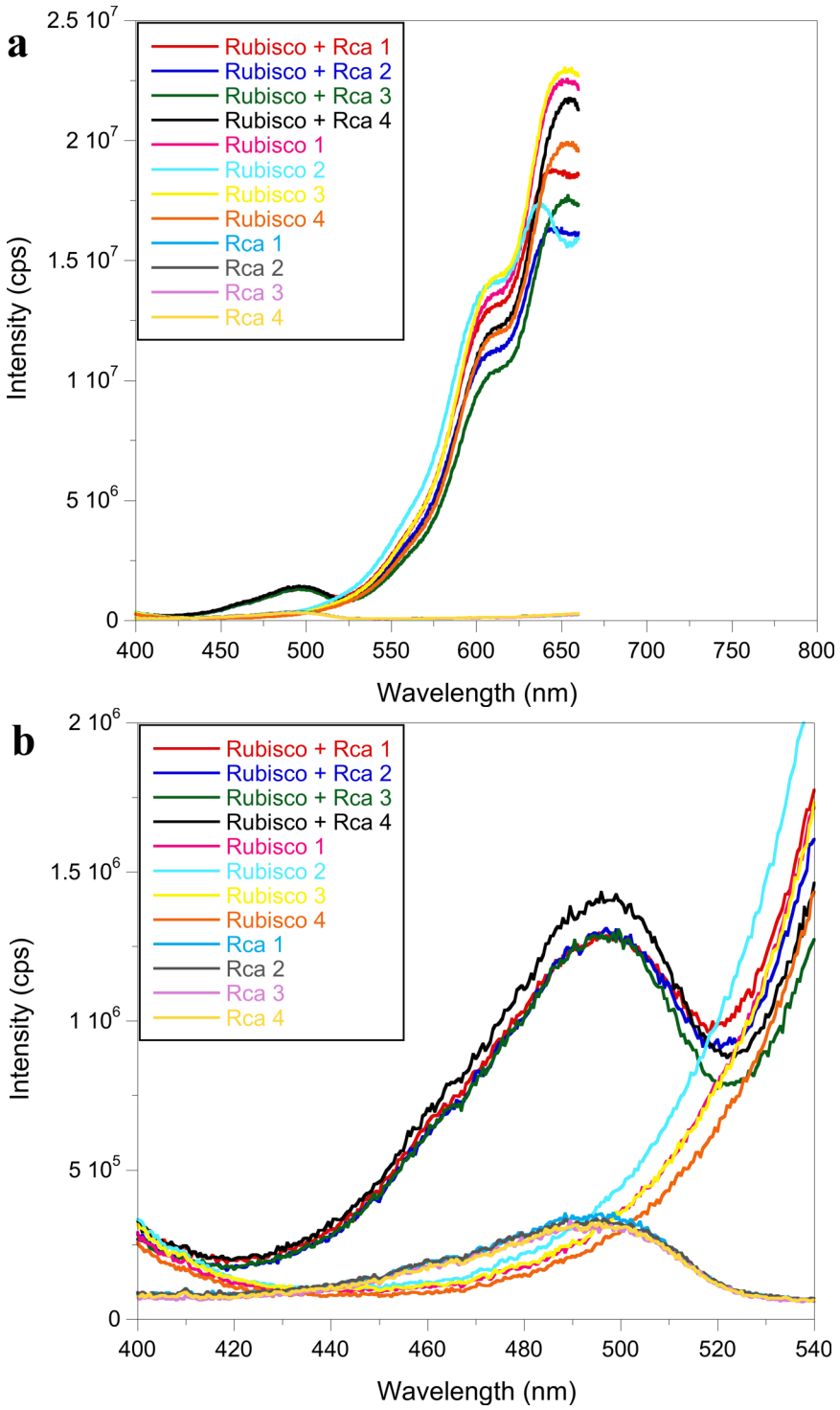

Figure 17. Excitation scans of Rubisco-Rca FRET binding assay. (a) Full excitation scan, (b) excitation scan zoomed in to show FRET signal. showing promising results. All Rca samples were labeled with Alexa-488 (1 dye per subunit), cotton Rubisco was labeled with Alexa-647 (3.5 dyes per L8S8).

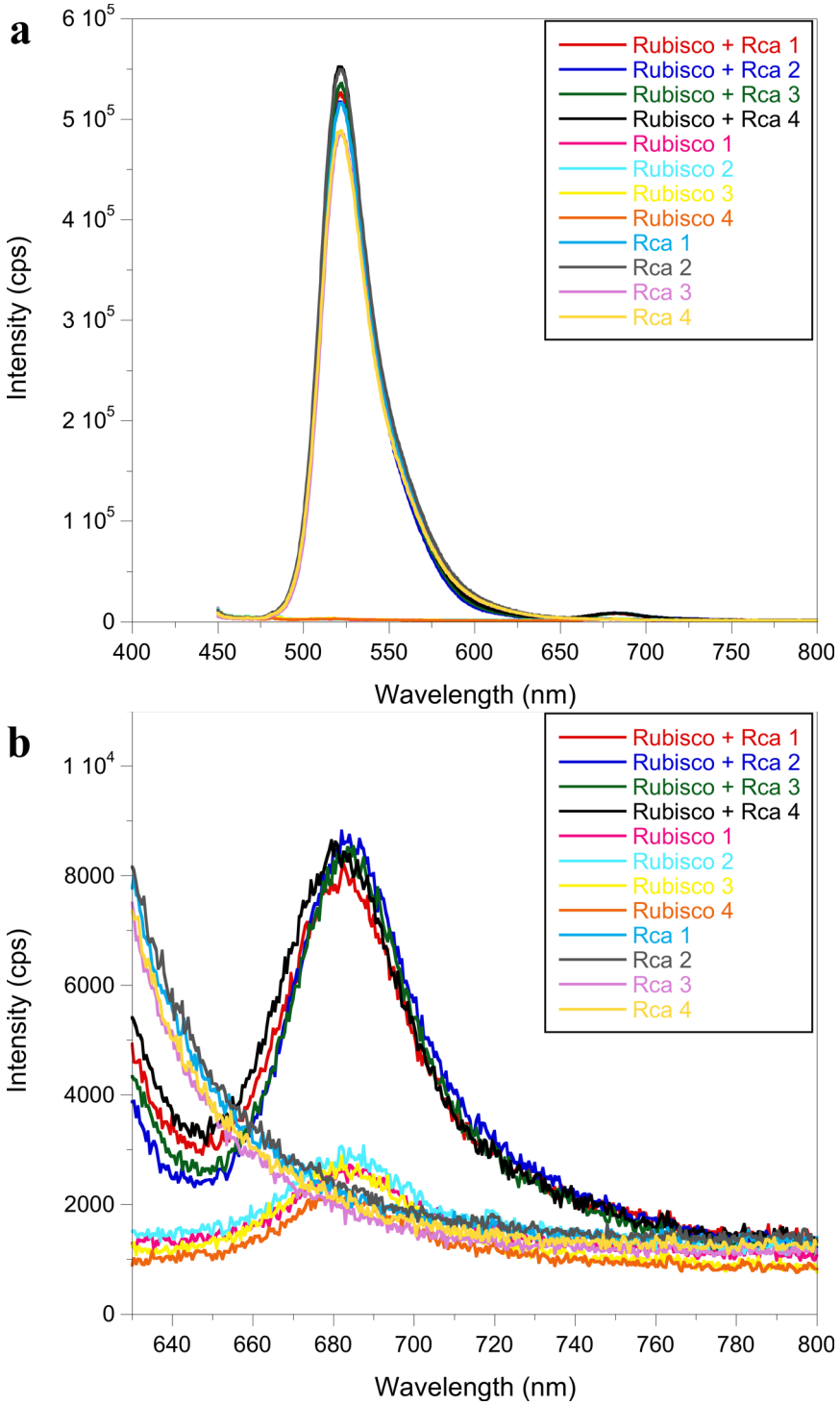

Figure 18. Emission scans of Rubisco-Rca FRET binding assay. (a) Full emission scan, (b) Emission scan zoomed in to show FRET signal. All Rca samples were labeled with Alexa-488 (1 dye per subunit), cotton Rubisco was labeled with Alexa-647 (3.5 dyes per L8S8).

To determine if the peak seen in figures 17 and 18 was due to interaction between Rubisco and Rca, a full set of controls were performed at the same concentration. Free dye was assayed alone, together and with protein samples. In the Rca-488 + free Alexa-647 control, there was a peak for both green and red dyes in the excitation scan. It was the only sample with a significant peak for the green dye, and indicates a possibility of FRET. It was speculated that free Alexa-647 attached to Rca, but the sample was run through a Sephadex gel-filtration column, then over HPLC and Alexa-647 was no longer present. In the Rubisco-647 + free Alexa-488 sample, there was a very small peak for free Alexa-488 dye, slightly increased from the Rca only and Alexa-488 samples due to a small amount of leakage from Rubisco-647. As expected, for the Rca-488 only and free Alexa-488 samples, there was a very small peak for Alexa-488 dye in the excitation scan. It was observed in the emission scans that Rca-488 samples are consistently lower in intensity than free Alexa-488 containing samples.

No discernable FRET signal was seen in either the excitation or the emission scans for the Rubisco-647 + Rca-488 sample. After excitation and emission scans, the Rubisco + Rca sample was extracted from the cuvette and placed on ice for 15 minutes. Scans were repeated after this incubation period, but there was no discernable signal change of either dye between these two samples. If binding were happening and the two C-terminal tails were in close enough proximity, FRET would occur. The FRET signal would be seen when excited at 495 nm with emission monitored at 672 nm in the excitation scan, and at 672 nm in the emission scan upon excitation at 420 nm. No definitive FRET signal was seen with the Rubisco-Rca sample over the control samples, and the high concentration of Alexa-647 in the cuvette was becoming problematic and

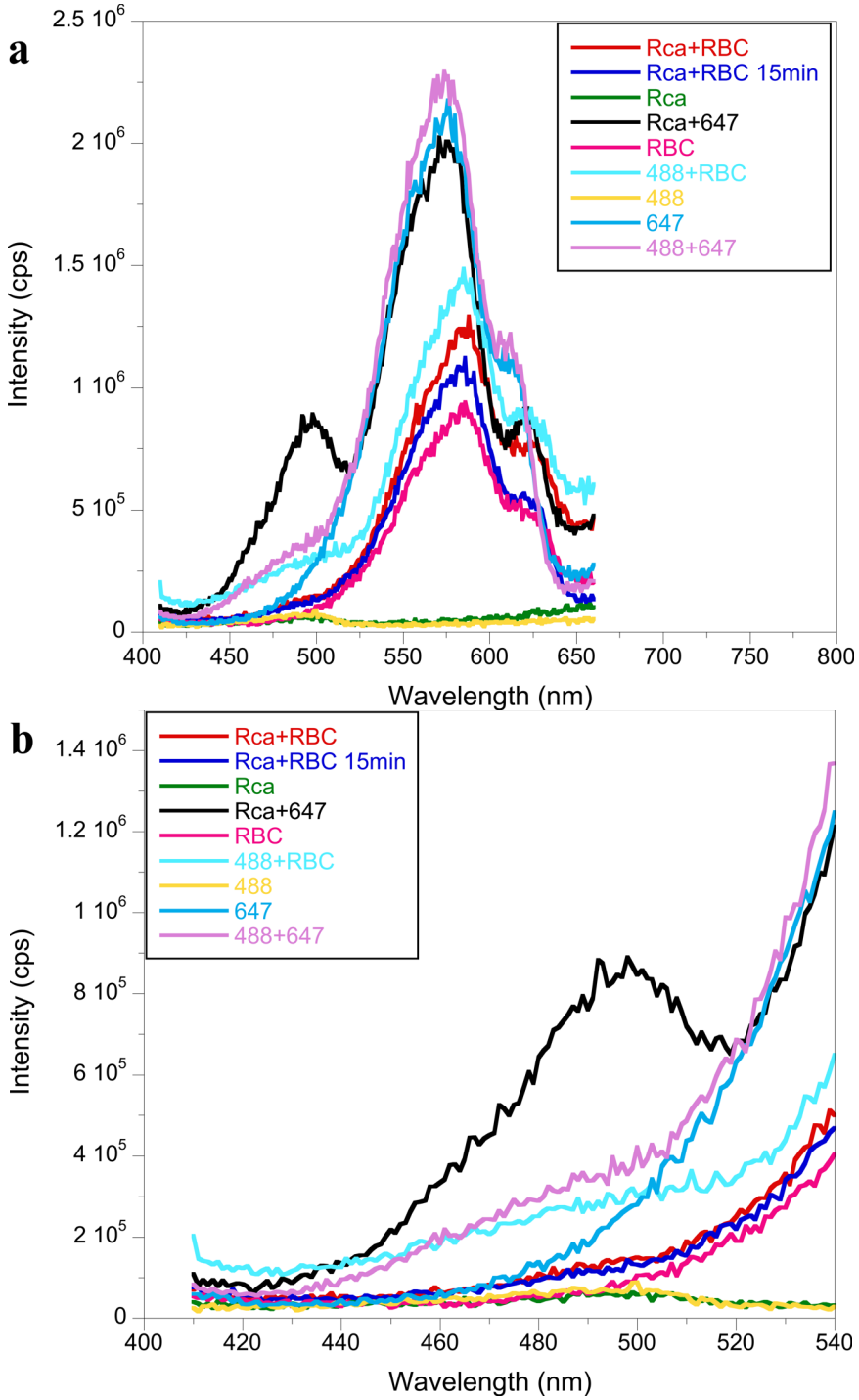

Figure 19. Excitation scans with full set of controls. (a) Full excitation scan with emission monitored at 672 nm of the Rubisco-Rca FRET Binding Assay.
(b) Excitation scan zoomed in to show FRET signal. All Rubisco samples (26.5 µM) were labeled with Alexa-647 (1 dye per L8S8), Rca samples (30 µM) were a mix of unlabeled with labeled with Alexa-488 (final 0.21 dyes per subunit). The presence of free dye is designated with 488 or 647.

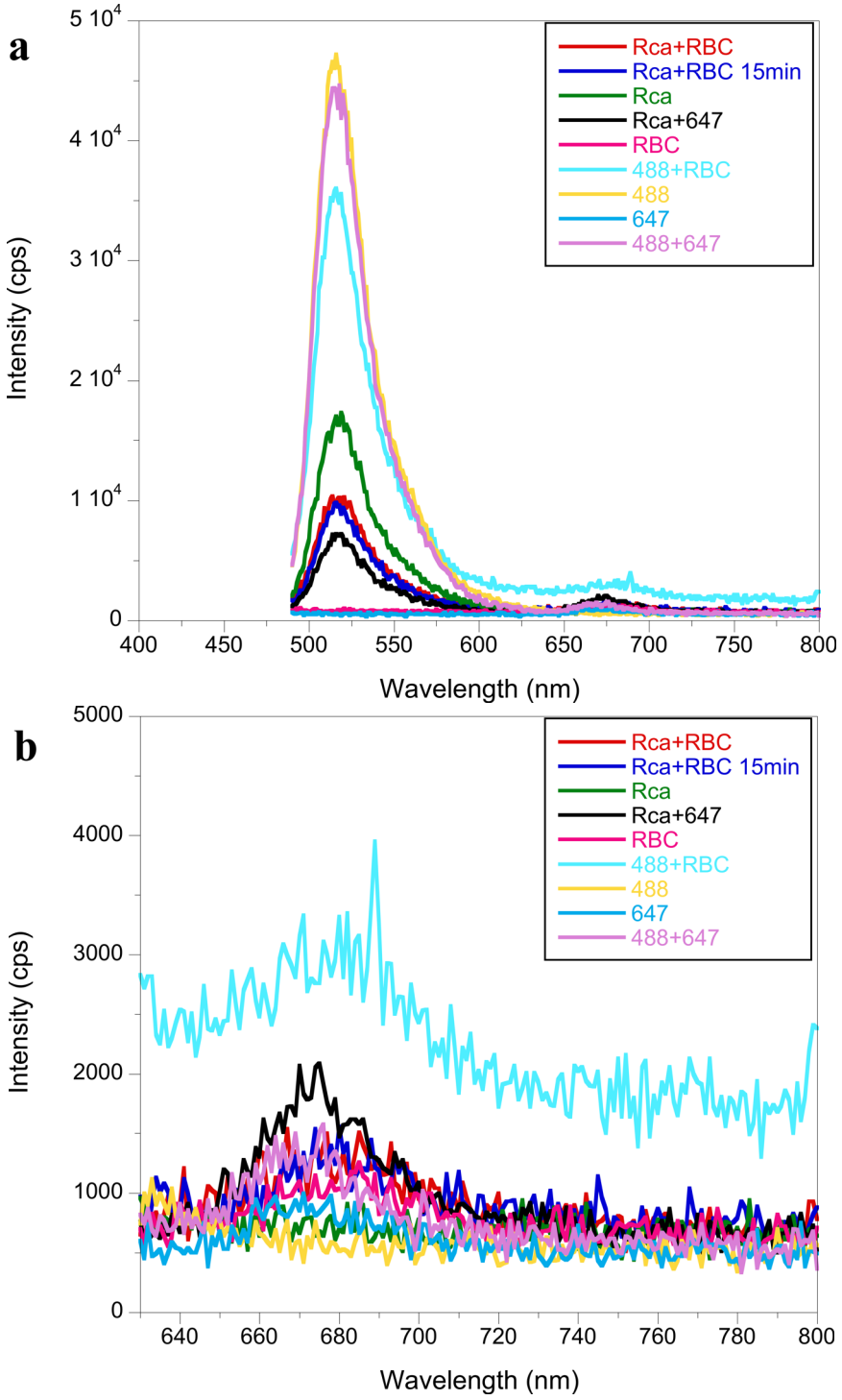

Figure 20. Emission scans with full set of controls. (a) Full emission scan with excitation at 420 nm of the Rubisco-Rca FRET binding assay. (b) Emission scan zoomed in to show FRET signal. All Rubisco samples (26.5 μM) were labeled with Alexa-647 (1 dye per L8S8), Rca samples (30 μM) were a mix of unlabeled with labeled with Alexa-488 (final 0.21 dyes per subunit). The presence of free dye is designated with 488 or 647.

skewing the excitation scans (with 1 dye per L8S8, the Alexa-647 concentration was 26.5 μM).

Crowding Agents Do Not Affect Fluorescence

Since no binding was seen in the FRET assay, crowding agents were introduced. To determine whether the crowding agent, Ficoll, was suitable to use in FRET-based binding assays, a free dye test was performed to examine any effect on the excitation and emission of the free dyes. Previously, excess Rubisco (24:1 L8S8:Rca_6) and crowding agents did not modify catalytic rates of tobacco Rca [59].

The excitation and emission spectra of free Alexa-488 and Alexa-647 were not altered by the addition of up to 20% Ficoll 70. In a separate experiment, up to 18% BSA was added with no spectral changes. We were hopeful that the introduction of these crowding agents to the Rubisco-Rca binding assay would increase the interaction enough to see a change in FRET signal, however, this was not the case for either Ficoll or BSA, with cotton or Chlamy Rubisco.

DISCUSSION

In this work, the primary goal was to develop a FRET-based assay to measure the strength of the Rubisco-Rca interaction as a function of Rca assembly and Rubisco activation state. Rubisco and Rca were labeled with fluorescent dyes to monitor their proximity by FRET. Although equilibrium constants were not determined, we did learn important information about developing the assay and what conditions did not work.

Labeling of Chlamy and cotton Rubisco were optimized, with reaction conditions at pH 7.2 and 2.5 dyes per large subunit leading to about half of all large subunits (~4 per L8S8) labeled in mutated Chlamy. In cotton, without an introduced cysteine, reaction

conditions at pH 7.5 and 4 dyes per large subunit gave 1-3 labels per L8S8. ATP hydrolysis is not affected when every chain is labeled, but Rubisco reactivation studies were not performed. If there is a bulky label on every large subunit C-terminal tail, binding may be inhibited, if the side-on interaction model is correct. However, if there is a smaller number of labels on each holoenzyme, there would be open sites adequate for binding, where a FRET signal should still be seen. In cotton Rubisco, since labeling was at non-specific sites, the label positions are not known. Since the labels are on the surface of Rubisco, these labels could be in positions that are hindering the binding of Rca.

If Rubisco continued to be purified from leaves, yields would allow for higher concentrations in the assay. Still, the dye concentration would remain an issue. Even at 1 dye per holoenzyme and the current Rubisco concentration of 30 μM, the Alexa-647 dye would show the peak shift caused by dimer formation and self-quenching. One option might be to switch dyes so Alexa-647 would be on Rca, and Alexa-488 on Rubisco. This way, every Rubisco would have a dye, and just a fraction of the Rca assemblies would, so that any reactivation event will have at least half the necessary components to show an increase in FRET.

In the chloroplast stroma, the concentrations of both Rubisco and Rca are much higher than feasible in a cuvette. Even though multiple crowding attempts with BSA and Ficoll were performed, the physiological conditions to promote binding may be significantly more crowded. In such a crowded environment, weak binding of Rca to Rubisco may be sufficient.

When Rca is in the hexameric state, it may be asymmetric, causing less stable binding. There may be nucleotide-imposed asymmetry, explaining the low affinity

binding constants. Rca undergoes large scale domain motions dependent on the nucleotide bound in the active site. In the future, effects of different nucleotides can be assayed in these interaction studies. ADP-AlF_x is a flexible transition state analog and may provide insight into binding states. Since flexibility allows for different conformations of Rca, ADP-AlF_x may provide enough variation between subunits in assemblies to achieve a Rubisco-binding competent conformation.

To be able to characterize the physical interaction between Rubisco and Rca, we attempted to develop a FRET assay, using Rca labeled with a green fluorophore, and Rubisco labeled with a red fluorophore. We were hoping to visualize Rubisco-Rca binding by FRET, determine binding constants and identify specific Rca residues that make direct contact with Rubisco by using truncation variants and mutations. Although initial data looked promising, this approach has not been fruitful, as no true FRET signal has been observed. One possibility is that under the conditions tested, Rca is not able to undergo the structural reorganizations necessary to achieve binding-competent conformations. Rca may also be asymmetric, leading to less stable binding of an already weak interaction. Binding of these two enzymes may be too fast to be seen in this assay, or there may not be enough bound in the correct conformations to give a detectable signal.

With the labeling of Rca and Chlamy Rubisco optimized, knowledge that Alexa-647 concentrations under 6 μM and crowding agents can be used without worry of optical effects, many more conditions can be examined for binding. Using the more active spinach Rca with *Chlamydomonas* Rubisco, the information gained in the development of the assay may lead to successful FRET-binding assays.

CHAPTER 3

SUBUNIT EXCHANGE IN OLIGOMERIC ASSEMBLIES OF SPINACH SHORT-FORM RUBISCO ACTIVASE

ABSTRACT

Spinacia oleracea-β (So-β) Rca was successfully labeled with green and red fluorophores and utilized in a Förster resonance energy transfer (FRET) assay to monitor subunit exchange kinetics. A striking nucleotide effect was observed that correlated with thermal stability, indicating oligomeric conformational rigidity is based on nucleotide state. While ATP-analogs slow exchange to near zero, ATP speeds up exchange, and the fastest rates are with ADP. The high thermal stability of So-β Rca under certain conditions suggests subunit-subunit interactions in assemblies that are sufficiently tight to prevent exchange. Under certain conditions, the quaternary structure is flexible and adaptable to environmental conditions. Three different types of assemblies can be deduced from the rates of subunit exchange: rigid types with extremely slow dissociation of individual protomers, tight assemblies with the physiological substrate ATP, and loose assemblies that provide fast exchange due to high ADP. In combination with assembly assays, subunit exchange assays and reactivation studies will provide critical information about the structure/function relationship of Rca in the presence of different nucleotides and thereby help characterize the Rca regulation mechanism.

INTRODUCTION

Rubisco represents the primary entry point of CO_2 into biomass, but it is easily inhibited by turnover-dependent production of tight binding substrate mimics [24]. Rubisco activase (Rca) catalyzes the rapid release of trapped inhibitors from the active

site of Rubisco to allow for continued carbon fixation. However, at increased temperatures, Rca is not able to keep up with the significantly increased rate of Rubisco inhibition, which limits photosynthesis [51]. Understanding the structure and stability of Rca under various conditions will help with increasing reactivation rates at high temperatures.

In the presence of ADP, or in the absence of nucleotide, Rca enzymes have a highly dynamic state *in vitro* and can form assemblies ranging from 1 to 16 subunits [72]. In spinach leaves, there is an equal amount of α–Rca and β–Rca isoforms [73]. The average oligomeric size of spinach Rca was obtained using diffusion constants obtained by analytical ultracentrifugation (AUC) [72]. At 0.2 mg/mL (4.8 μM), So-β-Rca was a tetramer in Mg-ADP and Mg-ATPγS conditions, and a trimer in apo. However, these are estimated average oligomeric sizes; a range of oligomers was seen in solution with larger complexes at higher concentrations. At the same 0.2 mg/mL concentration, So-α-Rca was less polydisperse and estimated as tetrameric under apo conditions, pentameric in Mg-ADP, and a closed-ring hexamer in Mg-ATPγS [72]. It has been proposed that the significantly increased thermostability of the hexameric structures provides increased resistance against denaturation at higher temperatures [72].

In vitro, a mixture of 50% α– and 50% β– isoforms was shown to act similarly to only α in that binding of ATPγS formed hexameric species, suggesting the α–isoform may act as a structural framework necessary for the β–isoform to form hexamers [72]. ATPγS has also been shown to significantly increase the thermostability of So-α-Rca, from 30 to 55°C, while ADP provided an increase to 36°C [38]. In So-β-Rca, ATPγS

increased thermostability from 30 to 41°C, and ADP to 40°C [38]. Thermostability with analogs is much higher in spinach than in other higher plants: in cotton-β Rca, thermostability with ATPγS-Mg was 44°C, the same as in ADP (45°C) or ATP (44°C) [47, 48].

Rca is heavily regulated by the ATP:ADP ratio in the chloroplast stroma and is responsible for maintaining Rubisco activity under high energy charge [52, 74]. The activity of spinach-β and cotton-β drops by 20% with a 1:3 ratio of ADP:ATP [37]. In tobacco Rca, a second magnesium binding site was found that may be a co-activation site [59, 75]. Magnesium binding involves at least 3 Rca subunits, and ATP may bind more tightly or may be hydrolyzed more rapidly when 2 magnesium ions are coordinated to the complex. The apparent K_d value for the second magnesium binding site is 6.8 ± 2.6 mM, and the catalytic efficiency increases by more than 8-fold with rising free magnesium [59]. For tobacco Rca, the proposed model at low magnesium is an open-ring hexamer, with ADP-bound, ATP-bound and free subunits. Increasing Mg^{2+} leads to binding at the co-activator site and may lead to formation of topologically closed hexameric rings [59].

AAA+ ATPase ClpX forms rigid-body units through interactions of the N-terminal AAA+ domain of one subunit with the C-terminal AAA+ domain of the next [53]. Even at saturating ATP concentrations, at least two subunits in each hexameric assembly were free of nucleotide [54]. In ClpX, three nucleotide binding states were found: low affinity, high affinity and free [58].

Under dark conditions, ATPase activity of the chloroplast F_1F_0-ATP synthase is inhibited by Mg^{2+}-ADP to prevent wasteful ATP hydrolysis [76, 77] Similarly, low

magnesium may prevent wasteful ATP hydrolysis by tobacco Rca in dark adapted chloroplasts [59], as well as promotes large aggregates in cotton-β Rca [48].

Here, the general question of the rate of quaternary rearrangement of Rca is addressed. Do Rca subunits exchange between different oligomeric species, and if so, is this process rapid and facile? If subunits exchange, the quaternary structure is more likely to be flexible and adaptable to environmental conditions. To answer this question, spinach β-Rca was chosen, because this variant has been shown to cross-react with *Chlamydomonas* Rubisco, and exhibits high reactivation activity.

METHODS

Nucleotide Purity

The average ADP contamination in commercial ATP preparations (>99%, Sigma) used in this study was determined to be 0.4803 % ± 0.2559 (n=3). The average ADP contamination in commercial ATPγS preparations (Roche) used in this study was determined to be 5.4187 % ± 0.4455 (n=15). These values were measured using the NADH-based ATPase assay described below. Commercial ADP preparations (Alfa Aesar) used in this study were more than 97% pure based on the manufacturer's specification.

Subcloning and Site-directed Mutagenesis

The gene coding for So-β-Rca, comprising residues 1-378 of α-Rca (alternative splicing product), was transferred from the pET23a(+) vector into the pHUE expression system using the SacII and NotI restriction sites. The pHUE system was a generous gift from Dr. Spencer Whitney (Australian National University) [78, 79], and allows for the

expression of a 6His-tagged ubiquitin fusion protein that is cleavable by a 6His-tagged deubiquitylating enzyme (DUB).

To provide a cysteine residue for covalent labeling, the T375C substitution was introduced into So-β-Rca (in pHUE plasmid), using the QuikChange site-directed mutagenesis kit (Agilent) and following the manufacturer's instructions. The entire coding sequence of the expression construct was verified by DNA sequencing. Full-length spinach β-Rca bearing the single site substitution was denoted So-β-Rca-T375C.

Protein Expression and Purification

The pHUE vector carrying the gene for So-β-Rca-T375C was transformed into *E. coli* strain BL21*(DE3) (Invitrogen). Bacterial cells were cultured in 3 L LB broth with 100 mg/L carbenicillin at 37°C until the OD_{600} reached 0.6, then induced by addition of 1 mM IPTG and grown at 25°C with shaking at 200 rpm for 8 hours. After centrifugation, the cells were frozen at -80°C.

Cell paste was suspended in 40 ml of 25 mM Tris-HCl pH 8.0, 150 mM NaCl, 10 mM Imidazole pH 8.0, 30% glycerol, 1 mM DTT, 0.1 mM ADP, 0.1 mM EDTA pH 8.0, 1 mM PMSF and 20 mg hen egg white lysozyme and then disrupted by 5 rounds of sonication (60 seconds on, 30 seconds off). The lysate was centrifuged at 15K rpm (17,600xg) and 4°C for 30 minutes, and the supernatant was passed through a 0.22 μm syringe filter before loading onto a nickel-nitrilotriacetic acid column (Qiagen). His-tagged protein was purified using an imidazole step gradient from 10 to 500 mM in 25 mM Tris-HCl pH 8.0, 150 mM NaCl, 1 mM DTT and 0.1 mM ADP. Fractions containing the His-tagged protein were pooled, EDTA was added to 1 mM, ADP to 0.5 mM and DTT to 1 mM. After addition of 0.4 mg of deubiquitylating enzyme (DUB)

for a final concentration of 11.4 μg/mL (0.27 μM), the sample was dialyzed overnight at 16°C against 1 L of 25 mM Tris-HCl pH 8.0, 40 mM NaCl, 1 mM EDTA pH 8.0, 0.05 mM ADP and 1 mM DTT. The next morning, the dialysis buffer was replaced with fresh buffer that contained 0.1 mM EDTA (instead of 1 mM), and dialysis continued at 16°C for 3 hours. The dialysate was reapplied to a Ni-NTA column, and So-β-Rca was collected in the early fractions. Protein fractions were concentrated and buffer-exchanged into 25 mM HEPES pH 7.2, 250 mM KCl, 5 mM $MgCl_2$, 10% glycerol, and 2 mM ATPγS. Aliquots were flash-frozen in liquid N_2 and stored at -80°C. Rca preparations were quantitated utilizing the Bradford method (n=9) with BSA as a standard.

Preparation of Deubiquitylating Enzyme (DUB)

6His-tagged DUB was expressed from the pHUsp2 vector and purified following published protocols [78]. Briefly, E. coli strain BL21*(DE3) (Invitrogen) transformed with the pHUsp2 vector carrying the gene for 6His-tagged DUB was cultured in LB-carbenicillin to OD_{600} of 0.8, then induced with IPTG for 4 hours. The cells were pelleted, stored at -80°C, and lysed by sonication. Protein purification entailed affinity chromatography using Ni-NTA chromatography. The pooled fractions were dialyzed against 1 liter of 50 mM Tris-HCl pH 8.0, 150 mM NaCl, 30% glycerol, 0.1 mM EDTA pH 8.0 and 2 mM BME. Protein was quantitated utilizing the Bradford method (n=9) with BSA as a standard, flash-frozen, and used with the His-tag attached.

General Protein-Dye Conjugation Strategy

So-β-Rca-T375C was covalently labeled at the C-terminal engineered T375C, using the thiol-directed fluorophores Alexa-488 C5-maleimide ($\lambda_{max\text{-}ex}$ = 494 nm, $\lambda_{max\text{-}em}$

= 519 nm) and Alexa-647 C2-maleimide ($\lambda_{max\text{-}ex}$ = 651 nm, $\lambda_{max\text{-}em}$ = 672 nm) (Molecular Probes, Inc.). Dye-conjugated protein was termed Rca-488, Rca-647, or Rca-488-647, depending on the reagents utilized in the labeling reaction. Unlike cotton Rca, spinach Rca could be labeled specifically at the C-terminus only in the presence of Mg-ATPγS. In the presence of ADP, labeling of several buried wild type cysteine residues were labeled as well, likely due to the high thermolability of spinach Rca in the presence of ADP. As reported previously, Mg-ATPγS raises the apparent thermal denaturation temperature $T_{m\text{-}app}$ from 25 to 60 °C, such that buried cysteine residues remain inaccessible to the labeling reagent. As a control experiment, wild-type So-β-Rca was subjected to an identical labeling procedure. Only the C-terminal Cys residue is derivatized, whereas the remaining thiol groups are not solvent-accessible, as demonstrated previously for cotton β-Rca [46]. Characterization by reverse-phase HPLC and by MALDI (see below) confirm that heterogeneity increases when the labeling reaction is carried out under conditions that render So-β-Rca metastable.

Protein-Dye Conjugation Methodology: Labeling with Alexa-488 and Alexa-647 Dyes

To generate Rca-488-647 for the label dilution assay (see below), multi-subunit assemblies of So-β-Rca-T375C were simultaneously labeled with both dyes (1:1, Alexa-488:Alexa-647). The initial reaction consisted of a 1:1 molar ratio of dye:Rca (total dye to Rca subunit concentration). To this end, 3.9 µL of 500 mM ATP, 124.7 µL of 50 mM HEPES pH 7.2, 7.66 µL of 3.22 mM Alexa-488 (dissolved in 50 mM HEPES pH 7.2) and 13.76 µL of 1.78 mM Alexa-647 were sequentially added to 200 µL of 245 µM Rca (dissolved in 50 mM HEPES pH 7.2, 250 mM KCl, 2 mM ATPγS). At this point, the

350-μL reaction contained 50 mM HEPES pH 7.2, 140 mM KCl, 5.57 mM ATP, 70 μM Alexa 488, 70 μM Alexa 647 and 140 μM Rca, and was incubated at 4°C. After 90 minutes, aliquots of dye were added to provide for an additional 1.9:1 molar ratio of total dye:Rca (14.2 μL of 3.22 mM Alexa-488 and 25.6 μL of 1.78 mM Alexa-647), resulting in a final reaction volume of 390 μL and composition of 50 mM HEPES pH 7.2, 125 mM KCl, 5 mM ATP, 180 μM Alexa-488, 180 μM Alexa-647 and 125 μM Rca. At this point, the sample was incubated overnight at 4°C. To remove excess free dye, 400 μL of saturated ammonium sulfate was added drop-wise, followed by 30 min incubation at 4°C. The pellet was collected by microcentrifugation in an eppendorf tube, suspended in 125 μL 25 mM HEPES pH 7.5, 250 mM KCl, 5 mM $MgCl_2$ and 10% glycerol, and desalted by two passes through a gel filtration spin column equilibrated in the same buffer (Sephadex G50-fine, 2 mL bed volume, 400 *g* centrifugation for 2 min). ATPγS was added to a final concentration of 2 mM, aliquots were flash-frozen in liquid nitrogen and stored at -80°C.

So-β-Rca-T375C preparations containing only one type of label were also prepared, and termed Rca-488 and Rca-647. These were used in the label mixing assay described below. The dye conjugation protocol was essentially identical to the dual-labeling protocol, except that the reaction was carried out in one step only. Alexa dye was combined with protein at a molar ratio of 3:1 (dye:Rca), incubated overnight, and desalted by means of a Sephadex column as described above.

HPLC, Spectrophotometric and Mass Spectrometric Analysis of Labeled Protein

Rca-488-647 was analyzed by reverse-phase HPLC (Agilent Technologies 1260 Infinity Quaternary LC system, Agilent Technologies 1100 Series Diode-Array detector)

on a C18 analytical column (Vydac, 218TP, 5μM, 250 x 4.6 mm) using a linear water/acetonitrile gradient with 0.1% trifluoroacetic acid. The eluent was monitored for protein and Alexa dye absorbance by OD_{220}, OD_{280}, OD_{490} and OD_{650}. Free dye was not observed in any of the Rca-488-647 samples. Protein-containing fractions were collected, and the absorbance was measured from 800 - 250 nm using 50% acetonitrile, 50% water, 0.1% TFA as a solvent blank (Shimadzu UV2401-PC Spectrophotometer).

The degree of labeling was calculated from the absorbance of each species, using the published (Molecular Probes, Inc.) extinction coefficients of each dye (Alexa-488: ε_{494} = 71,000 $M^{-1}cm^{-1}$; Alexa-647: ε_{650} = 239,000 $M^{-1}cm^{-1}$). The concentration of Rca was determined by OD_{280}, using an extinction coefficient calculated from the amino acid sequence (ε_{280} = 38,640 $M^{-1}cm^{-1}$). To correct for Alexa-488 contributions to the OD_{280}, the OD_{494} was multiplied by the correction factor 0.11, then subtracted from the OD_{280}. To correct for Alexa-647 contributions to the OD_{280}, the OD_{650} was multiplied by the correction factor 0.03, then subtracted from the OD_{280} (Molecular Probes, Inc.). In all Rca-488-647 samples used in this study, 90% of subunits were dye-conjugated, with a ratio of 1.7:1, Alexa-488:Alexa-647 (average of 0.57 Alexa-488 and 0.33 Alexa-647 dyes per subunit). Labeled protein was quantitated using the BCA method (n=6) with BSA as a standard [80]. MALDI mass spectrometry was carried out on an Applied Biosystems/MDS SCIEX 4800 MALDI TOF/TOF Analyzer, using a matrix of sinapinic acid.

Label Dilution Assay to Monitor Subunit Exchange Rates

Stock solutions were prepared containing either 50 μM label-free Rca or 50 μM Rca-488-647, each in buffer containing 1 mM ATPγS, 25 mM HEPES pH 7.5, 250 mM

KCl and 5 mM $MgCl_2$. The stocks were diluted 10-fold with buffer containing 25 mM HEPES pH 7.5, 250 mM KCl, 5 mM $MgCl_2$ and 10% glycerol. Fluorescence excitation and emission scans were collected on 5 μM Rca-488-647, using a Jobin Yvon Fluoromax-3 fluorimeter and a quartz microcuvette thermostatted at 25°C by a circulating water bath. Fluorescence was monitored in 1.0 nm increments with an integration time of 0.2 seconds. Excitation scans were collected from 410 nm to 680 nm with emission monitored at 685 nm, an excitation slit width of 2.0 nm and an emission slit width of 1.5 nm. Emission spectra were collected from 490 nm to 800 nm with excitation at 420 nm and a slit width of 2.0 nm for both excitation and emission. Subsequently, 20 μL of 5 μM Rca-488-647 were placed into the cuvette, 2 μL of 80 mM nucleotide (ATP, ADP or ATPγS) and 60 μL of 5 μM label-free Rca were added, and the solution was mixed by gentle pipetting (time zero). Final protein in the cuvette consisted of 1.25 μM Rca-488-647 and 3.75 μM label-free Rca (0.71 μM Alexa-488 and 0.41 μM Alexa-647 conjugated to protein) in a solution containing 2 mM nucleotide (ATP, ADP or ATPγS), 100 μM residual ATPγS, 25 mM HEPES pH 7.5, 250 mM KCl, 10% glycerol and either 5 mM $MgCl_2$, 2.1 mM $MgCl_2$ or 5 mM $MnCl_2$ (with ~100 nM residual $MgCl_2$). Upon mixing, excitation scans were collected every 5 minutes for 50 minutes, then every 10 minutes for another 100 minutes, then again after 24 hours. Emission scans were collected at 0, 45, 90, 135 and 150 minutes.

To prepare samples containing Mn^{2+} as the divalent cation, the protein stock solution (487 μM Rca in 2 mM ATPγS, 25 mM HEPES pH 7.5, 250 mM KCl, 5 mM $MgCl_2$) was diluted to 50 μM with 25 mM HEPES pH 7.5, 250 mM KCl and 5 mM $MnCl_2$, then concentrated and diluted three times at 4°C using a membrane concentrator

(10 kDa cutoff filter). Residual $MgCl_2$ was approximately 1 μM (corresponding to 100 nM in the cuvette). Subsequently, ATPγS was added to 1 mM.

To prepare samples with ADP and aluminum fluoride bound to the Rca active site (ADP-AlF_x), 2 μL of 80 mM ADP, 16 μL of 250 mM NaF, 8 μL of 50 μM Rca, and 54 μL buffer (25 mM HEPES pH 7.5, 250 mM KCl, 5 mM $MgCl_2$ and 10% glycerol) were mixed and incubated for 5 min at 30°C [81]. Subsequently, 0.8 μL of 0.2 M $AlCl_3$ was added, the sample was mixed and incubated for 10 min at 25°C. The final composition was 5 μM Rca in 2 mM ADP, 50 mM NaF, 2 mM $AlCl_3$, 25 mM HEPES pH 7.5, 250 mM KCl, 5 mM $MgCl_2$ and 10% glycerol.

Label Mixing Assay to Monitor Subunit Exchange Rates

To initiate the mixing of Rca subunits labeled with different dyes, Rca-488 was combined with Rca-647 in order to observe the rise of FRET as subunits exchange between different assemblies. To prepare a stock solution of 5 μM Rca containing an appropriate Alexa-488 concentration, a 5 μM stock was prepared containing 2.84 μM Rca-488 and 2.16 μM label-free Rca in 25 mM HEPES pH 7.5, 250 mM KCl, 5 mM $MgCl_2$, 10% glycerol and 100 μM ATPγS. Likewise, to prepare a stock solution of 5 μM Rca containing an appropriate Alexa-647 concentration, a stock was prepared containing 1.68 μM Rca-647 and 3.32 μM of label-free Rca in 25 mM HEPES pH 7.5, 250 mM KCl, 5 mM $MgCl_2$, 10% glycerol and 100 μM ATPγS. Immediately afterwards, 20 μL of each of the two stock solutions were transferred into the cuvette, 2 μL of 80 mM nucleotide were added, and 40 μL of 5 μM label-free Rca were added at time zero. The solution was mixed by gentle pipetting, and spectra were collected as a function of time as described above. The final composition of the sample in the cuvette was 0.71 μM Rca-488,

0.42 μM Rca-647, 3.75 μM label-free Rca, 2 mM nucleotide, 100 μM residual ATPγS, 25 mM HEPES pH 7.5, 250 mM KCl, 5 mM $MgCl_2$ and 10% glycerol. This provides the same final concentration of each Alexa label as in the label dilution assay.

FRET Correction Factors

Förster resonance energy transfer (FRET) was monitored by tracking the 685 nm emission upon excitation at 495 nm, using excitation spectra. Raw fluorescence intensities recorded in the label dilution assay were corrected for Alexa-488 emission leakage into the red channel, termed F_{Lk}, and for the direct excitation of Alexa-647 by green light, termed F_{Dir} (both determined with λ_{ex}=495 nm, λ_{em} = 685 nm) [82].

$$F_{raw} = F_{Lk} + F_{Dir} + F_{FRET} \qquad \text{Equation 3}$$

The correction factor for leakage CF_{Lk} was determined by subjecting a sample of Rca-488 to excitation and emission scans using instrumental parameters identical to those used in the label dilution assay. Rca preparations were combined to provide a solution of 0.71 μM Rca-488, 4.29 μM label-free Rca, 2 mM ATPγS, 25 mM HEPES pH 7.5, 250 mM KCl and 5 mM $MgCl_2$, and fluorescence spectra were collected every 5 min for 30 min. For each spectrum, CF_{Lk} was calculated by dividing the 685-nm emission (λ_{ex} = 495 nm) by the 515-nm emission (λ_{ex} = 420 nm). The average value of CF_{Lk} was calculated to be 1.4669 +/- 0.03801 (2.59%, n=7). For each time point of the label dilution assay, the data were corrected for F_{Lk} by multiplying the raw emission at 515 nm (λ_{ex}=420 nm) by CF_{Lk}, then subtracting the resulting value from the 685 nm emission (λ_{ex}=495 nm).

The correction factor for F_{Dir} was determined by collecting a series of excitation and emission scans over a 30 min time period on a sample containing Rca-647, with

instrumental parameters identical to those used in the label dilution assay. The sample contained 0.42 μM Rca-647, 4.58 μM label-free Rca, 2 mM ATPγS, 25 mM HEPES pH 7.5, 250 mM KCl and 5 mM $MgCl_2$. The correction factor CF_{Dir} was calculated by dividing the 685 nm emission observed with λ_{ex} = 495 nm by the 685-nm emission observed with λ_{ex} = 650 nm. The average value for CF_{Dir} was calculated to be 0.03167 +/- 0.000921 (2.91% error, n = 7). Data collected during the label dilution assay (see above) were corrected for F_{Dir} by multiplying the raw 685 nm emission (λ_{ex}=650 nm) by CF_{Dir}, then subtracting the resulting value from the 685 nm emission observed with λ_{ex}=495 nm.

Correction for Fluctuations in Red Dye Fluorescence

In all label dilution assays, the fluorescence of the red dye exhibited some variation around an average value. In assemblies lacking subunit exchange, the 685 nm emission upon 495 nm excitation followed closely the 685 nm emission upon 650 nm excitation. This observation suggests that both signals are equally affected by red dye fluctuations. Control experiments using free dye indicate that the fluorescence fluctuations of the red dye are a consequence of attachment to protein. The free dyes exhibit a reproducible and steady decrease in intensity of 13% over 60 min. To the contrary, attachment to Rca does not, on average, lead to a loss of fluorescence, but instead provides for larger deviations from the average value. Therefore, an additional, operational correction was carried out to control for these deviations. In this approach, the F_{Lk} and F_{Dir} corrected data were divided by the red dye intensity (λ_{ex} = 650 nm and λ_{em} = 685 nm) observed in the excitation scans.

Dye Stability Assays

The photostability of each dye attached to protein was examined in separate assays following the label dilution assay procedure. Stock solutions containing 50 μM Rca-488 or Rca-647 in the presence of 1 mM ATPγS were diluted to 5 μM protein with dilution buffer (25 mM HEPES pH 7.5, 250 mM KCl, 5 mM $MgCl_2$, 10% glycerol). To obtain 0.71 μM Rca-488 and 4.29 μM label-free Rca, 11.36 μL of 5 μM Rca-488, 2 μL of 80 mM ATPγS and 68.64 μL of 5 μM label-free Rca were added to the cuvette and gently mixed by pipetting. Similarly, to obtain 0.42 μM Rca-647 and 4.58 μM label-free Rca, 6.72 μL of 5 μM Rca-647, 2 μL of 80 mM ATPγS and 73.28 μL of 5 μM label-free Rca were added to the cuvette. Excitation scans were collected every 5 minutes for 50 minutes, then every 10 minutes for another 130 minutes. Each assay was performed in triplicate using independently prepared samples.

Free Dye Controls

A series of free dye controls were performed using 2.5 μM Alexa-488 and 2.5 μM Alexa-647 in 5 mM ATPγS, 25 mM HEPES pH 7.5, 250 mM KCl, 5 mM $MgCl_2$, and 10% glycerol. In the excitation scans, emission was monitored at 672 nm, and in the emission scans, the samples were excited at 420 nm. The variety of conditions examined included Alexa-488 alone, Alexa-647 alone, Alexa-488 plus Alexa-647 in the presence of label-free Rca, Alexa-488 plus Alexa-647 in the presence of bovine serum albumin (BSA), Alexa-488 in the presence of Rca-647, and Alexa-647 in the presence of Rca-488. In samples containing Rca or BSA, the total protein concentration was 210 μg/ml.

Interference by Cationic Species

To examine any effects of multi-valent cations on spectral properties, free dye behavior was examined in the presence of either 5 mM $MgCl_2$, 5 mM $MnCl_2$, 2 mM $AlCl_3$, or 10 mM $AlCl_3$ (all in 25 mM HEPES pH 7.5, 250 mM KCl, and 10% glycerol). All samples contained 0.71 μM Alexa-488 and 0.42 μM Alexa-647. Excitation scans with emission monitored at 685 nm were taken every 5 minutes for 30 minutes, and emission scans with excitation at 420 nm were taken initially and after 30 minutes.

Continuous ATPase Assays Based on Phosphate Production

This assay was carried out to compare the activity of label-free So-β-Rca-T375C with the activity of the same variant conjugated to Alexa-488 (Rca-488) or Alexa-647 (Rca-647). The rate of inorganic phosphate release upon ATP hydrolysis was monitored by an enzyme-coupled spectrophotometric assay [59, 70]. To assay phosphate production in a continuous fashion, the absorbance difference between the reactant and product species was monitored by absorbance at 360 nm as a function of time. To monitor residual phosphate in assay components, baseline scans were collected in the absence of Rca with and without ATP. To monitor ATP turnover by Rca, 704 μL working solution was added to the sample and reference cuvettes and the absorbance set to zero. 200 μL MESG stock, 30 μL PNP stock, 8 μL 0.5 M $MgCl_2$ stock and 50 μL Rca (in 25 mM HEPES pH 7.5, 250 mM KCl, 5 mM $MgCl_2$, 10% glycerol) were added to the sample cuvette, and the time scan was started. After 60 seconds, 8 μL ATP stock (500 mM) was added, the solution was mixed using a manual cuvette mixer, and the A_{360} was monitored for 300 seconds. The final composition of the sample in the cuvette was 55 mM HEPES pH 8.0, 50 mM Tris-HCl pH 7.5, 0.8 mM DTT, 200 μM MESG, 0.1 mM

Sodium Azide, 3 units PNP, 9 mM $MgCl_2$, 4 mM ATP, 5.3-8.5 μM Rca, 0.5% glycerol, 12.5 mM KCl, 1.25 mM HEPES pH 7.5 and 0.1 mM ATPγS. The baseline scan was subtracted from the response curve, and the slope was determined between 70 and 90 seconds, consistently the steepest part of the curve. Using a phosphate standard curve, the Rca turnover velocity was calculated (μM phosphate produced per second) and normalized with respect to Rca subunit concentration. Each reaction was carried out in triplicate, using independently prepared protein pools. Since the absorbance of Alexa-647 interferes with the Bradford assay, BCA assays were carried out to determine protein concentrations (n=9).

End-Point ATPase Assays Based on ADP Production

To determine the amount of ADP generated over the time course of subunit exchange, an enzyme-coupled spectrophotometric assay based on NADH oxidation was employed as an end-point assay [59, 83]. An appropriate protein stock was prepared (50 μM Rca in 25 mM HEPES pH 7.5, 250 mM KCl, 5 mM $MgCl_2$, 10% glycerol, 1 mM ATPγS), and a label dilution assay reaction was set up in an Eppendorf tube, with components identical to the reactions used when monitoring time-dependent FRET in the presence of either ATP-Mg or ATP-Mn. The reaction mixture contained 1.25 μM Rca-488-647, 3.75 μM label-free Rca, 0.1 mM residual ATPγS, 2 mM ATP and 5 mM Mg^{2+} or Mn^{2+}. At specific time points, 5 μL aliquots were withdrawn and added to a cuvette containing 15 μL buffer (25 mM HEPES, 250 mM KCl, 5 mM $MgCl_2$, 10% glycerol) and 475 μL NADH assay mix. NADH assay mix consisted of 100 mM Tricine pH 8.0, 20 mM KCl, 5 mM DTT, 5 mM $MgCl_2$, 2 mM phosphoenolpyruvate, 0.3 mM NADH, 1.3 – 2.2 U pyruvate kinase and 2 – 3.1 U lactate dehydrogenase (Sigma-Aldrich). The OD_{340}

was monitored for about 150 seconds, and the extinction coefficient of NADH (6,220 M^{-1} cm^{-1}) was used to calculate the amount of ADP present based on the net loss of absorbance. The NADH assay mix used for Mn^{2+}-containing Rca samples contained Mn^{2+} instead of Mg^{2+}. Control reactions with known amounts of ADP demonstrate that there is no difference in the response of the assay mix, whether it contains Mg^{2+} or Mn^{2+}. Pyruvate kinase activity is known to be accelerated in the presence of Mn^{2+}.

Continuous ATPase Assays Based on ADP Production

To compare ATP turnover of different Rca preparations, the enzyme-coupled assay monitoring NADH oxidation was employed in continuous mode [59, 83]. The reaction mixture contained 100 mM Tricine pH 8.0, 20 mM KCl, 5 mM DTT, 5 mM $MgCl_2$, 2 mM phosphoenolpyruvate, 0.3 mM NADH, 1.3 – 2.2 units (U) pyruvate kinase and 2 – 3.1 U lactate dehydrogenase (Sigma-Aldrich). 35 µL Rca stock (50 µM protein in 25 mM HEPES pH 7.5, 250 mM KCl, 5 mM $MgCl_2$, 10% glycerol, 1 mM ATPγS) were added to a cuvette containing assay mix to yield a final volume of 350 µL. The reference cell contained assay mix without NADH or PK/LDH. The OD_{340} was monitored for 50 seconds, or until a stable signal was obtained, 2 mM ATP or ATPγS were added and mixed manually, and the reaction was monitored for 300 seconds. Control experiments without Rca were used to determine the amount of ADP contamination in ATP and ATPγS preparations, and the response was subtracted from the data. The extinction coefficient of NADH (6,220 M^{-1} cm^{-1}) was used to calculate the rate of NADH loss from the steepest part of the curve over a 36 second range. For assays in the presence of Mn^{2+}, the magnesium salt in the assay mix and in the Rca stock solutions was replaced with 5 mM $MnCl_2$. To this end, Rca stock solutions were diluted to 50 µM with buffer

containing Mn^{2+}, then buffer-exchanged three times using a spin concentrator, until residual Mg^{2+} was less than 200 nM in the cuvette. The final reaction components in the cuvette were 100 mM Tricine pH 8.0, 45 mM KCl (20 mM from mix, 25 mM from Rca stock), 5 mM DTT, 5 mM $MgCl_2$ or $MnCl_2$, 2 mM phosphoenolpyruvate, 0.3 mM NADH, 1.3 – 2.2 U pyruvate kinase, 2 – 3.1 U lactate dehydrogenase, 5 μM Rca, 2.5 mM HEPES pH 7.5, 1% glycerol, 2 mM ATP and 0.1 mM ATPγS.

RESULTS

Development of a FRET-Based Subunit Exchange Assay

There is evidence that the activity of Rca is regulated by quaternary reorganization, where the hexamer is the most active and higher order oligomers are not very active [59]. Although information on the oligomeric size of spinach-β Rca is not known, subunits must be exchanging and rearranging to change position. Subunit exchange is important in both a scientific and practical sense. While rates of subunit exchange can provide insight into subunit-subunit interactions and the tightness of the assemblies, it is also critical for certain assays to understand the time frame for which subunits are fully equilibrated. Alexa-488 and Alexa-647 were chosen as FRET partners due to a large spectral separation, which avoids direct excitation of the acceptor, and their efficiency of energy transfer (figure 12).

Various preparations of spinach-β Rca-488 (Rca covalently labeled with Alexa-488), Rca-647 (Rca covalently labeled with Alexa-647) and Rca-488-647 (Rca covalently labeled with both Alexa-488 and Alexa-647) were generated and were tested to determine whether mixing of Rca-488 with Rca-647 lead to the formation of a FRET signal by collecting appropriate excitation and emission spectra, as FRET is expected to occur only

if green- and red-labeled subunits are located in the same multi-subunit complex (figure 21). Initially, samples containing between 1.25 μM and 20 μM total Rca were examined, and each concentration was tested using different ratios of labeled to unlabeled protein to optimize the signal. The density of the label was adjusted to exclude direct dye-dye interactions such as π-stacked dimers (as determined by control samples consisting of free dye without protein), and subunit mixing was monitored over a 24-hour time period at 5 μM Rca. Appropriate correction factors for leakage (*Lk*) of the green dye emission into the red channel (figures 22, 23), and direct excitation (*Dir*) of the red dye (figure 24) were determined using various control experiments, and these correction factors were applied to the individual excitation scans collected during the subunit mixing experiment (see Methods).

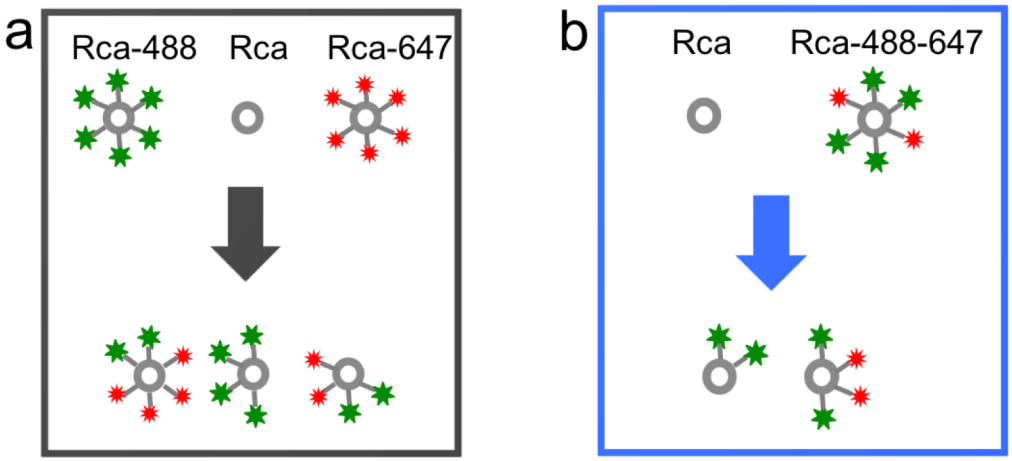

Figure 21. Schematic of subunit exchange in Rca. Rca (assumed to be a closed-ring hexamer, gray circle) labeled with Alexa-488 (green) and Alexa-647 (red) is mixed with label-free Rca. With time, subunits exchange between oligomers. (a) The label mixing assay starts with Rca labeled with Alexa-488 (Rca-488), Rca labeled with Alexa-647 (Rca-647), and label-free Rca. As subunits exchange, green and red labels move onto the same assemblies and produce a FRET signal. (b) The label dilution assay begins with label-free Rca and Rca labeled with both Alexa-488 and Alexa-647 (Rca-488-647). The FRET signal decreases as subunits exchange and green and red labels move onto other assemblies.

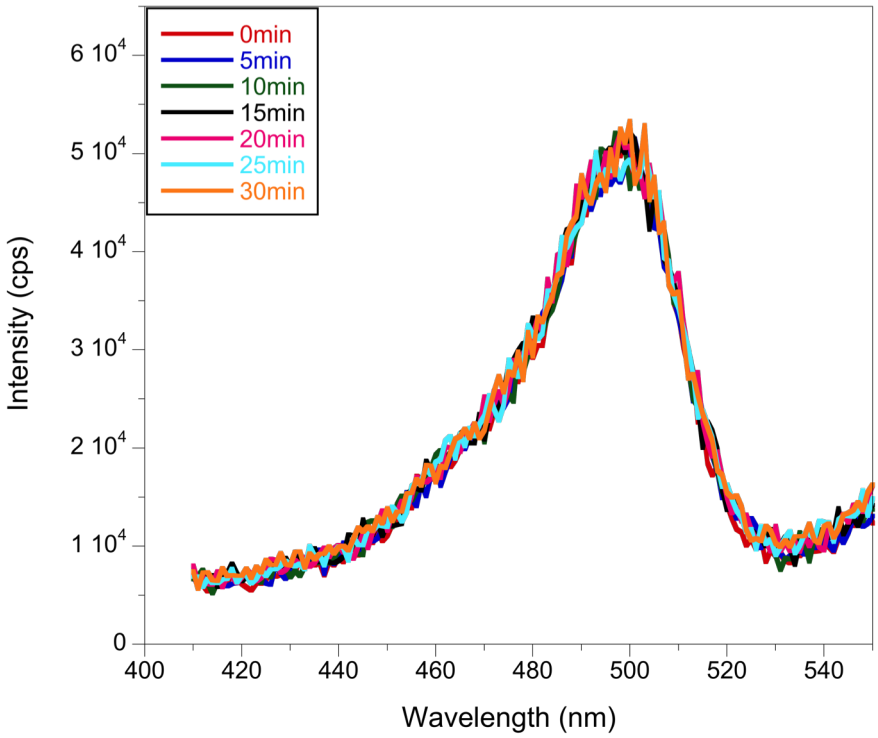

Figure 22. Excitation scan for the determination of the leakage correction factor. Excitation scan of 0.71 µM Rca-488 mixed with 4.29 µM unlabeled Rca used to determine the leakage correction factor for the label dilution assay. The ratio of this 495 nm peak to the 515 nm peak of the same sample in figure 23 is the *Lk* correction factor. This was then applied to the 515 nm fluorescence intensity in the label dilution subunit exchange assay to correct for *Lk* of the green dye at 495 nm.

The Label Mixing Assay Indicates Exchange of Dimers

In this modification of the assay, there is no initial FRET and the increase in emission upon 495 nm excitation is monitored. FRET occurs as subunits exchange between oligomers and Rca-488 and Rca-647 come into close proximity (figure 21) and is seen in the presence of ATP (figure 25). The sample containing ATPγS showed no significant increase in FRET intensity. Label mixing data was not corrected due to the initial fluorescence intensities being too close to noise level to accurately correct for *Lk* and *Dir*. It was found that the FRET signal was indeed increasing with time, indicating the exchange of subunits between multisubunit assemblies. The correspondence between

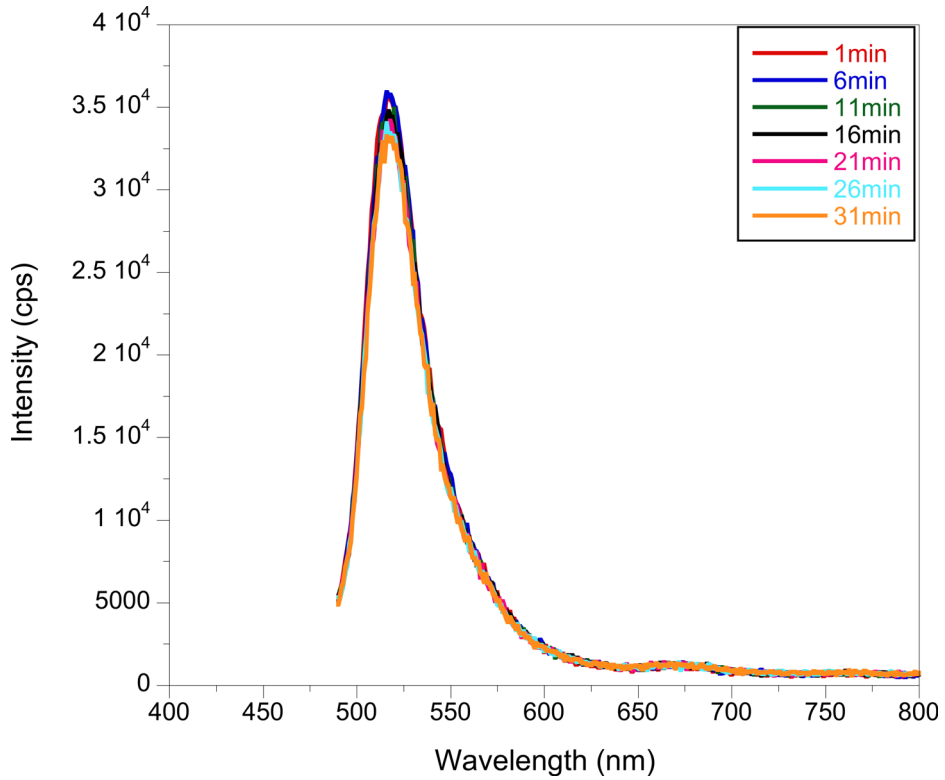

Figure 23. Emission scan for the determination of the leakage correction factor. Emission scan of 0.71 µM Rca-488 mixed with 4.29 µM unlabeled Rca was used to determine the leakage correction factor for the label dilution assay. The ratio of the 495 nm peak in figure 22 to this 515 nm peak is the *Lk* correction factor. This was then applied to the 515 nm fluorescence intensity in the label dilution subunit exchange assay to correct for *Lk* of the green dye at 495 nm.

excitation and emission spectra, and the clear isosbestic point in the emission spectra clearly supported an increase in FRET with time. However, the FRET signal remained weak even after prolonged incubation. We hypothesized that the weak signal may be the result of the exchange of dimeric Rca species. If so, mixing of an aliquot of Rca-488 with an aliquot of Rca-647 would lead to the mixing of dimers carrying two copies of the same dye, such that energy transfer would remain rather limited, even if all dimers (red or green) are randomly distributed. To address this issue, unlabeled protein was introduced, but the FRET signal remained relatively weak, in support of the dimer hypothesis.

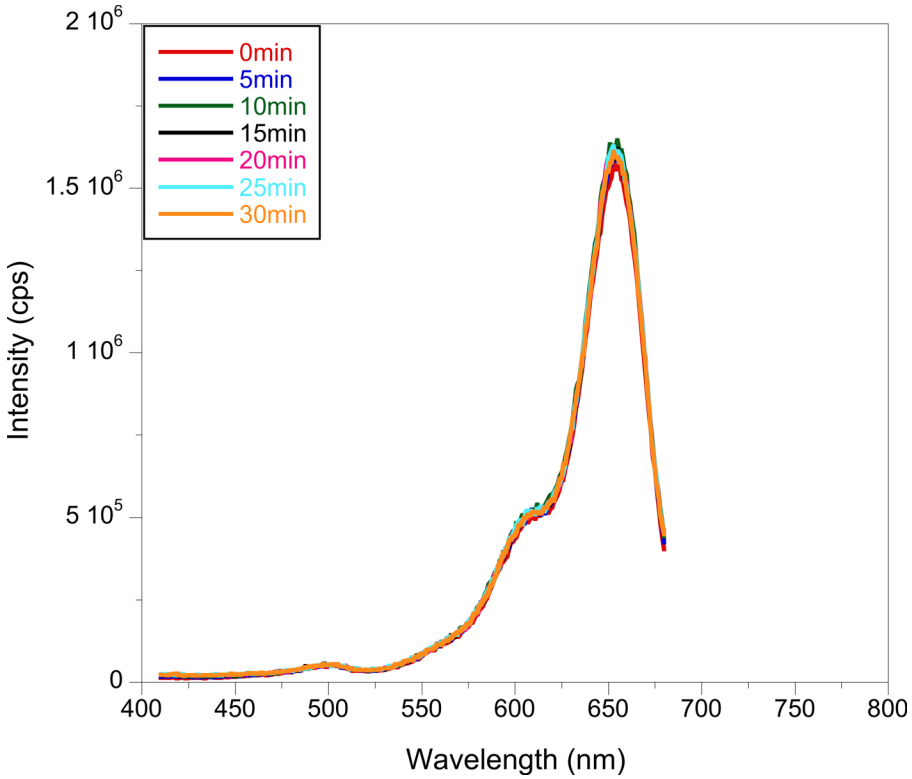

Figure 24. Excitation scan for the determination of the *Dir* correction factor. Excitation scan of 0.42 µM Rca-647 mixed with 4.58 µM unlabeled Rca was used to determine the *Dir* (direct excitation) correction factor for the Label Dilution Assay. The ratio of the 495 nm peak to the 650 nm peak is the *Dir* correction factor. This was then applied to the 650 nm fluorescence intensity in the label dilution subunit exchange assay to correct for *Dir* of the red dye.

The Label Dilution Assay Shows a Decrease in FRET

To improve the magnitude of the FRET signal, i.e. the signal-to-noise ratio, the reverse experiment was carried out. In this experiment, the starting material consisted of Rca preparations that were simultaneously labeled with green and red dyes (Rca-488-647). In this way, both labels are likely to be randomly distributed, such that adjacent Rca subunits may carry different labels (figure 21). It was found that indeed, the change of FRET upon dilution with unlabeled protein was very significant, and that a large fraction, but not all, of the FRET intensity was lost upon four-fold dilution (figure 26). The

correspondence between excitation and emission spectra, and the clear isosbestic point in the emission spectra supported a decrease in FRET with time. The best conditions for this experiment consisted of 5 μM Rca final, obtained by mixing 1.25 μM Rca-488-647 with 3.75 μM unlabeled Rca. Data were routinely collected over a 3 hour time interval, with no significant changes in fluorescence after 60 minutes.

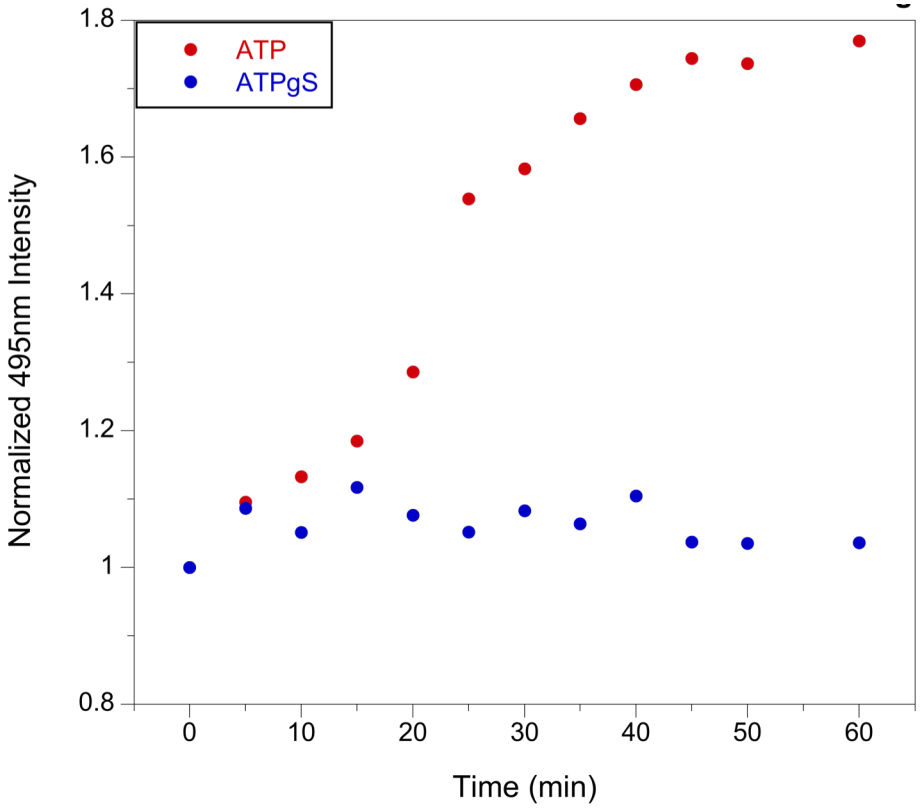

Figure 25. Time-dependent red dye emission observed during the label mixing assay. At time zero, Rca-488 and Rca-647 were mixed in the presence of either ATP or ATPγS. Upon 495 nm excitation, the 685 nm emission is plotted as a function of time. The data were not corrected for *Lk* and *Dir*, because in the label mixing assay, the raw signal was of similar magnitude as the calculated correction factor. The increase in intensity observed for the ATP-containing sample is consistent with an increase in FRET signal due to subunit exchange between oligomeric assemblies. To the contrary, intensity observed for the ATPγS-containing sample remains relatively constant, suggesting that either the subunit exchange rate is extremely slow, or that the assembly state is dominated by dimeric species carrying the same label.

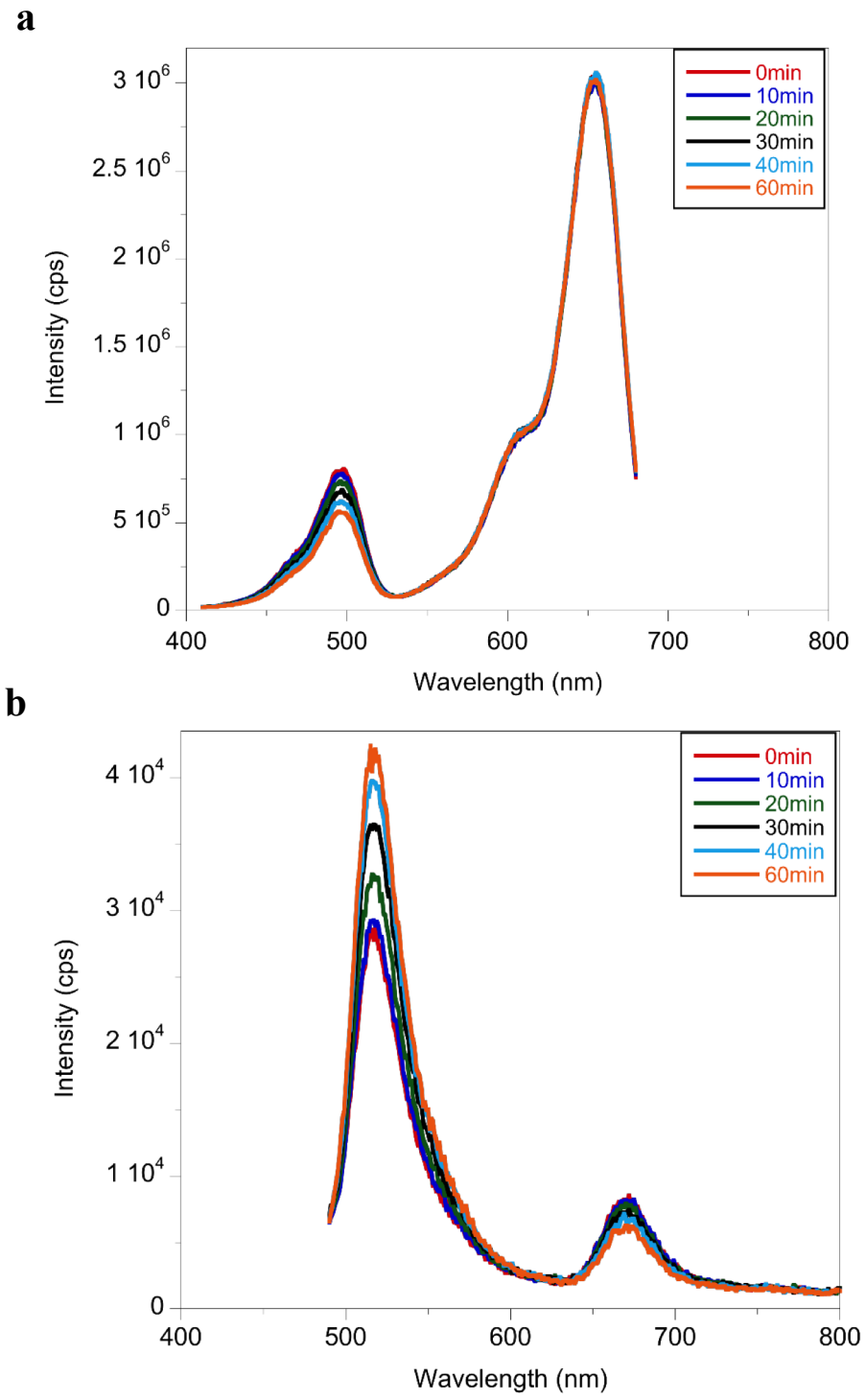

Figure 26. Raw excitation and emission scans in the label dilution assay. (a) Excitation scan with emission monitored at 685 nm of 1.25 µM Rca-488-647 and 3.75 µM unlabeled Rca in Mg-ATP. (b) Emission scan with excitation at 420 nm of 1.25 µM Rca-488-647 and 3.75 µM unlabeled Rca in Mg-ATP shows a clear isosbestic point around 630 nm.

Both Assays Confirm a Change in FRET Due to Subunit Exchange

Excitation and emission spectra in the label mixing assay confirmed the decrease in FRET signal seen in the label dilution assay is due to loss of FRET, rather than loss of photostability of the dyes. In figures 27 and 28, neither the label mixing nor the label dilution data is corrected. Both assays seem to follow the same sigmoidal trend in the presence of ATP-Mg^{2+}: slow for the first 10 minutes, then speed up until 40 minutes, and then begin to level off. In both assays, subunits take about 50 minutes to reach equilibrium (figure 27). Once the system reached equilibrium, the level of FRET seen in the label mixing assay was five-fold lower than in the label dilution assay (figure 28). The stark discrepancy between the FRET levels in the two assays further suggests

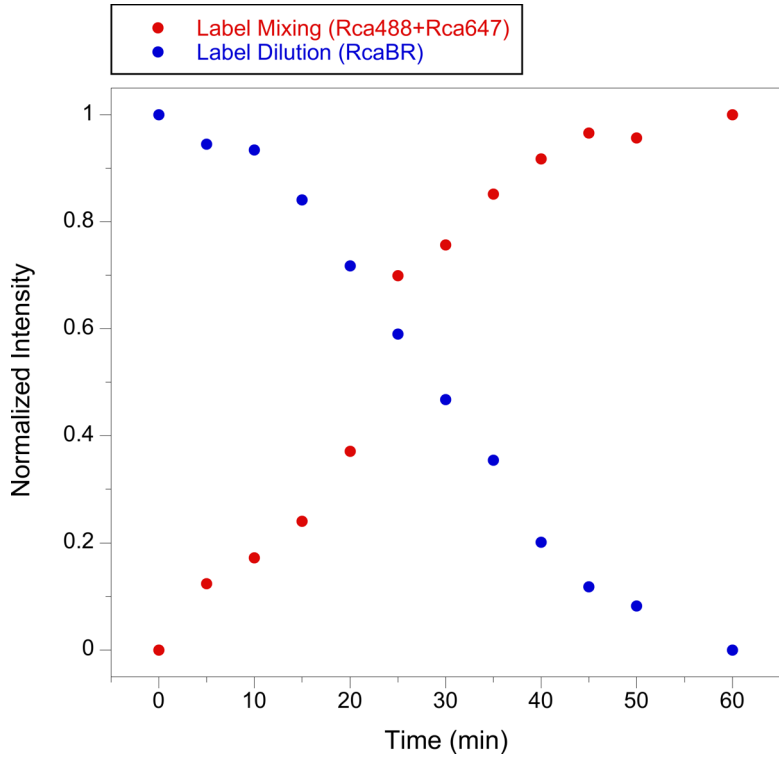

Figure 27. Comparison of label mixing and label dilution assays in the presence of Mg·ATP. The observed 685-nm emission intensity (λ_{ex} = 495 nm) was normalized with respect to its minimum and maximum value obtained over a 60 min time interval (data not corrected for *Lk* and *Dir*).

subunits are exchanging as dimers. If single protomers were exchanging freely between oligomeric assemblies, the FRET signal once the system reached equilibrium would be approximately equal to that in the label dilution assay, since both assays consisted of the same concentrations of dye and (labeled/unlabeled) Rca. Although both variations of the assay were successful in giving changes in FRET, the label mixing assay gave a smaller overall intensity change, and was much closer to noise. In addition to the increase in emission when exciting the green dye, there was also an increase when exciting the red dye. This may have been due to random dye fluctuations (figures 31, 36), but the increase when exciting at 495 nm could not be accurately interpreted to see if the signal increase

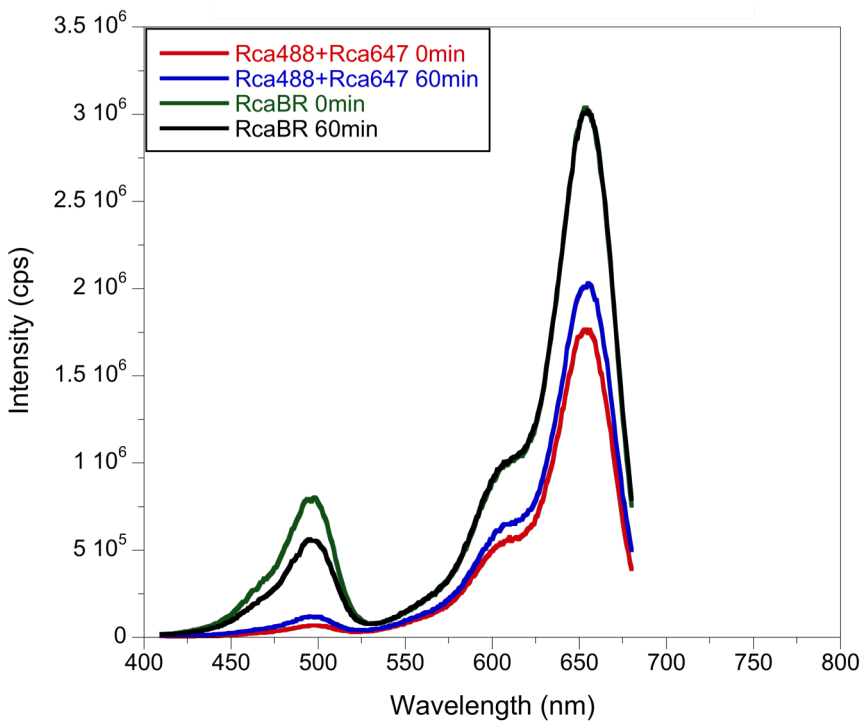

Figure 28. Excitation spectra of label mixing and label dilution assays in the presence of Mg·ATP. Shown are typical spectra collected at time t = 0 and t = 60 min (λ_{em} = 685 nm). The label composition is identical in the two assays (see Methods). In the label mixing assay, a 77% increase in fluorescence intensity is observed at λ_{ex} = 495 nm (change in arbitrary fluorescence units is 53,050 cps over 60 min). In the label dilution assay, a 28.5% decrease in fluorescence intensity is observed at λ_{ex} = 495 nm (change in arbitrary fluorescence units is 224,750 cps).

was truly due to FRET. Due to this, the label dilution assay was used to further examine subunit exchange under various nucleotide and divalent conditions.

Subunit Exchange Occurs in the Presence of ATP and ADP

For the following conditions, it was found that the FRET intensity decreases as a function of time upon mixing dual-labeled Rca with unlabeled Rca: 2 mM ATP with 5 mM Mg^{2+}; 2 mM ATP with 2.1 mM Mg^{2+}; 2 mM ATP with 5 mM Mn^{2+}; 2 mM ADP with 5 mM Mg^{2+}; 2 mM ADP with 5 mM Mn^{2+}; 1.5 mM ATP, 0.5 mM ADP with 5 mM Mg^{2+} (figure 29). Most of the response is observed within the first 50 minutes, suggesting that subunit exchange is fully equilibrated within this timeframe. Spiking with additional ATP has only a minor effect, and does not modify the extent of FRET loss, suggesting that the system has in fact fully equilibrated.

In the presence of ATP, red emission upon green excitation (λ_{ex} = 495 nm; λ_{em} = 685 nm) decreases, whereas red emission upon red excitation slightly increases (λ_{ex} = 650 nm; λ_{em} = 685 nm) (figure 30). These observations are consistent with a decrease in FRET. Once the intensity upon excitation at 495 nm due to FRET (F_{FRET}) was calculated by subtracting *Lk* and *Dir* (equation 3), each data point was normalized by total red dye intensity (I_{650nm}), with respect to time. Both dyes showed a similar rate of signal loss over the time course (figure 30). Normalizing with respect to total red dye at each time point should account for any dye fluctuations occurring during the assay. Dye fluctuations were seen in all conditions of the label dilution subunit exchange assay (figure 31). A trend based on nucleotide was not seen. While some conditions gave dramatically increased signal and wide standard deviations, when all 27 independent trials were averaged, the

intensity was very close to 1 during the entire 60 minute time course and the standard deviation narrowed (figure 31b).

The Rate of Subunit Exchange Depends on the Amount of ADP Present

With the physiological substrate ATP-Mg, there is a biphasic curve, starting with a lag phase of about 5 minutes where almost no exchange is occurring, then subunit

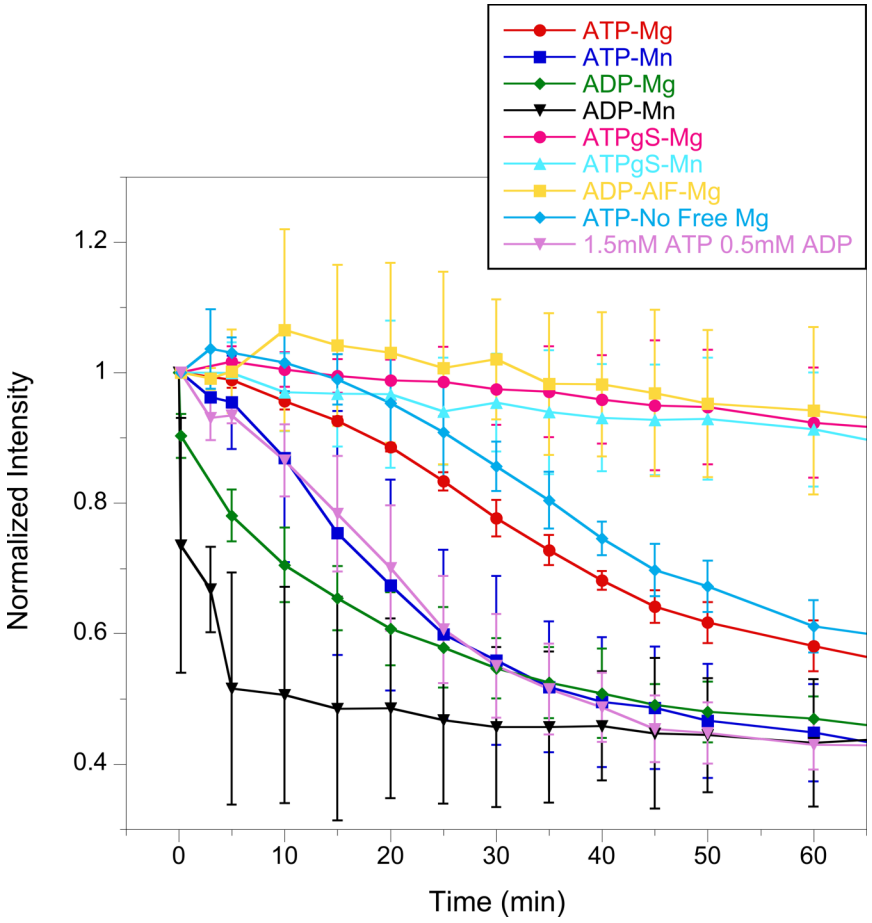

Figure 29. **Time-dependent changes in FRET intensity observed in the label dilution assay.** For each experiment, 1.25 µM Rca-488-647 was combined with 3.75 µM label-free Rca at time zero. The 685-nm emission intensity (λ_{ex} = 495-nm) was monitored as a function of time, corrected for leakage and direct excitation and normalized with respect to initial values. Three independent data sets were collected for each nucleotide and cation condition. All samples contained a total of 2 mM nucleotide and 5 mM magnesium or manganese ions, with the exception of one condition, which consisted of 2 mM ATP and 2.1 mM Mg^{2+} (0.1 mM free Mg^{2+}, labeled as "ATP-No Free Mg").

mixing speeds up until leveling off around 45 minutes (figure 32). Exchange in the presence of manganese was significantly faster than in magnesium. Instead of the lag period seen in magnesium, the ATP sample showed a slow and steady initial rate of exchange before leveling off around 35 minutes. Manganese loosens up the subunit-subunit interactions and makes them more facile. There is a proposed cation binding site that mediates these interactions, and manganese has been shown to not mediate this contact as efficiently as magnesium. In the presence of ADP-Mg, there is a monophasic exchange curve showing immediate and rapid loss of FRET, suggesting ADP destabilizes

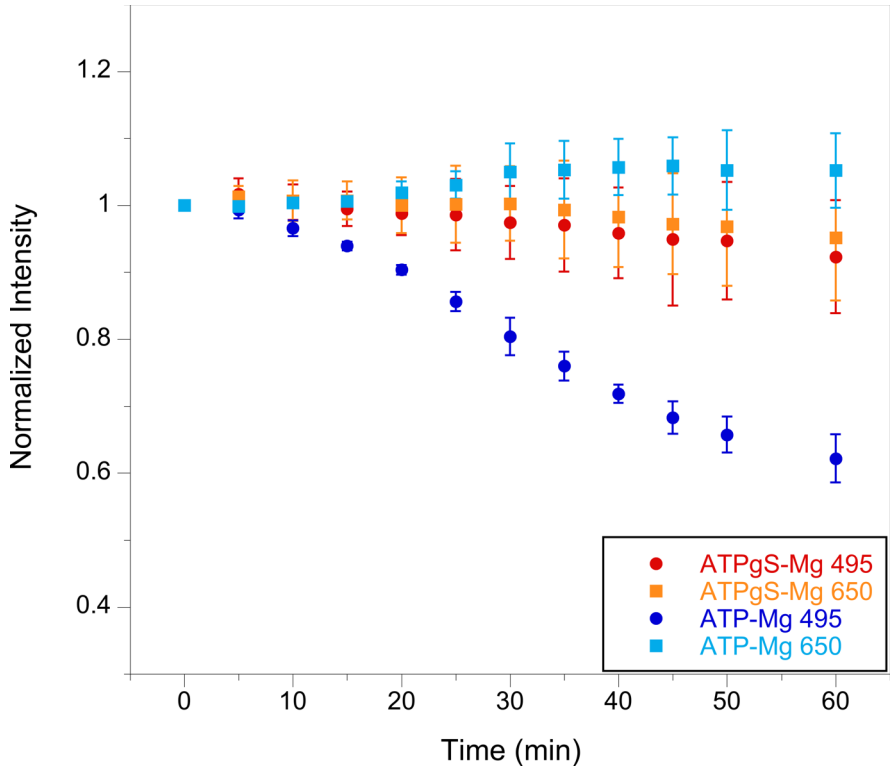

Figure 30. Time-dependent changes in red fluorescence upon green and red excitation, as observed with the label dilution subunit exchange assay. Upon mixing of Rca-488-647 with label-free Rca in the presence of either 2 mM ATP (dark and light blue) or 2 mM ATPγS (red and orange), the 685-nm emission was monitored as a function of excitation wavelength. The data for λ_{ex} = 495 nm are shown in blue and red, and the data for λ_{ex} = 650 nm are shown in light blue and orange. The data for λ_{ex} = 495 nm were corrected for leakage and direct excitation (*Lk* and *Dir*).

subunit-subunit interactions. The combination of ADP with manganese speeds up exchange even more. During the 5 minute lag period of the Mg-ATP subunit exchange

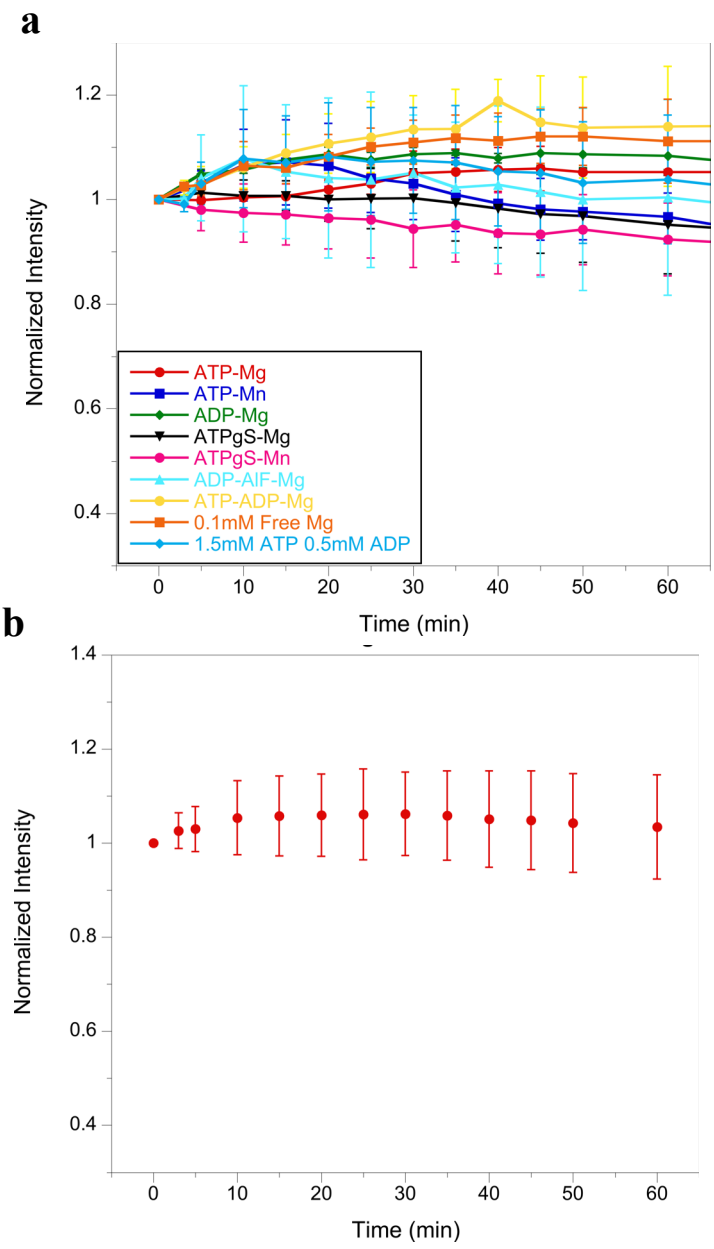

Figure 31. Time-dependent fluorescence variations observed in the label dilution assay upon direct excitation of the red dye. (a) The 685-nm emission (λ_{ex} = 650 nm) was monitored as a function of time upon mixing of 1.25 µM Rca-488-647 with 3.75 µM label-free Rca in the presence of various nucleotides and divalent cations. (b) All 27 trials were averaged.

sample, approximately 420 μM ADP accumulated (figure 33), suggesting about 0.5 mM ADP is the threshold needed to catalyze subunit exchange. The label dilution subunit exchange assay wasperformed with 0.5 mM ADP and 1.5 mM ATP in Mg^{2+}, and did not show the same initial lag period as the ATP-Mg sample did. Instead, steady exchange

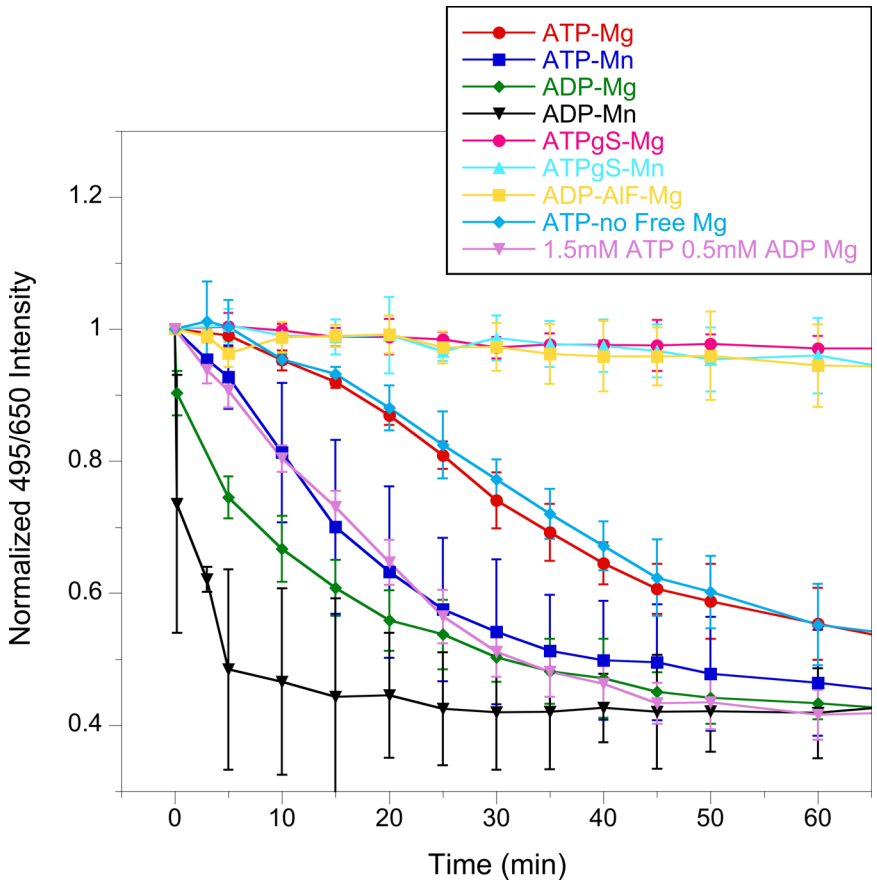

Figure 32. **Time-dependent changes in FRET intensity observed in the label dilution assay upon adjustments for the observed variability in red dye fluorescence.** For each experiment, 1.25 μM Rca-488-647 was combined with 3.75 μM label-free Rca at time zero. The 685-nm emission intensity (λ_{ex} = 495-nm) was monitored as a function of time, and corrected for leakage and direct excitation. *To account for variations in red fluorescence upon direct excitation of Rca-647, each corrected data point was divided by the 685-nm emission observed upon 650-nm excitation.* The resulting values were normalized with respect to initial values. Three independent data sets were collected for each nucleotide and cation condition. All samples contained a total of 2 mM nucleotide and 5 mM magnesium or manganese ions, with the exception of one condition, which consisted of 2 mM ATP, 2.1 mM total Mg^{2+} (0.1 mM free Mg^{2+}, labeled as "ATP-No Free Mg").

occurred immediately, until leveling off around 35 minutes. Exchange was not nearly as rapid as for all ADP, but confirmed 0.5 mM ADP promotes immediate exchange with no time needed to accumulate additional ADP. The lack of a lag period in this sample confirms some ADP is needed for exchange to occur. The larger the ADP fraction is, the faster the exchange rate. Conversely, the ATP-Mn sample does not show a lag period, and the rate of ADP accumulation is slower, suggesting Mn^{2+} alone is enough to loosen up assemblies.

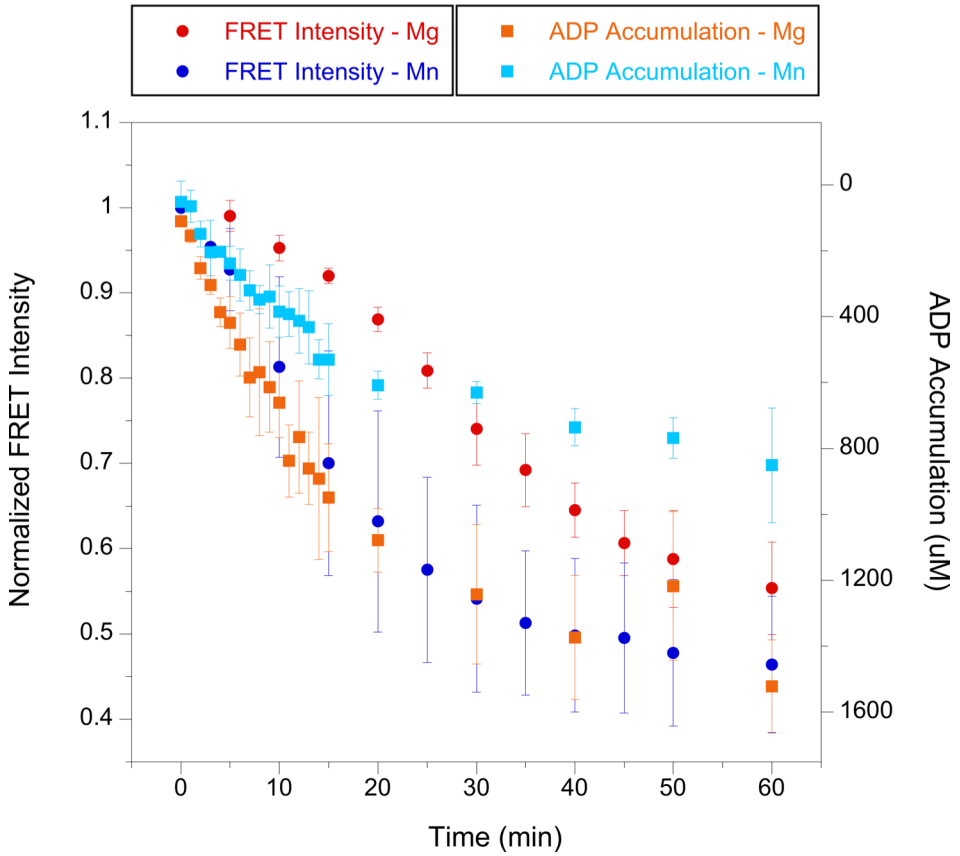

Figure 33. Time-dependent ADP accumulation, as compared to the loss of FRET observed in the label dilution assay. In both assays, 1.25 µM Rca-488-647 were combined with 3.75 µM label-free Rca at time zero. ADP accumulation was coupled to NADH production in an enzyme-linked assay. At time zero, samples contained 2 mM ATP and 5 mM Mg^{2+} or 5 mM Mn^{2+}.

Subunit Exchange is Inhibited by Analogs

If ADP is eliminated completely by using the ATP analog ATPγS or flexible transition state analog ADP-AlF_x, subunit exchange is inhibited almost completely (figure 32). Identity of the divalent cation present does not affect subunit exchange in the presence of ATPγS as it does in both ATP and ADP. The disruption effect of manganese on subunit-subunit interactions is not strong enough to break the interactions formed by the presence of ATPγS.

Subunit Exchange is Correlated with Thermal Stability

The transition state analog ADP-AlF_x provides substantial stabilization in the presence of magnesium ions, with an apparent T_m of almost 50°C (table 5). The high thermal stability of spinach β-Rca in the presence of ATPγS and magnesium or manganese indicates subunit-subunit interactions in ring-like assemblies that are tight enough to prevent exchange. Lower thermostability lends itself to more dynamic movements and looser assemblies. The closer the melting temperature is to ambient temperature, the more prone to dissociation. The three distinct rates of subunit exchange can be grouped into three assembly categories: rigid types with extremely slow exchange of individual subunits, tight assemblies with ATP, and loose assemblies that provide fast exchange due to high ADP.

Table 5. Apparent melting temperatures "T_ms" for So-β-Rca(1-378) expressed from pHUE. Thermofluor data were collected and analyzed by Dr. J. Nathan Henderson.

Nucleotides	No divalents	5 mM Mg^{2+}	5 mM Mn^{2+}
No nucleotide	25.6 ± 0.0°C	24.4 ± 1.0°C	25.4 ± 0.5°C
2 mM ADP	35.0 ± 0.2°C	34.0 ± 0.3°C	37.2 ± 0.0°C
2 mM ATP	28.2 ± 0.0°C	35.3 ± 0.2°C	38.2 ± 0.5°C
2 mM ATPγS	41.6 ± 0.2°C	59.7 ± 0.3°C	60.6 ± 0.2°C
2 mM ADP-AlF_x	37.1 ± 0.3°C	49.1 ± 2.2°C	36.5 ± 0.3°C

C-terminal Labeling of Spinach-β Rca Does Not Affect ATPase or Reactivation Activity

ATPase activity assays were carried out on spinach-β-Rca-T375C with covalently attached Alexa dyes to determine if covalent labeling modifies the ATPase activities of spinach-β Rca. Previously, ATPase assays based on MESG (phosphate production measurements) were carried out on cotton-β Rca using preparations that contained 0, 25, 50, 75 and 100% Alexa-488 labeled subunits. It was determined that covalently bound Alexa-488 does not affect the ATPase activity of cotton-β Rca (table 4). Here, the ATPase activity of green-labeled spinach-β Rca (Rca-488), red-labeled spinach-β Rca (Rca-647) and spinach-β Rca without label were compared. Again, no differences in activity between any of these preparations were found (table 6), indicating that the C-terminal derivatization does not affect the rate of ATP turnover in any way. The average turnover rate was measured to be 13 min^{-1}, similar to that measured by the NADH assay (15 min^{-1}) under similar conditions (table 7).

Table 6. Turnover rates of spinach-β Rca with or without a C-terminal label.

	Turnover Rate (min^{-1})	Standard Deviation
Unlabeled Rca	13.079	1.479
Rca-488	13.323	1.843
Rca-647	13.629	2.225

Utilizing a continuous, four-enzyme-linked spectrophotometric assay to monitor the carboxylation activity of Rubisco, a k_{cat} value of 2.26 s^{-1} ± 0.13 s^{-1} and a K_m value of 42.1 μM ± 6.65 μM were determined for wild-type *Chlamydomonas* Rubisco produced in our lab. These values were collected between 0 and 150 μM RuBP under saturating

carbon dioxide conditions. The linking enzymes consisted of phosphoglycerate mutase, enolase, pyruvate kinase and lactate dehydrogenase. Rubisco reactivation assays were performed by Matthew Hilton.

ATP and ATPγS Turnover is Moderately Affected by Replacement of Magnesium with Manganese Ions

Utilizing the NADH-based ATPase assay, turnover numbers of 5 μM spinach β-Rca-T375C in the presence of either magnesium or manganese ions were compared. A series of ADP standards were performed in each assay mix to verify the response of each assay was accurate and the consistent (figure 34). In the presence of ATP and Mg^{2+}, the

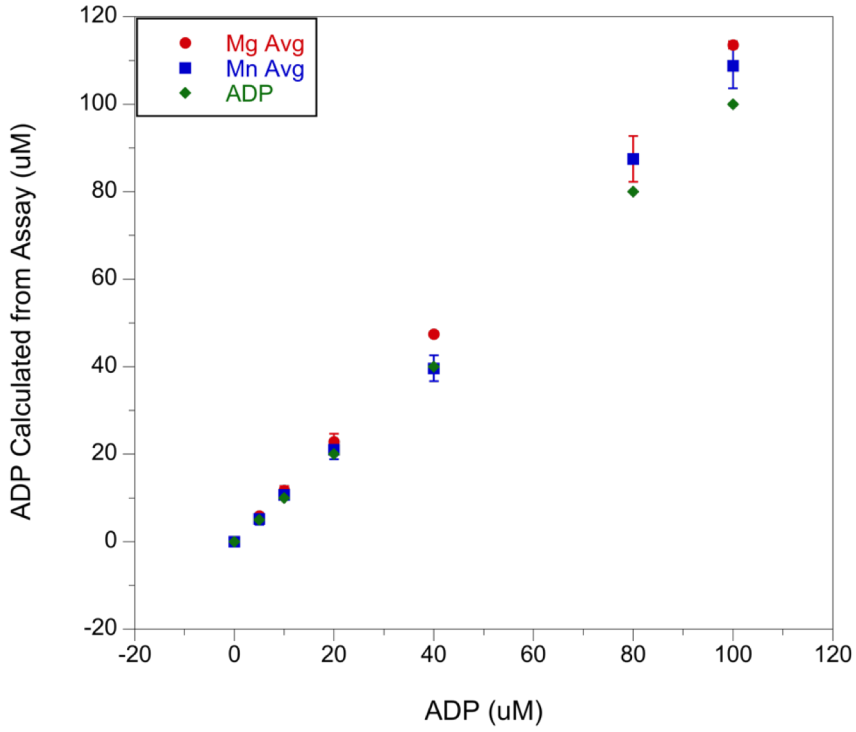

Figure 34. ADP standards in the continuous ATPase assay based on ADP production. Assay mix was prepared with either $MgCl_2$ (red) or $MnCl_2$ (blue). The theoretical concentration of ADP is shown in green, and along the x-axis. The average of three independent trials, with standard deviation is shown. Samples to test ADP accumulation fell in the 0-30 μM range.

turnover rate was measured to be 15.4 ± 0.5 min^{-1} (table 7). Similarly, the turnover rate in the presence of ATP and Mn^{2+} was measured to be 18.2 ± 0.9 min^{-1}. The turnover numbers indicate that manganese cations can substitute for magnesium cations to activate ATP-bound Rca towards hydrolysis. Manganese ions accelerate turnover and accelerate subunit exchange, suggesting faster turnover is coupled to faster exchange.

Table 7. ATP and ATPγS turnover rates of spinach Rca.

	ATP turnover (min^{-1})	ATPγS turnover (min^{-1})
Mg^{2+}	15.43 ± 0.5352	0.3723 ± 0.0845
Mn^{2+}	18.26 ± 1.2629	0.3677 ± 0.0921

Turnover of ATPγS by spinach β-Rca-T375C was also measured in the presence of either Mg^{2+} or Mn^{2+} ions, and found that the turnover rate is about 0.4 min^{-1}, irrespective of the divalent cation. Low concentrations of ATPγS were found to inhibit ATP turnover of spinach β-Rca-T375C (figure 35). Because ATPγS turns over so slowly, some sites may get stuck in a tight or locked state and block those sites from binding ATP. The extremely slow rates of turnover and subunit exchange in ATP analogs, along with inhibitory effects on ATP turnover, further suggest active ATP hydrolysis is coupled to subunit exchange.

Low Concentrations of ADP Do Not Affect ATP Turnover

In tobacco Rca, concentrations up to 140 μM ADP were shown to inhibit activity [59]. To examine whether the regulation of spinach-β Rca is affected by low concentrations of ADP, ATPase activity assays to test for ADP inhibition or ADP activation of spinach β-Rca-T375C were performed. Extensive collection of turnover

data in the presence of small amounts of ADP (10 μM to 180 μM) demonstrate that within this concentration range, ADP neither inhibits nor activates spinach-β Rca (figure 35). Due to commercial ADP preparations containing some amount of phosphate, this assay could not tolerate ADP concentrations over 180 μM. 0.18 mM ADP is not able to compete with 2 mM ATP for binding to the active site, therefore, at concentrations up to 180 μM, ADP does not bind at an appreciable rate to promote subunit exchange. ADP accumulates to about 200 μM after 3 minutes (figure 33), which is still within the 5 minute lag period before exchange occurs.

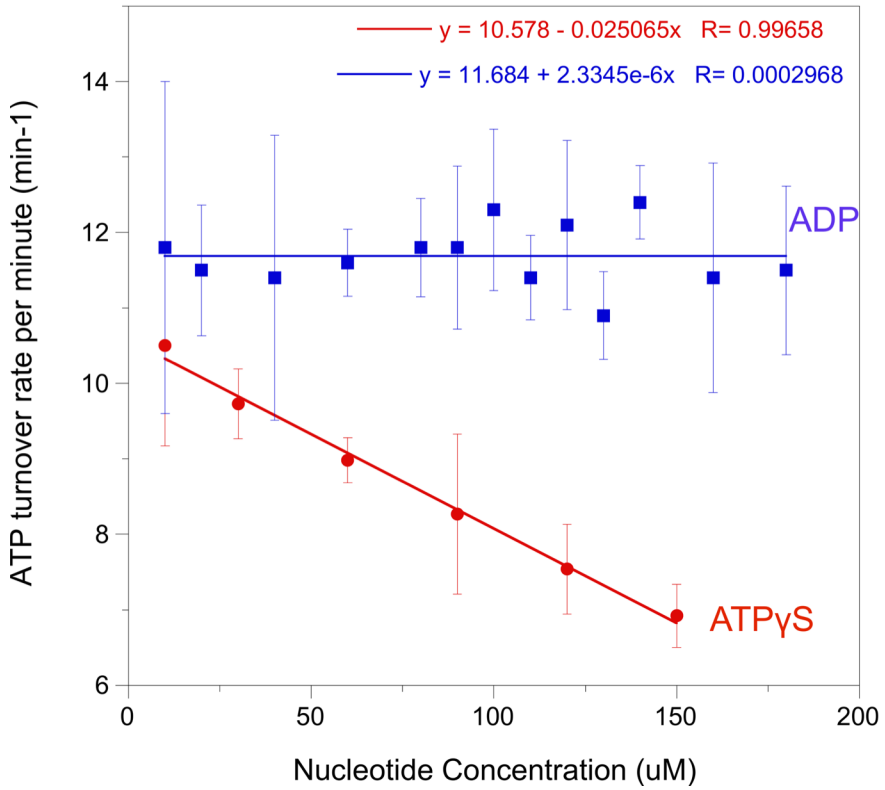

Figure 35. Turnover rates of So-β-Rca in the presence of added ADP or ATPγS using the continuous MESG assay. Samples contained 5 μM Rca, 2 mM ATP and corresponding amount of additional ADP or ATPγS. Data were fit to a linear regression line.

Dye Stability

Both protein-derivatized dyes showed small fluctuations over 60 minutes: at 60 minutes, on average Rca-488 and Rca-647 decreased <1% of initial signal (figure 36). Time course spectra of an individual trial showed greater fluctuations than an average of 5 trials (figure 36), indicating dye instability in both green and red dyes is random. Decreasing the number of emission scans did not diminish the signal loss. Typically, samples in the label dilution assay showed a similar fluctuation range in the red dye signal over 60 minutes (figure 31).

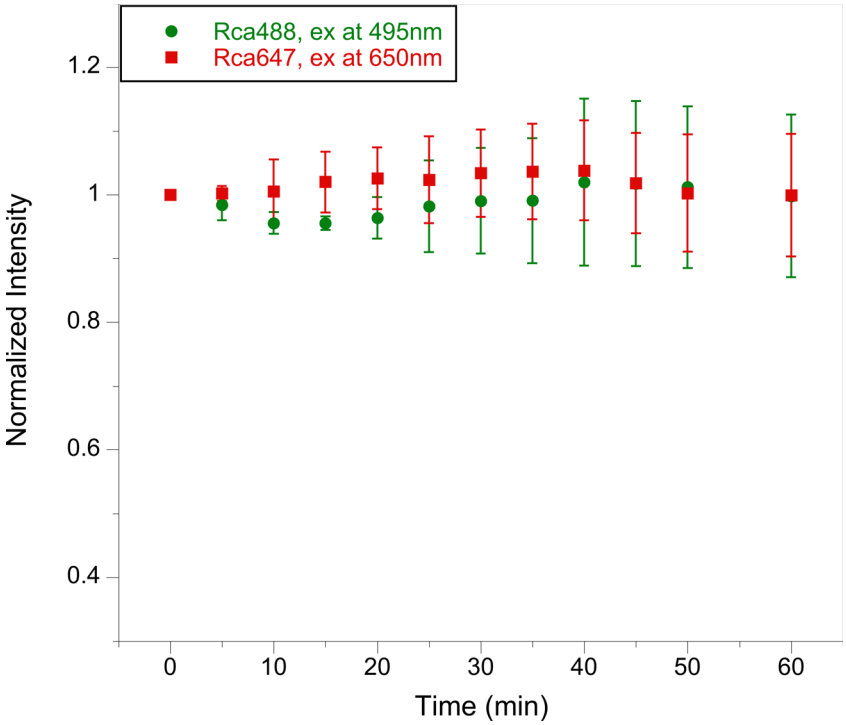

Figure 36. Optical stability of Alexa-488 and Alexa-647 dyes upon covalent attachment to protein. Preparations of Rca-488 and Rca-647 were mixed with label-free Rca to obtain 5 μM subunit concentration in 2 mM ATPγS. Time-dependent excitation and emission scans were collected with five independent repetitions, using experimental parameters identical to those used in the label dilution assay. Rca-488 preparations were excited at 495 nm and emission was monitored at 535 nm. Rca-647 preparations were excited at 650 nm, with emission monitored at 685 nm. The data were normalized with respect to the value obtained at time zero.

For the free dye (no protein), the emission of the red dye decreases more substantially when free than when attached to protein (figure 37). When Alexa is attached to protein, there is no average red dye signal change over 60 minutes as a function of cation (Mg^{2+} vs Mn^{2+}). After 60 minutes, fluorescence decreases in both dye derivatized protein and free dye, up to 25% signal loss after 180 minutes (λ_{ex} = 650 nm, λ_{em} = 685 nm).

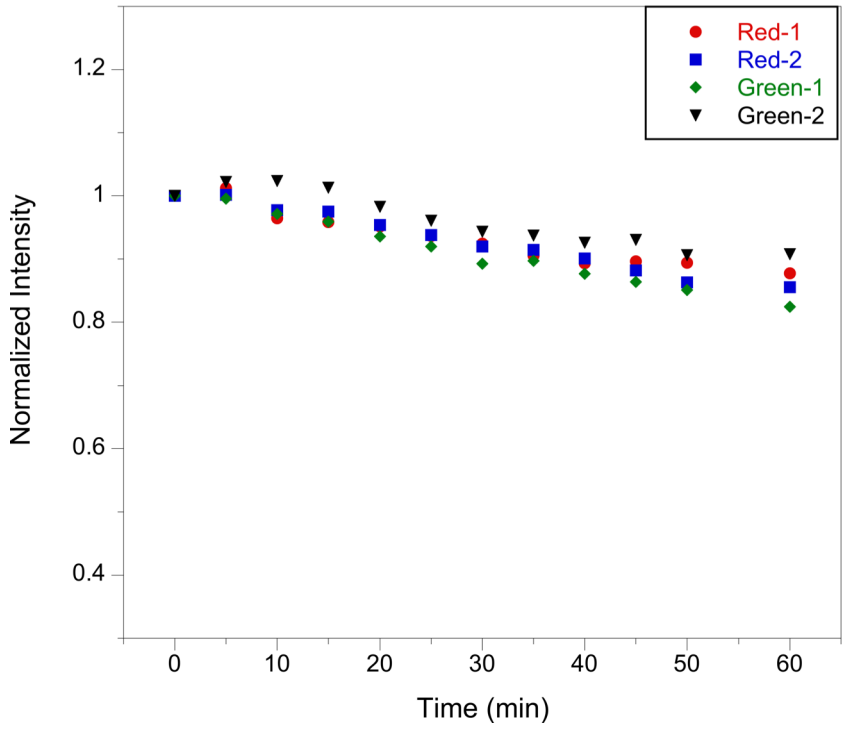

Figure 37. Optical stability of free Alexa-488 and Alexa-647 dyes. Time-dependent excitation and emission scans were collected with two independent repetitions, using experimental parameters identical to those used in the label dilution assay. Green Alexa-488 samples were excited at 420 nm and emission was monitored at 515 nm. Red Alexa-647 samples were excited at 650 nm, with emission monitored at 685 nm. The data were normalized with respect to the value obtained at time zero.

Trolox is a water-soluble analog of vitamin E that is known to be a reductant that quenches triplet states via electron transfer [84]. However, the addition of 3 mM Trolox did not significantly affect fluorescence intensity of either dye in combined free dye

(19% red dye signal loss vs 14% without Trolox, over 180 min; 19% green dye signal loss vs 21% without Trolox, over 180 min) or Rca-488/Rca-647 time course control assays (23% signal loss vs 17% without Trolox, over 180 min), and was not used in the data shown.

$MgCl_2$, $MnCl_2$ and 2 mM $AlCl_3$ did not present any significant changes to the free dye spectra over the 30 minute time course (figures 38, 39). However, with 10 mM $AlCl_3$, there was a four-fold decrease in red dye intensity in the excitation spectra, with a two-fold increase in green dye intensity compared to all other samples (figure 38). The emission spectra showed a similar trend, with a two-fold decrease in green dye intensity

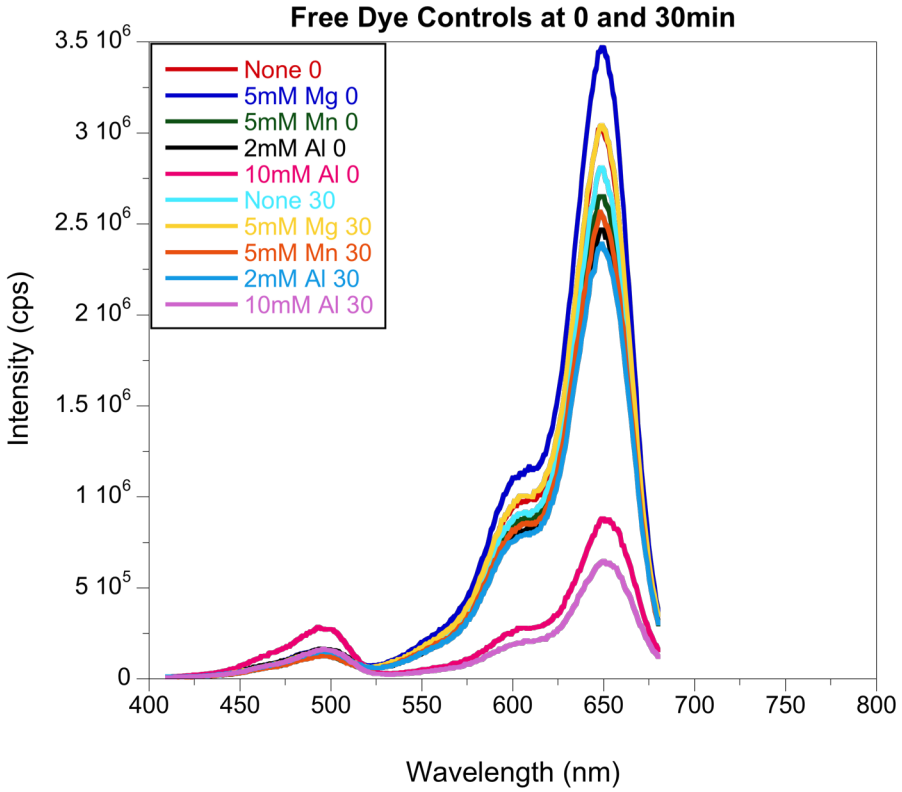

Figure 38. Excitation spectra of free dyes in the presence of various cationic species. Excitation spectra (λ_{em} = 685 nm) of 0.71 µM Alexa-488 and 0.42 µM Alexa-647 with stated concentrations of $MgCl_2$, $MnCl_2$ or $AlCl_3$ at 0 and 30 minutes. 10 mM $AlCl_3$ leads to substantial quenching of Alexa-647 fluorescence. 2 mM Mn^{2+} and 2 mM Al^{3+} appear to quench mildly.

and slight increase in red dye intensity (figure 39). The drastic drop in overall intensity paired with an emission increase upon 495 nm excitation suggested if FRET were occurring in the Rca samples under these conditions, results could not be interpreted. Since $AlCl_3$ is a component in making ADP-AlF_x, the label dilution assay data in the presence of 10 mM ADP-AlF_x are not reliable and are therefore not shown.

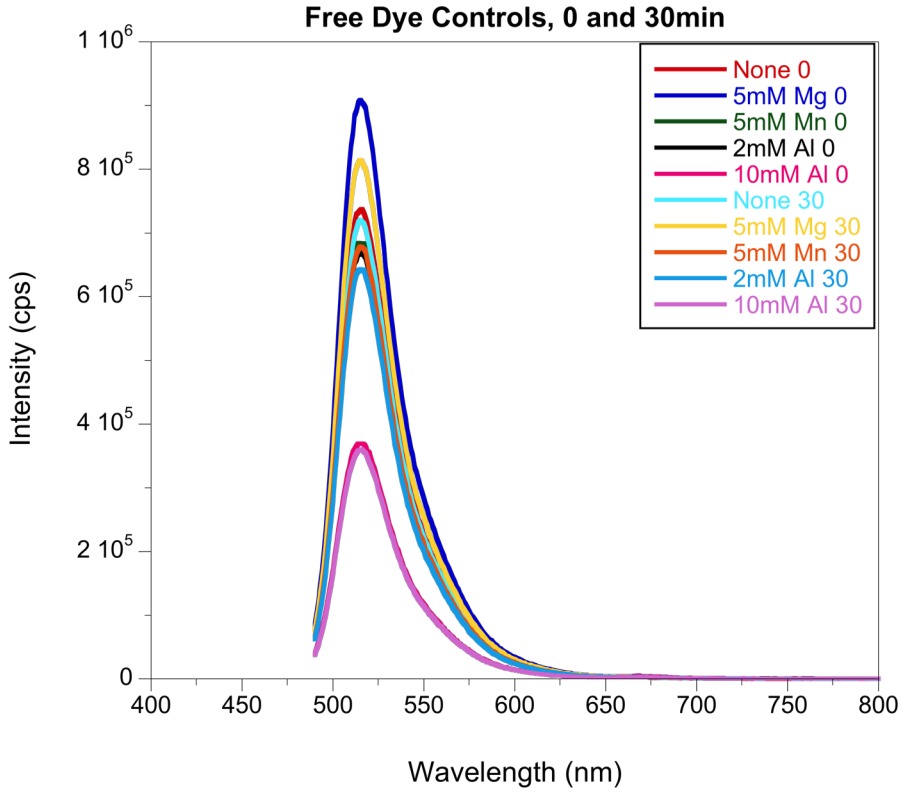

Figure 39. Emission spectra of free dyes in the presence of various cationic species. Emission scans (λ_{ex} = 420 nm) of 0.71 µM Alexa-488 and 0.42 µM Alexa-647 with stated concentrations of $MgCl_2$, $MnCl_2$ or $AlCl_3$ at 0 and 30 minutes. 10 mM $AlCl_3$ leads to substantial quenching of Alexa-488 fluorescence. 2 mM Mn^{2+} and 2 mM Al^{3+} appear to quench mildly.

Alexa Dye is Attached to the Introduced C-terminal Cysteine

Excitation and emission scans collected during the first 15 minutes of the Rca labeling reaction shows attachment of green and red dyes to subunits in the same oligomer, as evidenced by an increase in the FRET signal. An increase in red dye

emission (λ_{em} = 672 nm) upon excitation of the green dye (λ_{ex} = 495 nm) in both emission and excitation scans, and a decrease in the emission of the green dye (λ_{em} = 515 nm) upon excitation of the green dye (λ_{ex} = 420 nm) in the emission scan, are events consistent with an increase in FRET (figures 40, 41). In the samples with BSA, neither the emission intensity at 685 nm observed upon excitation at 495 nm (figure 42), nor the emission intensities observed at 530 nm and 672 nm upon excitation at 420 nm (figure 43) exhibit any time dependence, and are inconsistent with FRET. This observation

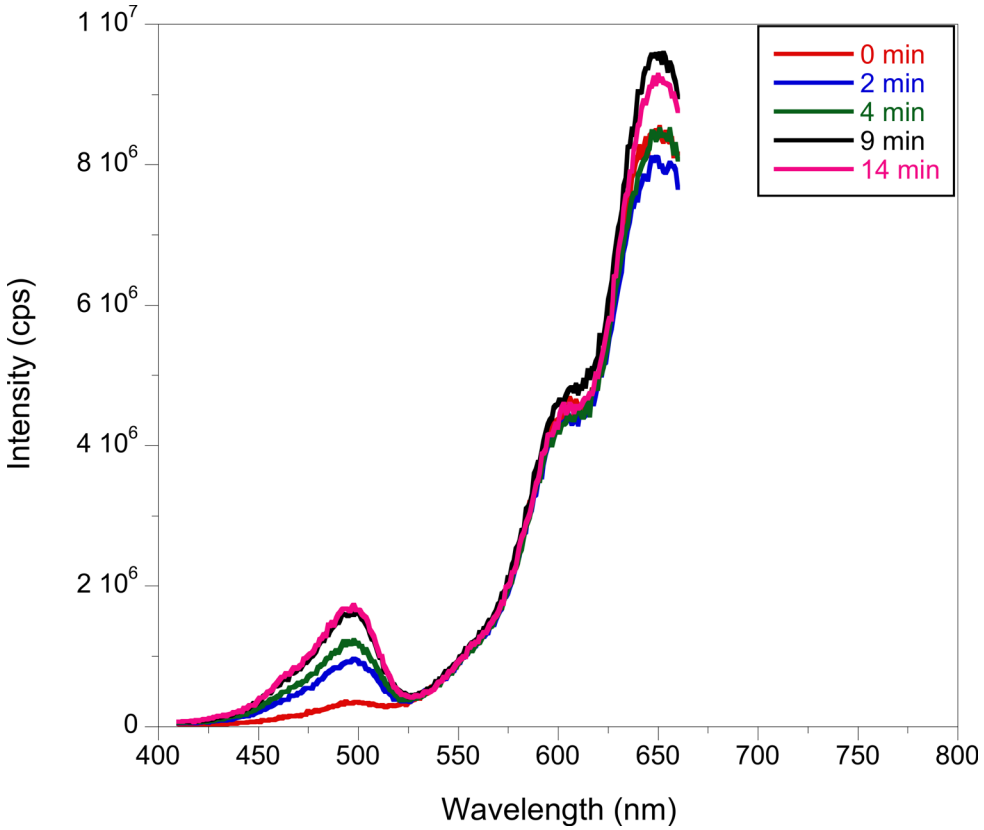

Figure 40. Excitation scans collected during the Rca labeling reaction (λ_{em} = 672 nm). The reaction mixture contained 2.5 µM Alexa-488, 2.5 µM Alexa-647 and 5 µM label-free Rca in the presence of 5 mM ATPγS. During the labeling reaction, oligomeric assemblies of Rca are derivatized with Alexa-488 and Alexa-647 dyes. Attachment of green and red dyes to subunits in the same oligomer leads to FRET, as observed by an increase in emission upon excitation of the green dye (λ_{ex} = 495 nm). Direct excitation of the red dye at 650 nm leads to emission intensities that vary within the error of the experiment (see figures 31, 36).

indicates that individual BSA monomers are not derivatized simultaneously with both green and red dyes. Likewise, non-specific adsorption of both dyes onto individual BSA monomers appears unlikely. Additionally, wild-type So-β-Rca subjected to an identical labeling procedure was found to remain label-free, indicating that in So-β-Rca-T375C, the label only reacts with the introduced cysteine.

Comparing the raw emission upon 495 nm excitation (directly exciting the green dye while monitoring red dye emission) between various samples in 5 mM ATPγS showed no significant increase or decrease at the FRET signal wavelength (λ_{ex} = 495 nm,

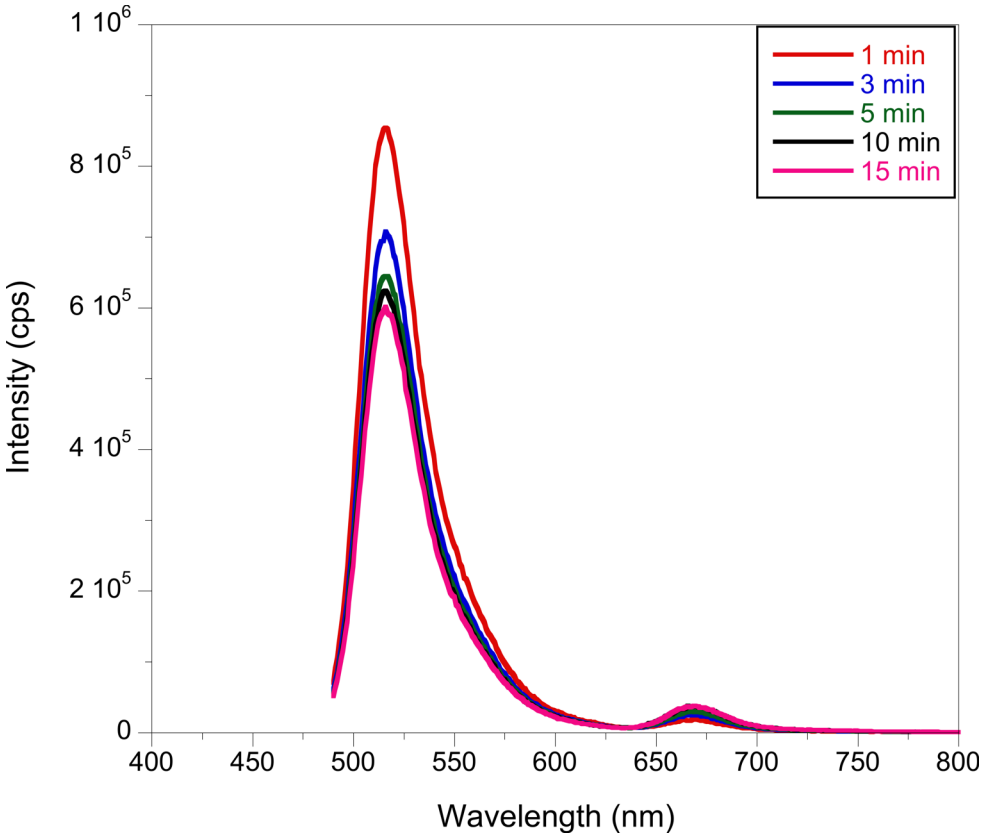

Figure 41. Emission scans collected during the Rca labeling reaction (λ_{ex} = 420 nm). The reaction mixture contained 2.5 μM Alexa-488, 2.5 μM Alexa-647 and 5 μM label-free Rca in the presence of 5 mM ATPγS. During the labeling reaction, oligomeric assemblies of Rca are derivatized with Alexa-488 and Alexa-647 dyes. Attachment of green and red dyes to subunits in the same oligomer leads to FRET, as observed by a decrease in the emission of the green dye (λ_{em} = 515 nm), and an increase in the emission of the red dye (λ_{em} = 670 nm).

λ_{em} = 672 nm), except in the case of both free dyes with unlabeled Rca (figure 44). This shows the dye covalently attached to Rca is stable and not free to rearrange onto other subunits, nor does the free dye attach to labeled or unlabeled Rca in a high enough occurrence to increase FRET between the dyes. A baseline signal is present and consistent in all samples due to *Lk* and *Dir*. Free Alexa-488 and free Alexa-647 were added to unlabeled Rca (RcaUL) in the cuvette and the FRET signal increased as a function of time (figures 40, 41). Experiments with one free dye plus labeled Rca did not show an increase of FRET, indicating all accessible labeling sites were occupied (figure 44). The Rca488 + Rca647 + RcaUL sample did not show evidence of FRET, indicating

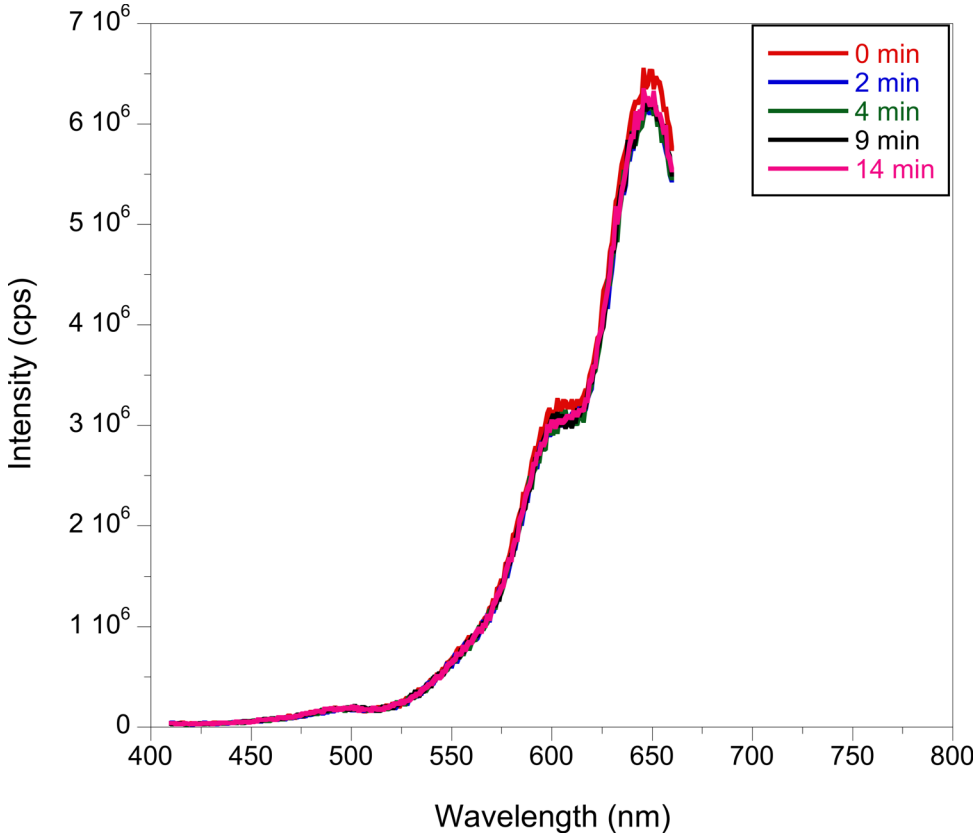

Figure 42. Excitation scans collected during a BSA labeling reaction (λ_{em} = 672 nm). The reaction mixture contained 2.5 µM Alexa-488, 2.5 µM Alexa-647 and 0.21 mg/mL BSA in the presence of 5 mM ATPγS. The emission intensity observed upon excitation at 495 nm does not exhibit any time dependence, and is inconsistent with FRET.

no subunit exchange is occurring in ATPγS (which later experiments confirmed). Dual-labeling of Rca oligomers leads to FRET, whereas labeling with one dye only does not lead to FRET (figure 44), therefore, labeled Rca samples (Rca-488 and Rca-647) do not get additionally labeled in the presence of free dye. Free dye can be used in control experiments, since any FRET signal is coming from the dyes reacting with the protein.

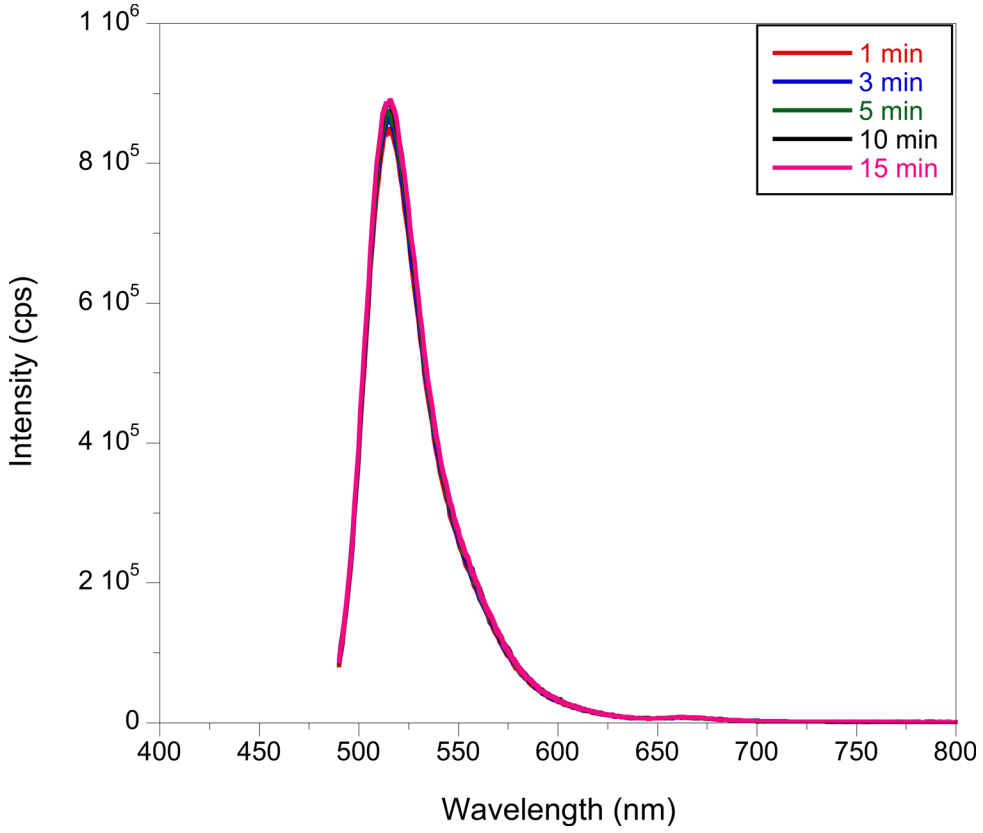

Figure 43. Emission scans collected during a BSA labeling reaction (λ_{ex} = 420 nm). The reaction mixture contained 2.5 µM Alexa-488, 2.5 µM Alexa-647 and 0.21 mg/mL BSA in the presence of 5 mM ATPγS. The emission intensities observed at 530 nm and 672 nm do not exhibit any time dependence, and are therefore inconsistent with FRET. This observation indicates that BSA, which is monomeric, does not simultaneously react with both green and red dyes. In addition, non-specific adsorption of both dyes onto the protein surface appears unlikely.

ATP Regeneration System

An ATP regeneration system was introduced into the FRET-based subunit exchange assays. Since the effect on accelerating subunit exchange was relatively minor,

whether the ATP regeneration system is capable of eliminating ADP to a point where ADP will not inhibit Rca was tested. Using the NADH assay, it was found that ADP accumulates fairly substantially before the regeneration system becomes active, providing a rationale for its poor performance in the subunit exchange assay.

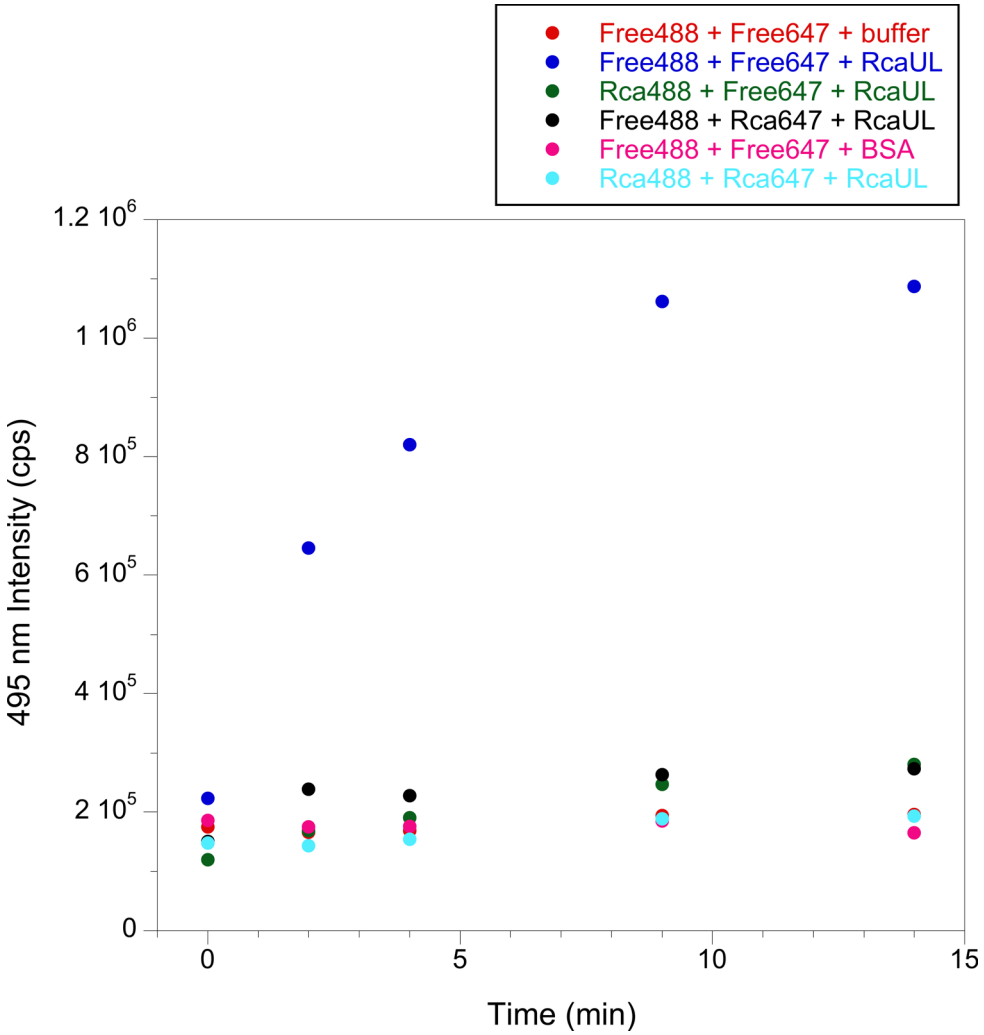

Figure 44. Time course of the Rca dual-labeling reaction compared to various control reactions. The raw 672-nm emission intensity is plotted as a function of time (λ_{ex} = 495 nm). Samples contain various combinations of free Alexa dyes and protein preparations with and without covalent label. All samples contained 2.5 µM Alexa-488 (free or protein-attached), 2.5 µM Alexa-647 (free or protein-attached) and 5 mM ATPγS. Dual-labeling of Rca oligomers leads to FRET, whereas labeling with one dye only does not lead to FRET. Samples containing free dyes in buffer with or without BSA do not exhibit FRET. Unlabeled Rca is indicated as RcaUL.

Analytical Data on Alexa Derivatized Rca Preparations

To verify the identity of Alexa-derivatized Rca, protein preparations were analyzed by reverse phase HPLC (figure 45). All Rca eluted at 53% ACN, whereas free Alexa-488 eluted at 29% ACN and free Alexa-647 eluted at 18% ACN. No free dye was present in any of the Rca labeling preparations (Rca-488, Rca-647 or Rca-488-647). Eluted protein was collected to analyze further by absorbance spectra and MALDI.

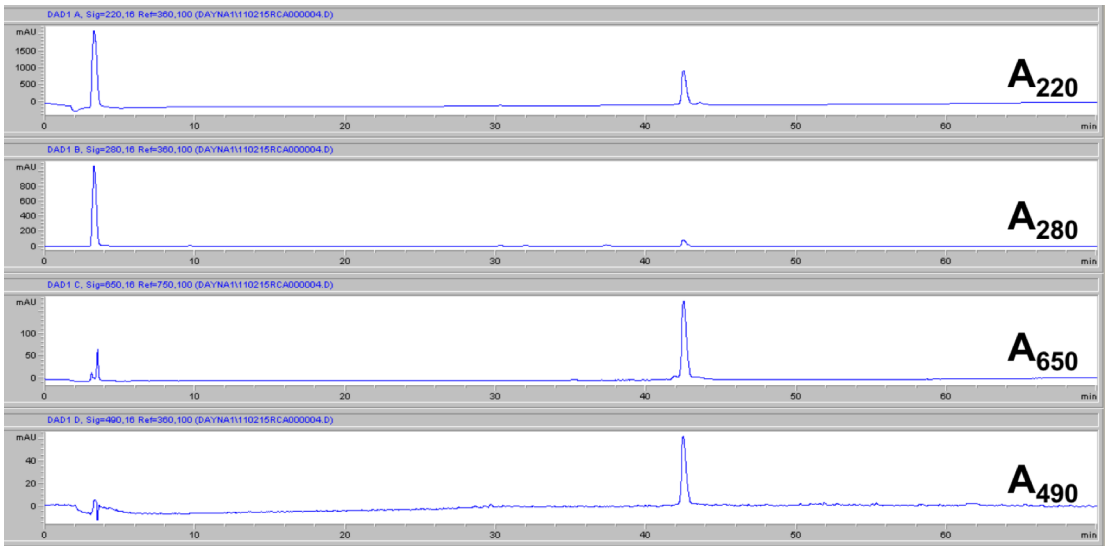

Figure 45. HPLC chromatogram of Rca-488-647. Reverse-phase HPLC chromatogram of Alexa-labeled Rca monitored at 220 nm (top), 280 nm (upper middle), 650 nm (lower middle) and 490 nm (bottom). The chromatograms indicate that the Rca preparation is covalently labeled with both Alexa-488 and Alexa-647 and does not contain any traces of free Alexa dye.

The labeling efficiency was calculated from the absorbance spectra (figure 46, equations 1, 2). In Rca-488-647 samples, 90% of subunits were dye-conjugated, with a ratio of 1.7:1, Alexa-488:Alexa-647 (average of 0.57 Alexa-488 and 0.33 Alexa-647 dyes per subunit), indicating Alexa-488 is more easily derivatized. The individual Rca-488 and Rca-647 labeling reactions provided labeling efficiencies close to 1 dye per subunit.

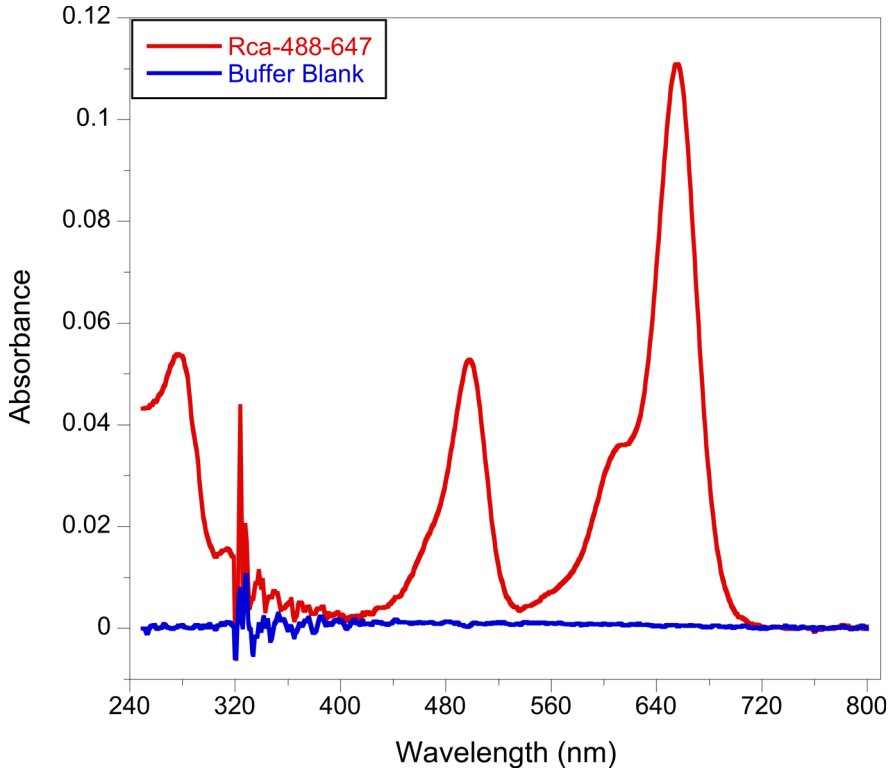

Figure 46. Absorbance spectra of Rca-488-647. The labeling efficiency was determined as 0.57 Alexa-488 dyes and 0.33 Alexa-647 dyes per subunit, giving an average of 90% of subunits labeled.

MALDI spectra on labeled Rca (Rca-488, Rca-647 and Rca-488-647) confirmed a homogeneous pool of 1 label per subunit (table 8, figure 47). Wild-type So-β-Rca subjected to the dual-labeling procedure had a measured mass of 41994 Da, consistent with the theoretical mass of unlabeled wild-type So-β-Rca of 41924 Da.

Table 8. Theoretical and measured masses of So-β-Rca by MALDI.

	Theoretical Mass (Da)	Measured Mass (Da)
So-β-T375C	41925	42011
So-β-T375C-488	42646	42652
So-β-T375C-647	43175	43078

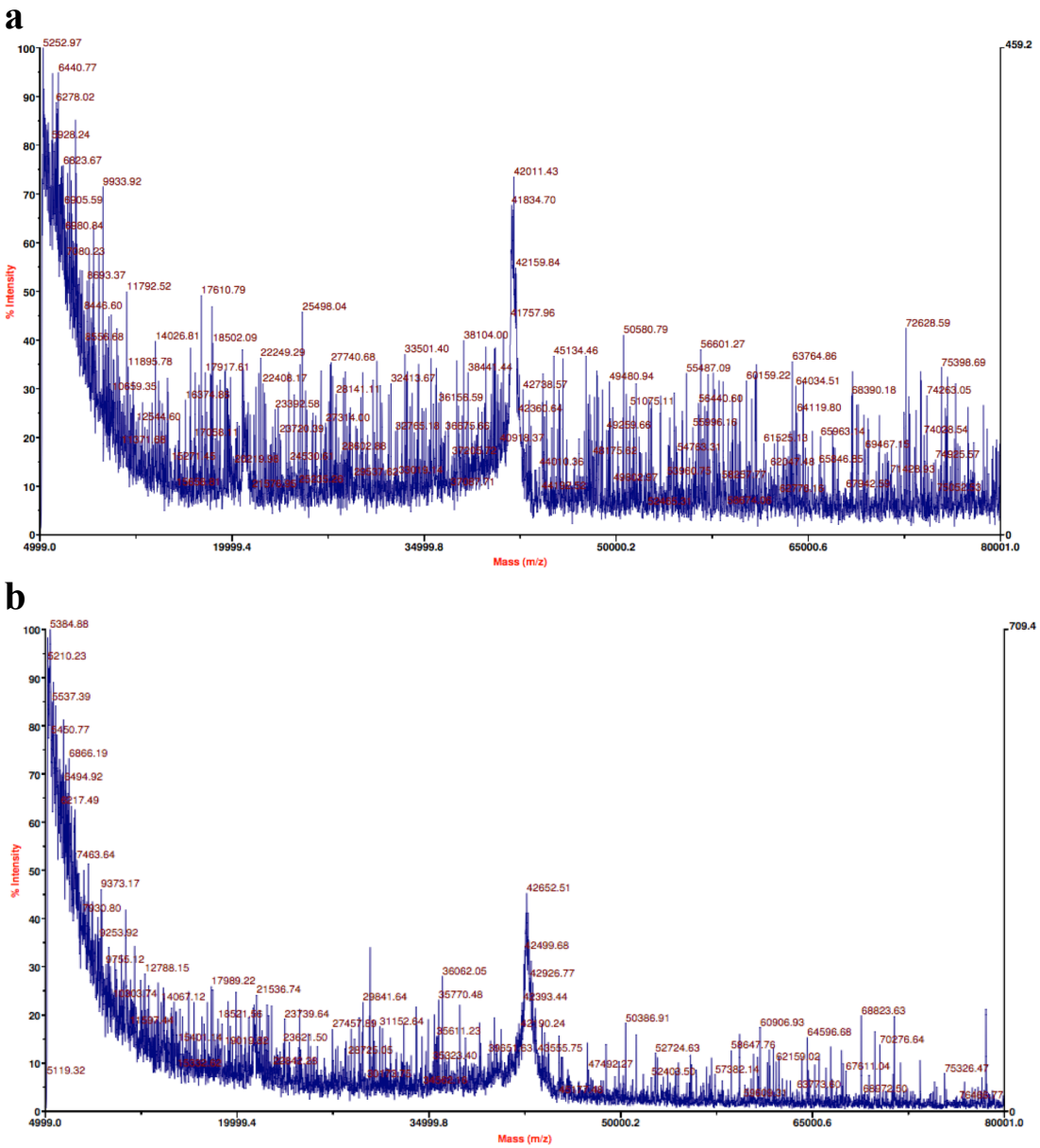

Figure 47. MALDI spectra of unlabeled and labeled spinach Rca. Spectra were collected on unlabeled and labeled cotton Rca preparations, and compared to their theoretical values. (a) The unlabeled Rca spectrum exhibits a main peak with m/z = 42011 (z=1). The calculated mass is 41925 Da. (b) The Rca-488 protein spectrum exhibits a main peak with m/z = 42652 (z=1). The calculated mass is 42646 Da. The error of this instrument is estimated to be about 100 Da for a protein of this size.

DISCUSSION

So-β-Rca was successfully labeled with green and red fluorophores and utilized in a FRET-based assay to monitor subunit exchange kinetics. A striking nucleotide effect was observed that correlated with thermal stability, indicating oligomeric conformational rigidity is based on nucleotide state. With physiological ATP, there is moderate thermostability and slow subunit exchange, consistent with tight assemblies; with ADP, moderate thermostability, fast subunit exchange, and no inhibitory effects on turnover between 10 and 180 μM, corresponding with loose assemblies; and in the presence of ATPγS, there is high thermostability, very limited subunit exchange, and an inhibitory effect on turnover indicating rigid assemblies. The high thermal stability of So-β-Rca under certain conditions suggests subunit-subunit interactions in assemblies that are sufficiently tight to prevent exchange.

In Rca, the model of biological regulation is that quaternary reorganization serves as the regulatory mechanism. Rca activity is concentration dependent, where smaller order oligomers show higher activity, hexamers reactivate Rubisco, and large aggregates serve as storage mechanisms [63, 85].

A Tight Binding Event May Occur in ClpX

The bacterial ClpXP is a AAA+ protease that consists of peptidase ClpP and hexameric motor ClpX. ClpX is a closely related homolog to Rca, with 10% sequence identity between the AAA+ domains. Recently, the complete mechanochemical ATPase cycle of the ClpX motor was characterized by using dual-trap optical tweezers to track a single ClpX molecule (figure 48) [86]. After ATP binds to the motor, the complex is proposed to go through an irreversible tight binding event before hydrolysis. Release of

phosphate is proposed to be the force generating step to pull the substrate through the central pore of ClpX and into the barrel of ClpP [87]. It is proposed the subunits go through conformational switching after each ATPase cycle to convert between the three nucleotide binding states: high-affinity, low-affinity, and free [54, 58]. Similarly, three conformational states are present in tobacco Rca in assemblies with about 6 subunits: ATP-bound, ADP-bound, and free [59].

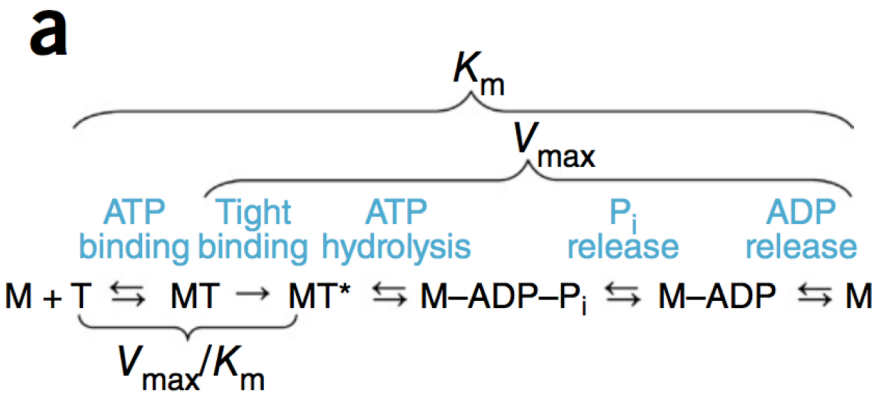

Figure 48. Scheme of the ATPase cycle in a ClpX motor. (Figure used from Rodriguez-Aliaga, P., Ramirez, L., Kim, F., Bustamante, C., and Martin, A., *Substrate-translocating loops regulate mechanochemical coupling and power production in AAA+ protease ClpXP*. Nat Struct Mol Biol, 2016. **23**(11): p. 974-981, with permission from Nature Publishing Group, page 136)

If Rca goes through a similar ATPase cycle, ATP binds, then goes through a tight binding event to produce the tight binding state. Once hydrolysis occurs, ADP is loosely bound and then is released, opening up Rca to bind another ATP molecule. This may also explain the locked conformation in the presence of ATPγS. Since ATPγS is an ATP mimic, it can bind and go through the tight binding event. However, since ATPγS is hydrolyzed extremely slowly, these sites are trapped in the tight binding state. The conformational change induced by the tight binding state may lock the subunits and prevent subunit exchange. In the hexameric ClpX, no more than four subunits can be

bound to nucleotide at one time, and it was found that two or more subunits bound to ATPγS stalled the motor [86]. If Rca is present as a hexamer, it is possible the binding of ATPγS to two or more subunits could halt subunit exchange.

Comparison of Spinach Rca to Tobacco Rca

In tobacco, the K_i value for ADP was 37 ± 7.0 μM, about one third the value of K_m for ATP, meaning tighter product binding compared with substrate [59]. This does not seem to be the case in spinach, since ADP does not inhibit ATP turnover from 0 – 180 μM. With tobacco Rca, 30% of ATPase activity is lost when 140 μM ADP is present [59], whereas in spinach Rca, 0% of activity is lost. In tobacco Rca, there is no catalytic activation by μM concentrations of ADP and 2 mM ATP, however, in ClpX, a jump in ATPase activity was seen in the presence of 100 μM ADP, suggesting ADP promotes a catalytically activated conformation [88]. In tobacco Rca, the Hill coefficient for ATP hydrolysis in the absence of ADP is 1.0, whereas in the presence of 132 μM ADP, the Hill coefficient is 1.9, suggesting the presence of ADP is critical in facilitating functional communication between subunits [59]. In spinach Rca, ADP accelerates exchange, but the relationship between subunit exchange and subunit cooperativity is not yet understood.

In tobacco, a second magnesium binding site was found that may be a co-activation site [59, 75]. Increasing free Mg^{2+} leads to cooperative binding at this site and an 8-fold increase in catalytic efficiency is seen, suggesting high magnesium may lead to formation of topologically closed hexameric rings [59], while at low magnesium, the proposed model is an open-ring hexamer, with ADP-bound, ATP-bound and free subunits. It has been proposed that the significantly increased thermostability of the

hexameric structures provides increased resistance against denaturation at higher temperatures [72]. Here, a change is not seen in the subunit exchange rate with very little free magnesium. If the second magnesium ion serves as a co-activator in spinach Rca, this may suggest the tightness of ATP binding or hydrolysis do not affect subunit exchange. Even as ADP accumulates, the lack of free magnesium does not affect subunit exchange. This may suggest subunit exchange is not affected by open vs closed ring conformations.

Subunit Rearrangements May Be Regulated by ADP

There is evidence that the activity of Rca is regulated by quaternary reorganization, where the hexamer is the most active and higher order oligomers are not very active [59]. If quaternary reorganization is regulatory, stabilized forms of Rca will respond more slowly to fluctuations in ADP and Mg. Although information is unknown on the oligomeric size, subunits must be exchanging and rearranging to change position.

In cotton Rca, low or no free magnesium promotes large aggregates, and higher than 3 mM free magnesium promotes hexamer formation [48]. Under dark conditions, ATPase activity of the chloroplast F_1F_0-ATP synthase is inhibited by Mg^{2+}-ADP to prevent wasteful ATP hydrolysis [76, 77]. Similarly, low magnesium may prevent wasteful ATP hydrolysis by Rca in dark adapted chloroplasts [59]. Taken together, these data suggest large aggregates may be storage mechanisms. In low magnesium, Rca forms large aggregates that are not very active, in order to conserve ATP for when it is needed to reactivate Rubisco.

If Rca is engineered to be more thermostable, it may slow down its rearrangement rate in response to light. We propose that light regulation of Rubisco activity may be

mediated by ADP and Mg-dependent subunit rearrangements. Although the level of ADP accumulation in leaves is unknown due to the difficulty of measuring ADP in live plants, the proposed model utilizes changes in ADP and magnesium as a regulation mechanism. During times of high light, Rca forms a closed ring hexamer ready for Rubisco reactivation. In low light, ADP increases and Mg^{2+} decreases, which forms an open ring hexamer. During the night, ADP increases, and Mg^{2+} decreases to form a large, inactive aggregates. Subunit exchange data supports more facile exchange in the presence of high ADP.

Assembly Mechanism of Spinach-β Rca

To-date, efforts in the lab to decipher the assembly mechanism of spinach-β Rca fluorescence correlation spectroscopy (FCS) has not been successful. FCS performed by Andrew Serban found all spinach-β Rca preparations to be highly polydisperse, much more so than preparations of tobacco and cotton β-Rca. The presence of large aggregates is likely a result of the much reduced thermostability of spinach compared to tobacco and cotton Rca in the presence of ADP. Efforts are being made to improve the properties of these protein preparations, and therefore the quality of the FCS data.

Future Outlook

From this work, we propose Rca subunits exchange as dimers. To prove this, an additional cysteine residue could be introduced to cross-link two subunits. The dimers could be labeled with Alexa-488 and Alexa-647, and the label mixing assay (or both mixing and dilution assays) could be performed to see if the changes in FRET are similar. If so, subunits are in fact exchanging as dimers. Subunit rearrangement may be coupled to Rubisco reactivation. To address this, the label dilution assay can be performed in the

presence of Rubisco. Further development on the Rubisco-Rca FRET binding assay may also grant insight into the relationship between subunit rearrangement and reactivation. Information on the assembly and oligomeric size under different nucleotide and divalent conditions can be used with our subunit exchange results to further understand quaternary reorganization and regulation.

CHAPTER 4

DISCUSSION

The primary carbon fixing enzyme Rubisco maintains its activity through release of trapped inhibitors by Rubisco activase (Rca). Yet, very little is understood about how the two interact. Extensive effort was made to develop FRET-based assays to understand the physical interaction between Rubisco and Rca, as well as understand subunit exchange in Rca. While the Rubisco-Rca binding FRET assay remains to be fully optimized, valuable information was determined about assay conditions, and it led to examination of the structural adjustments of Rca. In the spinach short-form Rca label dilution subunit exchange assay, it was discovered that subunit exchange is nucleotide dependent and correlated with thermostability, with ADP giving the fastest exchange, ATP giving slower exchange and ATPγS preventing exchange. Manganese, like ADP, destabilizes subunit-subunit interactions for rapid and facile exchange between oligomers. Three different types of assemblies were deduced from the rates of subunit exchange: rigid types with extremely slow dissociation of individual protomers, tight assemblies with the physiological substrate ATP, and loose assemblies that provide fast exchange due to high ADP.

Comparison Between Rca from Different Species

At a single concentration, Rca from all species is present in a variety of assembly states, dependent on species and nucleotide conditions. In fluorescence correlation spectroscopy (FCS) assembly studies in our lab, all preparations of spinach-β Rca were found to be highly polydisperse, much more so than preparations of tobacco and cotton-β Rca. The assembly mechanism of cotton was published, where hexamers are the primary

oligomer (70-80%) in the presence of ATP [48]. Preliminary FCS data shows an altered assembly mechanism of tobacco-β Rca. By analytical ultracentrifugation, wild type tobacco showed the same heterogeneous mixtures of assembly states for both Mg-ADP and Mg-ATPγS [72]. Under some conditions, hexamers may dominate at 5 μM in tobacco [72], while only 50% may be hexameric in cotton at 5 μM [48]. Stable, closed ring hexamers were seen in tobacco mutants R294V in ATP [43] and R294A in ATPγS [65]. In ATPγS, hexamers form in spinach-α, but not in spinach-β [72]. Surprisingly, a mixture of spinach α and β also forms hexamers, suggesting the α-isoform acts as a structural scaffold [72]. In cotton-β, a hexamer forms in ATPγS [48], but shows a continuous assembly to form a spiral aggregate in ADP [46]. Also in cotton-β Rca, low or no free magnesium promotes large aggregates, while higher than 3 mM free magnesium promotes hexamer formation [48]. Additionally, there is a correlation between assembly state and thermostability. It has been proposed that the significantly increased thermostability of the hexameric structures provides increased resistance against denaturation at higher temperatures [72].

At 2 μM, cotton-β Rca has a dramatic decrease in ATPase and reactivation activity compared with cotton-α Rca, while a mixture of the two isoforms showed the same activity as α-Rca [37]. Turnover rates for cotton-β in Mg^{2+} presented here (0.7 ± 0.3 min^{-1}, table 4) were approximately 5-fold lower than previously determined (3.7 ± 1.9 min^{-1}) using the same construct [48]. The exact same conditions in tobacco-β gave turnover rates of 8.3 ± 0.3 min^{-1} [59]. Tobacco Rca turnover in Mn^{2+} dropped 32-fold to 0.26 ± 0.02 min^{-1}, indicating catalytic activation is specific to magnesium coordination and is not a general divalent cation effect [59]. Seen here in spinach-β Rca, the presence

of manganese rather than magnesium does not dramatically decrease turnover rates, but instead slightly increases rates (table 7). In spinach, high thermostability is seen in ADP-AlF_x-Mg^{2+}, but surprisingly, manganese cations do not provide an equivalent stabilization, suggesting that manganese cannot coordinate to the transition state analog of hydrolysis (but can in fact coordinate to the true transition state, as shown by turnover measurements).

Although Rca from different species behaves differently kinetically and mechanistically, information gained from both FRET assays can be helpful to understand Rca from all species. Rca subunit exchange rates may be relevant to the structural adjustments generating Rubisco-binding competent conformations of Rca. In combination with assembly assays, subunit exchange assays and reactivation studies will provide critical information about the structure/function relationship of Rca in the presence of different nucleotides. This work will help to build the Rca regulation mechanism, and in turn provide valuable insight into the Rubisco reactivation mechanism.

Future Direction

Going forward, information gained about Rca subunit exchange can be used to reexamine the physical interaction between Rubisco and Rca using the FRET-binding assay. Since subunit exchange and hydrolysis occur in the presence of ATP, getting the system to provide a detectable FRET signal in ATP would be the first step. Hydrolysis is critical for Rubisco reactivation, and may also be necessary for binding. Because of the limited hydrolysis and locked conformation in ATPγS, it may prevent Rubisco-Rca binding, and therefore, reactivation. Reactivation studies in the presence of ATPγS, to

confirm Rca cannot reactivate under these conditions, would be interesting. Although ADP inhibits reactivation activity [35], binding may still occur. ADP-AlF_x is a flexible transition state analog and may provide insight into binding states. Since flexibility allows for different conformations of Rca, ADP-AlF_x may provide enough variation between subunits in assemblies to achieve a Rubisco-binding competent conformation. Even though this analog locks Rca in rigid states, the interaction with Rubisco may still occur. It is possible the conformational states are slightly different between ATPγS and ADP-AlF_x. Since it was seen that subunit exchange is more rapid and facile in manganese, reactivation and binding in the presence of manganese could be examined.

Rubisco reactivation using labeled Rubisco was not performed. Due to the minimal yields obtained by *Chlamydomonas* Rubisco purification and additional loss during the labeling reaction, sample volumes were too low to adequately inhibit using current methods. Considering the most likely binding model is side-on, where the Rca hexamer lays flat with the central pore over two Rubisco active sites [6], it is possible the C-terminal dye on Rubisco is hindering binding. Also, since labeling of wild type cotton Rubisco was non-specific, dye locations are unknown, but could also be blocking binding. Before attempting to rework the assay, reactivation studies should be performed to verify Rca can reactivate labeled Rubisco.

The dye to protein ratio also remains problematic. In order to get a decent FRET signal, most Rubisco and Rca assemblies should contain a dye, but concentrations high enough to get consistent binding will lead to concentration-dependent dye artifacts. At appropriate dye concentrations (perhaps 1 dye per 5 Rubisco holoenzymes at 25 μM and 1 dye per Rca, assumed as a hexamer), FRET would only be detected for 20% of the

binding events, and there could be significant noise. The dye and protein concentrations will need to continue to be examined. Another alteration to consider is using a single molecule approach, as a bulk measurement may be too noisy to detect a signal under these conditions.

The time course of the assay will likely need to be lengthened, and the specific excitation and emission wavelengths examined, rather than looking at full excitation and/or emission scans. Binding between Rubisco and Rca is thought to be weak and transient [36], therefore, it is likely a binding event could happen on a second-long time scale rather than minutes, and perhaps with significant amounts of time between events. Now that it is known subunit exchange (and quaternary reorganization) occurs on an hour-long time scale, the Rubisco-Rca interaction assay can be altered to hopefully catch the occurrences of binding.

Much of the FRET-binding assay development was performed with cotton Rubisco and cotton Rca, which are known to not reactivate efficiently together. Since preliminary work has already been done on *Chlamydomonas* Rubisco and spinach-β Rca, they can easily be introduced to the binding assay to see if any results change or FRET is seen. Efforts are underway in the Wachter lab to understand assembly in tobacco Rca, and this information could be beneficial to the subunit exchange experiments. Using a range of concentrations that give primarily one assembly state could provide information on which oligomer may bind to Rubisco. In this case, tobacco Rubisco must also be prepared and labeled, as tobacco Rca cannot reactivate cotton, Chlamy or spinach Rubisco.

Even if no change in FRET is seen within a condition in the Rubisco-Rca binding assay, comparing the level of FRET over a range of nucleotides may lead to important binding information. For example, if the baseline level of FRET in ATP-Mg^{2+} samples is double that of ATPγS- Mg^{2+} samples, it would suggest binding is more stable in the presence of ATP. Previously, in the binding assay, extensive controls were performed imitating dye concentrations of labeled protein, but they were never identical conditions. By using the subunit exchange assay methodology of the exact same labeled protein conditions with only nucleotide or divalent as the variable, much more relevant information can be learned. This will require a much greater yield of Rubisco, which is currently being addressed in the lab using both mutated *Chlamydomonas* and wild-type tobacco plants.

To further understand subunit exchange in Rca, unlabeled, inhibited Rubisco could be introduced into the subunit exchange assay to see if exchange is altered when Rca is performing its reactivation duties. Since spinach Rca in leaves is comprised of about 50% α– and 50% β–isoforms [72], a mix of the two would be interesting to examine. In our lab, extensive efforts were made to isolate 100% oxidized and 100% reduced spinach-α, with very little success, but a mix of the two isoforms may provide insight into subunit exchange in physiologically relevant conditions.

There is a lack of knowledge of relevant Rca states and stoichiometries of Rubisco-bound species. Once this assay is fully optimized, binding constants can be determined and specific Rca residues that make direct contact with Rubisco can be identified by using truncation variants and mutations. This binding assay will provide insight into Rca states able to interact with Rubisco, as well as define conditions to

generate bound states for structural analysis, a step in deciphering the Rubisco reactivation mechanism.

REFERENCES

1. Melillo, J.M., Richmond, T., Yohe, G. W., *Climate Change Impacts in the United States: The Third National Climate Assessment*, U.S.G.C.R. Program, Editor. 2014.

2. Andersson, I. and Backlund, A., *Structure and function of Rubisco.* Plant Physiology and Biochemistry, 2008. **46**: p. 275-291.

3. Kitano, K., Maeda, N., Fukui, T., Atomi, H., Imanaka, T., and Miki, K., *Crystal Structure of a Novel-Type Archaeal Rubisco with Pentagonal Symmetry.* Structure, 2001. **9**(6): p. 473-481.

4. Ashida, H., Danchin, A., and Yokota, A., *Was photosynthetic RuBisCO recruited by acquisitive evolution from RuBisCO-like proteins involved in sulfur metabolism?* Research in Microbiology, 2005. **156**(5): p. 611-618.

5. Maeda, N., Kitano, K., Fukui, T., Ezaki, S., Atomi, H., Miki, K., and Imanaka, T., *Ribulose bisphosphate carboxylase/oxygenase from the hyperthermophilic archaeon Pyrococcus kodakaraensis KOD1 is composed solely of large subunits and forms a pentagonal structure1.* Journal of Molecular Biology, 1999. **293**(1): p. 57-66.

6. Wachter, R.M., Salvucci, M.E., Carmo-Silva, A.E., Barta, C., Genkov, T., and Spreitzer, R.J., *Activation of interspecies-hybrid Rubisco enzymes to assess different models for the Rubisco-Rubisco activase interaction.* Photosynth. Res., 2013. **117**: p. 557-566.

7. Spreitzer, R.J., *Role of the small subunit in ribulose-1,5-bisphosphate carboxylase/oxygenase.* Archives of Biochemistry and Biophysics, 2003. **414**(2): p. 141-149.

8. Tabita, F.R., *Microbial ribulose 1, 5-bisphosphate carboxylase/oxygenase: a different perspective.* Photosynthesis Research, 1999. **60**(1): p. 1-28.

9. Delwiche, C.F. and Palmer, J.D., *Rampant horizontal transfer and duplication of Rubisco genes in eubacteria and plastids.* Molecular Biology and Evolution, 1996. **13**(6): p. 873-882.

10. Joshi, J., Mueller-Cajar, O., Tsai, Y.-C.C., Hartl, F.U., and Hayer-Hartl, M., *Role of Small Subunit in Mediating Assembly of Red-type Form 1 Rubisco.* Journal of Biological Chemistry, 2014.

11. Falkowski, P.G., Katz, M.E., Knoll, A.H., Quigg, A., Raven, J.A., Schofield, O., and Taylor, F.J.R., *The Evolution of Modern Eukaryotic Phytoplankton.* Science, 2004. **305**(5682): p. 354-360.

12. Whitney, S.M., Baldet, P., Hudson, G.S., and Andrews, T.J., *Form I Rubiscos from non-green algae are expressed abundantly but not assembled in tobacco chloroplasts.* The Plant Journal, 2001. **26**(5): p. 535-547.

13. Whitney, S.M., Houtz, R.L., and Alonso, H., *Advancing Our Understanding and Capacity to Engineer Nature's CO2-Sequestering Enzyme, Rubisco.* Plant Physiology, 2011. **155**(1): p. 27-35.

14. Taylor, T.C. and Andersson, I., *Structural transitions during activation and ligand binding in hexadecameric Rubisco inferred from the crystal structure of the activated unliganded spinach enzyme.* Nat. Struct. Biol., 1996. **3**: p. 95-101.

15. Spreitzer, R.J. and Salvucci, M.E., *Rubisco: Structure, regulatory interactions, and possibilities for a better enzyme.* Annu. Rev. Plant Biol., 2002. **53**: p. 449-475.

16. Lorimer, G.H.M., H. M. , *Carbamate formation on the epsilon-amino group of a lysyl residue as the basis for the activation of ribulosebisphosphate carboxylase by CO2 and Mg2+.* Biochemistry, 1980. **19**: p. 5321-8.

17. Parry, M.A.J., Keys, A.J., Madgwick, P.J., Carmo-Silva, A.E., and Andralojc, P.J., *Rubisco regulation: a role for inhibitors.* Journal of Experimental Botany, 2008. **59**(7): p. 1569-1580.

18. Prasad, M.N.V. and Prasad, M.R.N., *Plant Ecophysiology*. 1997: Wiley.

19. Griffiths, H., *Plant biology: Designs on Rubisco.* Nature, 2006. **441**(7096): p. 940-941.

20. Jordan, D.B. and Chollet, R., *Inhibition of ribulose bisphosphate carboxylase by substrate ribulose 1,5-bisphosphate.* Journal of Biological Chemistry, 1983. **258**(22): p. 13752-8.

21. Gutteridge, S., Parry, M.A.J., Burton, S., Keys, A.J., Mudd, A., Feeney, J., Servaites, J.C., and Pierce, J., *A nocturnal inhibitor of carboxylation in leaves.* Nature, 1986. **324**(6094): p. 274-276.

22. Zhu, G.H. and Jensen, R.G., *XYLULOSE 1,5-BISPHOSPHATE SYNTHESIZED BY RIBULOSE 1,5-BISPHOSPHATE CARBOXYLASE OXYGENASE DURING CATALYSIS BINDS TO DECARBAMYLATED ENZYME.* Plant Physiology, 1991. **97**(4): p. 1348-1353.

23. Medrano, H., Parry, M.A.J., Socias, X., and Lawlor, D.W., *Long term water stress inactivates Rubisco in subterranean clover.* Annals of Applied Biology, 1997. **131**(3): p. 491-501.

24. Pearce, F.G. and Andrews, T.J., *The relationship between side reactions and slow inhibition of ribulose-bisphosphate carboxylase revealed by a loop 6 mutant of the Tobacco enzyme.* J. Biol. Chem., 2003. **278**: p. 32526-32536.

25. Kim, K. and Portis, A.R., *Oxygen-dependent H2O2 production by Rubisco.* FEBS Lett., 2004. **571**: p. 124-128.

26. Andersson, I., *Catalysis and regulation in Rubisco.* J. Exp. Bot., 2008. **59**: p. 1555-1568.

27. Salvucci, M.E., Rajagopalan, K., Sievert, G., Haley, B.E., and Watt, D.S., *Photoaffinity labeling of ribulose-1,5-bisphosphate carboxylase/oxygenase activase with ATP gamma-benzophenone. Identification of the ATP gamma-phosphate binding domain.* Journal of Biological Chemistry, 1993. **268**(19): p. 14239-14244.

28. van de Loo, F.J. and Salvucci, M.E., *Involvement of two aspartate residues of Rubisco activase in coordination of the ATP-g-phosphate and subunit cooperativity.* Biochemistry, 1998. **37**: p. 4621-4625.

29. Ogura, T., Whiteheart, S.W., and Wilkinson, A.J., *Conserved arginine residues implicated in ATP hydrolysis, nucleotide sensing, and inter-subunit interactions in AAA and AAA+ ATPases.* J. Struct. Biol., 2004. **146**: p. 106-112.

30. Li, C., Salvucci, M.E., and Portis, A.R.J., *Two residues of Rubisco activase involved in recognition of the Rubisco substrate.* J. Biol. Chem., 2005. **280**: p. 24864-24869.

31. Salvucci, M.E., Chavan, A.J., Klein, R.R., Rajagopolan, K., and Haley, B.E., *Photoaffinity labeling of the ATP binding domain of Rubisco activase and a separate domain involved in the activation of ribulose-1,5-bisphosphate carboxylase/oxygenase.* Biochemistry, 1994. **33**(49): p. 14879-14886.

32. Tsai, Y.-C.C., Lapina, M.C., Bhushan, S., and Mueller-Cajar, O., *Identification and characterization of multiple rubisco activases in chemoautotrophic bacteria.* Nature Communications, 2015. **6**: p. 8883.

33. Mueller-Cajar, O., Stotz, M., and Bracher, A., *Maintaining photosynthetic CO2 fixation via protein remodelling: the Rubisco activases.* Photosynth. Res., 2013. **119**: p. 191-201.

34. Mueller-Cajar, O., Stotz, M., Wendler, P., Hartl, F.U., Bracher, A., and Hayer-Hartl, M., *Structure and function of the AAA+ protein CbbX, a red-type Rubisco activase.* Nature, 2011. **479**: p. 194-199.

35. Robinson, S.P. and Portis, A.R., *Adenosine triphosphate hydrolysis by purified rubisco activase.* Archives of Biochemistry and Biophysics, 1989. **268**(1): p. 93-99.

36. Portis, A.R., *Rubisco activase - Rubisco's catalytic chaperone.* Photosynth. Res., 2003. **75**: p. 11-27.

37. Salvucci, M.E., van de Loo, F.J., and Stecher, D., *Two isoforms of Rubisco activase in cotton, the products of separate genes not alternative splicing.* Planta, 2003. **216**: p. 736-744.

38. Crafts-Brandner, S.J., van de Loo, F.J., and Salvucci, M.E., *The two forms of ribulose-1,5-bisphosphate carboxylase/oxygenase activase differ in sensitivity to elevated temperature.* Plant Physiol., 1997. **114**: p. 439-444.

39. Shen, J.B., Orozco, E.M., and Ogren, W.L., *Expression of the two isoforms of spinach ribulose 1,5-bisphosphate carboxylase activase and essentiality of the conserved lysine in the consensus nucleotide-binding domain.* Journal of Biological Chemistry, 1991. **266**(14): p. 8963-8968.

40. Zhang, N., Schuermann, P., and Portis, A.R.J., *Characterization of the regulatory function of the 46-kD isoform of Rubisco activase from Arabidopsis.* Photosynth. Res., 2001. **68**: p. 29-37.

41. Wang, D. and Portis, A.R., *Increased sensitivity of oxidized large isoform of ribulose-1,5-bisphosphate carboxylase/oxygenase (Rubisco) activase to ADP inhibition is due to an interaction between its carboxyl extension and nucleotide-binding pocket.* Journal of Biological Chemistry, 2006. **281**(35): p. 25241-25249.

42. Henderson, J.N., Kuriata, A.M., Fromme, R., Salvucci, M.E., and Wachter, R.M., *Atomic resolution X-ray structure of the substrate recognition domain of higher plant ribulose-bisphosphate carboxylase/oxygenase (Rubisco) activase.* J. Biol. Chem., 2011. **286**: p. 35683-35688.

43. Stotz, M., Mueller-Cajar, O., Ciniawsky, S., Wendler, P., Hartl, F.U., Bracher, A., and Hayer-Hartl, M., *Structure of green-type Rubisco activase from tobacco.* Nat. Struct. Mol. Biol., 2011. **18**: p. 1366-1370.

44. Smith, G.R., Contreras-Moreira, B., Zhang, X., and Bates, P.A., *A link between sequence conservation and domain motion within the AAA+ family.* J. Struct. Biol., 2004. **146**: p. 189-204.

45. Hasse, D., Larsson, A.M., and Andersson, I., *Structure of Arabidopsis thaliana Rubisco activase.* Acta Crystallogr., 2015. **D71**: p. 800-808.

46. Chakraborty, M., Kuriata, A.M., Henderson, J.N., Salvucci, M.E., Wachter, R.M., and Levitus, M., *Protein oligomerization monitored by fluorescence fluctuation*

spectroscopy: Self-assembly of rubisco activase. Biophys. J., 2012. **103**: p. 949-958.

47. Henderson, J.N., Hazra, S., Dunkle, A.M., Salvucci, M.E., and Wachter, R.M., *Biophysical characterization of higher plant Rubisco activase.* Biochim. Biophys. Acta, 2013. **1834**(1): p. 87-97.

48. Kuriata, A.M., Chakraborty, M., Henderson, J.N., Hazra, S., Serban, A.J., Pham, T.V.T., Levitus, M., and Wachter, R.M., *ATP and magnesium promote cotton short-form ribulose-1,5-bisphosphate carboxylase/oxygenase (Rubisco) activase hexamer formation at low micromolar concentrations.* Biochemistry, 2014. **53**: p. 7232-7246.

49. Crafts-Brandner, S.J. and Salvucci, M.E., *Rubisco activase constrains the photosynthetic potential of leaves at high temperature and CO2.* Proc. Natl. Acad. Sci. USA, 2000. **97**: p. 13430-13435.

50. Salvucci, M.E. and Crafts-Brandner, S.J., *Relationship between the heat tolerance of photosynthesis and the thermal stability of rubisco activase in plants from contrasting thermal environments.* Plant Physiol., 2004. **134**: p. 1460-1470.

51. Feller, U., Crafts-Brandner, S.J., and Salvucci, M.E., *Moderately high temperatures inhibit ribulose-1,5-bisphosphate carboxylase/oxygenase (Rubisco) activase-mediated activation of Rubisco.* Plant Physiol., 1998. **116**(2): p. 539-546.

52. Barta, C., Dunkle, A.M., Wachter, R.M., and Salvucci, M.E., *Structural changes associated with the acute thermal instability of Rubisco activase.* Arch. Biochem. Biophys., 2010. **499**: p. 17-25.

53. Glynn, S.E., Martin, A., Nager, A.R., Baker, T.A., and Sauer, R.T., *Structures of asymmetric ClpX hexamers reveal nucleotide-dependent motions in a AAA+ protein unfolding machine.* Cell, 2009. **139**: p. 144-756.

54. Hersch, G.L., Burton, R.E., Bolon, D.N., Baker, T.A., and Sauer, R.T., *Asymmetric interactions of ATP with the AAA+ ClpX6 unfoldase: Allosteric control of a protein machine.* Cell, 2005. **121**: p. 1017-1027.

55. Bochtler, M., Hartmann, C., Song, H.K., Bourenkov, G.P., Bartunik, H.D., and Huber, R., *The structures of HslU and the ATP-dependent protease HslU-HslV.* Nature, 2000. **403**: p. 800-805.

56. Wang, J., Song, J.J., Franklin, M.C., Kamtekar, S., Im, Y.J., Rho, S.H., Seong, I.S., Lee, C.S., Chung, C.H., and Eom, S.H., *Crystal structures of the HslVU peptidase-ATPase complex reveal an ATP-dependent proteolysis mechanism.* Structure, 2001. **9**: p. 177-184.

57. Wang, J., Song, J.J., Seong, I.S., Franklin, M.C., Kamtekar, S., Eom, S.H., and Chung, C.H., *Nucleotide-dependent conformational changes in a protease-associated ATPase HslU.* Structure, 2001. **9**: p. 1107-1116.

58. Stinson, B.M., Nager, A.R., Glynn, S.E., Schmitz, K.R., Baker, T.A., and Sauer, R.T., *Nucleotide binding and conformational switching in the hexameric ring of a AAA+ machine.* Cell, 2013. **153**: p. 628-639.

59. Hazra, S., Henderson, J.N., Liles, K., Hilton, M.T., and Wachter, R.M., *Regulation of ribulose-1,5-bisphosphate carboxylase/oxygenase (Rubisco) activase: Product inhibition, cooperativity, and magnesium activation.* J. Biol. Chem., 2015. **290**(40): p. 24222-24236.

60. Wang, Z.Y., Snyder, G.W., Esau, B.D., Portis, A.R., and Ogren, W.L., *Species-dependent variation in the interaction of substrate-bound ribulose-1,5-bisphosphate carboxylase oxygenase (Rubisco) and Rubisco activase.* Plant Physiol., 1992. **100**(4): p. 1858-1862.

61. Lan, Y. and Mott, K.A., *Determination of apparent Km values for ribulose 1,5-bisphosphate carboxylase/oxygenase (Rubisco) activase using the spectrophotometric assay of Rubisco activity.* Plant Physiol., 1991. **95**: p. 604-609.

62. Robinson, S.P., Streusand, V.J., Chatfield, J.M., and Portis, A.R., *Purification and Assay of Rubisco Activase from Leaves.* Plant Physiology, 1988. **88**(4): p. 1008-1014.

63. Keown, J.R., Griffin, M.D.W., Mertens, H.D.T., and Pearce, F.G., *Small oligomers of ribulose-bisphosphate carboxylase/oxygenase (Rubisco) activase are required for biological activity.* J. Biol. Chem., 2013. **288**(28): p. 20607-20615.

64. Li, C., Wang, D., and Portis, A.R.J., *Identification of critical arginine residues in the functioning of Rubisco activase.* Arch. Biochem. Biophys., 2006. **450**: p. 176-182.

65. Blayney, M.J., Whitney, S.M., and Beck, J.L., *NanoESI mass spectrometry of Rubisco and Rubisco activase structures and their interactions with nucleotides and sugar phosphates.* J. Am. Soc. Mass Spectrum, 2011. **22**: p. 1588-1601.

66. van de Loo, F.J. and Salvucci, M.E., *Activation of ribulose-1,5-bisphosphate carboxylase/oxygenase (Rubisco) involves Rubisco activase Trp16.* Biochemistry, 1996. **35**: p. 8143-8148.

67. Marin-Navarro, J. and Moreno, J., *Cysteine 449 and 459 modulate the reduction-oxidation conformational changes of ribulose 1,5-bisphosphate carboxylase/oxygenase and the translocation of the enzyme to membranes during stress.* Plant, Cell and Environment, 2006. **29**: p. 898-908.

68. Salvucci, M.E., *Potential for interactions between the carboxy- and amino-termini of Rubisco activase subunits.* FEBS Lett., 2004. **560**: p. 205-209.

69. *Alexa Fluor® 488 Protein Labeling Kit* 2006: Molecular Probes Product Information.

70. Webb, M.R., *A continuous spectrophotometric assay for inorganic phosphate and for measuring phosphate release kinetics in biological systems* Proc. Nat. Acad. Sci. USA, 1992. **89**(11): p. 4884-4887.

71. Dhar, A., Samiotakis, A., Ebbinghaus, S., Nienhaus, L., Homouz, D., Gruebele, M., and Cheung, M.S., *Structure, function, and folding of phosphoglycerate kinase are strongly perturbed by macromolecular crowding.* Proc. Nat. Acad. Sci. USA, 2010. **107**(41): p. 17586-17591.

72. Keown, J.R. and Pearce, F.G., *Structural characterization of spinach ribulose-1,5-biophosphate carboxylase/oxygenase activase isoforms reveals hexameric assemblies with increased thermal stability.* Biochem. J., 2014. **464**: p. 413-423.

73. Salvucci, M.E., Werneke, J.M., Ogren, W.L., and Portis, A.R., *Purification and Species Distribution of Rubisco Activase.* Plant Physiology, 1987. **84**(3): p. 930-936.

74. Carmo-Silva, A.E. and Salvucci, M.E., *The activity of Rubisco's molecular chaperone, Rubisco activase, in leaf extracts.* Photosynthesis Research, 2011. **108**(2-3): p. 143-155.

75. Frasch, W.D., Spano, M., and LoBrutto, R., *VO2+ as a probe of metal binding sites in Rubisco activase*, in *Photosynthesis: From Light to Biosphere*, P. Mathis, Editor. 1995, Kluwer Academic Publishers: Netherlands. p. 257-260.

76. Digel, J.G., Moore, N.D., and McCarty, R.E., *Influence of Divalent Cations on Nucleotide Exchange and ATPase Activity of Chloroplast Coupling Factor 1.* Biochemistry, 1998. **37**(49): p. 17209-17215.

77. Keis, S., Stocker, A., Dimroth, P., and Cook, G.M., *Inhibition of ATP Hydrolysis by Thermoalkaliphilic F(1)F(o)-ATP Synthase Is Controlled by the C Terminus of the ε Subunit.* Journal of Bacteriology, 2006. **188**(11): p. 3796-3804.

78. Baker, R.T., Catanzariti, A.M., Karunasekara, Y., Soboleva, T.A., Sharwood, R., Whitney, S., and Board, P.G., *Using deubiquitylating enzymes as research tools*, in *Ubiquitin and Protein Degradation, Part A*, R.J. Deshaies, Editor. 2005. p. 540-554.

79. Catanzariti, A.M., Soboleva, T.A., Jans, D.A., Board, P.G., and Baker, R.T., *An efficient system for high-level expression and easy purification of authentic recombinant proteins.* Protein Science, 2004. **13**(5): p. 1331-1339.

80. Smith, P.K., Krohn, R.I., Hermanson, G.T., Mallia, A.K., Gartner, F.H., Provenzano, M.D., Fujimoto, E.K., Goeke, N.M., Olson, B.J., and Klenk, D.C., *Measurement of protein using bicinchoninic acid.* Anal. Biochem., 1985. **150**: p. 76-85.

81. Xu, H., Gu, B.H., Nixon, B.T., and Hoover, T.R., *Purification and characterization of the AAA+ domain of Sinorhizobium meliloti DctD, a sigma(54)-dependent transcriptional activator.* Journal of Bacteriology, 2004. **186**(11): p. 3499-3507.

82. Lee, N.K., Kapanidis, A.N., Wang, Y., Michalet, X., Mukhopadhyay, J., Ebright, R.H., and Weiss, S., *Accurate FRET measurements within single diffusing biomolecules using alternating-laser excitation.* Biophysical Journal, 2005. **88**(4): p. 2939-2953.

83. Salvucci, M.E., *Subunit interactions of Rubisco activase - polyethylene glycol promotes self-association, stimulates ATPase and activation activities, and enhances interactions with Rubisco.* . Arch. Biochem. Biophys., 1992. **298**: p. 688-696.

84. Lambert, C.R. and Kochevar, I.E., *Electron Transfer Quenching of the Rose Bangal Triplet State.* Photochem. Photobiol., 1997. **66**: p. 15-25.

85. Hazra, S. and Wachter, R., *Unpublished Work*. 2015.

86. Rodriguez-Aliaga, P., Ramirez, L., Kim, F., Bustamante, C., and Martin, A., *Substrate-translocating loops regulate mechanochemical coupling and power production in AAA+ protease ClpXP.* Nat Struct Mol Biol, 2016. **23**(11): p. 974-981.

87. Sen, M., Maillard, R.A., Nyquist, K., Rodriguez-Aliaga, P., Presse, S., Martin, A., and Bustamante, C., *The ClpXP Protease Unfolds Substrates Using a Constant Rate of Pulling but Different Gears.* Cell, 2013. **155**(3): p. 636-646.

88. Stinson, B.M., Baytshtok, V., Schmitz, K.R., Baker, T.A., and Sauer, R.T., *Subunit asymmetry and roles of conformational switching in the hexameric AAA+ ring of ClpX.* Nat. Struct. Mol. Biol., 2015. **22**: p. 411-416.

89. Kennis, J.T.M., van Stokkum, I.H.M., Peterson, D.S., Pandit, A., and Wachter, R.M., *Ultrafast Proton Shuttling in Psammocora Cyan Fluorescent Protein.* J. Phys. Chem. B, 2013. **117**(38): p. 11134-11143.

90. Alieva, N.O., Konzen, K.A., Field, S.F., Meleshkevitch, E.A., Hunt, M.E., Beltran-Ramirez, V., Miller, D.J., Wiedenmann, J., Salih, A., and Matz, M.V., *Diversity and evolution of coral fluorescent proteins.* PLoS ONE, 2008. **3**: p. e2680.

91. Chudakov, D.M., Matz, M.V., Lukyanov, S., and Lukyanov, K.A., *Fluorescent proteins and their applications in imaging living cells and tissues.* Physiol Rev, 2010. **90**(3): p. 1103-63.

92. Tsien, R.Y., *The Green Fluorescent Protein.* Ann. Rev. Biochem., 1998. **67**: p. 509-544.

93. Markwardt, M.L., Kremers, G.-J., Kraft, C.A., Ray, K., Cranfill, P.J.C., Wilson, K.A., Day, R.N., Wachter, R.M., Davidson, M.W., and Rizzo, M.A., *An Improved Cerulean Fluorescent Protein with Enhanced Brightness and Reduced Reversible Photoswitching.* PLoS ONE, 2011. **6**(3).

94. Watkins, J.L., Kim, H., Markwardt, M.L., Chen, L., Fromme, R., Rizzo, M.A., and Wachter, R.M., *The 1.6 A resolution structure of a FRET-optimized Cerulean fluorescent protein.* Acta Crystallographica Section D, 2013. **69**(5): p. 767-773.

95. Goedhart, J., von Stetten, D., Noirclerc-Savoye, M., Lelimousin, M., Joosen, L., Hink, M.A., van Weeren, L., Gadella, T.W.J., and Royant, A., *Structure-guided evolution of cyan fluorescent proteins towards a quantum yield of 93%.* Nat. Communications, 2012. **3**: p. 1738/1-1738/9.

96. Kogure, T., Kawano, H., Abe, Y., and Miyawaki, A., *Fluorescence imaging using a fluorescent protein with a large Stokes shift.* Methods, 2008. **45**: p. 223-226.

97. Ai, H.W., Henderson, J.N., Remington, S.J., and Campbell, R.E., *Directed evolution of a monomeric, bright and photostable version of Clavularia cyan fluorescent protein: structural characterization and applications in fluorescence imaging.* Biochem. J., 2006. **400**: p. 531-540.

98. Carlson, H.J. and Campbell, R.E., *Genetically encoded FRET-based biosensors for multiparameter fluorescence imaging.* Curr. Opin. Biotechnol., 2009. **20**: p. 19-27.

99. Chattoraj, M., King, B.A., Bublitz, G.U., and Boxer, S.G., *Ultra-fast excited state dynamics in Green Fluorescent Protein: Multiple states and proton transfer.* Proc. Natl. Acad. Sci. USA, 1996. **93**: p. 8362-8367.

100. Winkler, K., Lindner, J.R., Subramaniam, V., Jovin, T.M., and Vohringer, P., *Ultrafast dynamics in the excited state of green fluorescent protein (wt) studied by frequency-resolved femtosecond pump-probe spectroscopy.* Physical Chemistry Chemical Physics, 2002. **4**(6): p. 1072-1081.

101. Kennis, J.T.M., Larsen, D.S., van Stokkum, I.H.M., Vengris, M., van Thor, J.J., and van Grondelle, R., *Uncovering the hidden ground state of green fluorescent protein.* Proceedings of the National Academy of Sciences of the United States of America, 2004. **101**(52): p. 17988-17993.

102. Creemers, T.M.H., Lock, A.J., Subramaniam, V., Jovin, T.M., and Volker, S., *Three photoconvertible forms of green fluorescent protein identified by spectral hole-burning.* Nat. Struct. Biol., 1999. **6**: p. 557-560.

103. Brejc, K., Sixma, T.K., Kitts, P.A., Kain, S.R., Tsien, R.Y., Ormö, M., and Remington, S.J., *Structural basis for dual excitation and photoisomerization of the Aequorea victoria Green Fluorescent Protein. Proc. Natl. Acad. Sci. USA.*, 1997. **94**: p. 2306-2311.

104. Toh, K.C., Stojković, E.A., van Stokkum, I.H.M., Moffat, K., and Kennis, J.T.M., *Proton-transfer and hydrogen-bond interactions determine fluorescence quantum yield and photochemical efficiency of bacteriophytochrome.* Proceedings of the National Academy of Sciences, 2010. **107**(20): p. 9170-9175.

105. Toh, K.C., Stojkovic, E.A., van Stokkum, I.H.M., Moffat, K., and Kennis, J.T.M., *Fluorescence quantum yield and photochemistry of bacteriophytochrome constructs.* Physical Chemistry Chemical Physics, 2011. **13**(25): p. 11985-11997.

106. Carroll, E.C., Song, S.-H., Kumauchi, M., van Stokkum, I.H.M., Jailaubekov, A., Hoff, W.D., and Larsen, D.S., *Subpicosecond Excited-State Proton Transfer Preceding Isomerization During the Photorecovery of Photoactive Yellow Protein.* The Journal of Physical Chemistry Letters, 2010. **1**(19): p. 2793-2799.

107. Kennis, J.T.M., Crosson, S., Gauden, M., van Stokkum, I.H.M., Moffat, K., and van Grondelle, R., *Primary Reactions of the LOV2 Domain of Phototropin, a Plant Blue-Light Photoreceptor.* Biochemistry, 2003. **42**(12): p. 3385-3392.

108. Mathes, T., van Stokkum, I.H.M., Stierl, M., and Kennis, J.T.M., *Redox Modulation of Flavin and Tyrosine Determines Photoinduced Proton-coupled Electron Transfer and Photoactivation of BLUF Photoreceptors.* Journal of Biological Chemistry, 2012. **287**(38): p. 31725-31738.

109. Toh, K.C., van Stokkum, I.H.M., Hendriks, J., Alexandre, M.T.A., Arents, J.C., Perez, M.A., van Grondelle, R., Hellingwerf, K.J., and Kennis, J.T.M., *On the signaling mechanism and the absence of photoreversibility in the AppA BLUF domain.* Biophysical Journal, 2008. **95**(1): p. 312-321.

110. Gauden, M., van Stokkum, I.H.M., Key, J.M., Luehrs, D.C., Van Grondelle, R., Hegemann, P., and Kennis, J.T.M., *Hydrogen-bond switching through a radical pair mechanism in a flavin-binding photoreceptor.* Proceedings of the National Academy of Sciences of the United States of America, 2006. **103**(29): p. 10895-10900.

111. Bonetti, C., Mathes, T., van Stokkum, I.H.M., Mullen, K.M., Groot, M.-L., van Grondelle, R., Hegemann, P., and Kennis, J.T.M., *Hydrogen Bond Switching among Flavin and Amino Acid Side Chains in the BLUF Photoreceptor Observed*

by Ultrafast Infrared Spectroscopy. Biophysical Journal, 2008. **95**(10): p. 4790-4802.

112. Kennis, J.T.M. and Groot, M.-L., *Ultrafast spectroscopy of biological photoreceptors.* Current Opinion in Structural Biology, 2007. **17**(5): p. 623-630.

113. Immeln, D., Weigel, A., Kottke, T., and Pérez Lustres, J.L., *Primary Events in the Blue Light Sensor Plant Cryptochrome: Intraprotein Electron and Proton Transfer Revealed by Femtosecond Spectroscopy.* Journal of the American Chemical Society, 2012. **134**(30): p. 12536-12546.

114. Mathes, T., van Stokkum, I.H.M., Bonetti, C., Hegemann, P., and Kennis, J.T.M., *The Hydrogen-Bond Switch Reaction of the Blrb Bluf Domain of Rhodobacter sphaeroides.* The Journal of Physical Chemistry B, 2011. **115**(24): p. 7963-7971.

115. Gauden, M., Grinstead, J.S., Laan, W., van Stokkum, I.H.M., Avila-Perez, M., Toh, K.C., Boelens, R., Kaptein, R., van Grondelle, R., Hellingwerf, K.J., and Kennis, J.T.M., *On the Role of Aromatic Side Chains in the Photoactivation of BLUF Domains.* Biochemistry, 2007. **46**(25): p. 7405-7415.

116. Malo, G.D., Wang, M., Wu, D., Stelling, A.L., Tonge, P.J., and Wachter, R.M., *Crystal structure and Raman studies of dsFP483, a cyan fluorescent protein from Discosoma striata.* J. Mol. Biol., 2008. **378**: p. 869-884.

117. Remington, S.J., Wachter, R.M., Yarbrough, D.K., Branchaud, B.P., Anderson, D.C., Kallio, K., and Lukyanov, K.A., *zFP538, a yellow fluorescent protein from Zoanthus, contains a novel three-ring chromophore.* Biochemistry, 2005. **44**: p. 202-212.

118. Pletneva, N., Pletnev, V., Tikhonova, T., Pakhomov, A.A., Popov, V., Martynov, V.I., Wlodawer, A., Dauter, Z., and Pletnev, S., *Refined crystal structures of red and green fluorescent proteins from the button polyp Zoanthus.* Acta Crystallographica Section D, 2007. **63**(10): p. 1082-1093.

119. Henderson, J.N. and Remington, S.J., *Crystal structures and mutational analysis of amFP486, a cyan fluorescent protein from Anemonia majano.* Proc. Natl. Acad. Sci. USA, 2005. **102**: p. 12712-12717.

120. Field, S.F., Bulina, M.Y., Kelmanson, I.V., Bielawski, J.P., and Matz, M.V., *Adaptive evolution of multicolored fluorescent proteins in reef-building corals.* J. Mol. Evol., 2006. **62**: p. 332-339.

APPENDIX A

BIOCHEMICAL CHARACTERIZATION OF A NOVEL CYAN FLUORESCENT PROTEIN, PSAMFP488

INTRODUCTION

Cyan, green, yellow, and red fluorescent proteins (FPs) homologous to green fluorescent protein (GFP) are used extensively as model systems to study fundamental processes in photobiology, such as the capture of light energy by protein-embedded chromophores, color tuning by the protein matrix, energy conversion by Förster resonance energy transfer (FRET), and excited-state proton transfer (ESPT) reactions. Cyan fluorescent proteins (CFPs) derived from marine organisms of the class Anthozoa bear a chromophore chemically identical to that found in GFP. However, their emission spectra are blue-shifted from the default green state. Typically, members of the cyan color class exhibit absorption maxima from 430 to 460 nm and emission maxima from 474 to 496 nm [90, 91]. Recently, a novel cyan fluorescent protein (CFP), termed psamFP488 in this work, was isolated from the genus *Psammocora* of reef building corals (order *Scleractinia*, family *Siderastreidae*) [90]. Surprisingly, psamFP488 is one of only two proteins that were reported to display a substantially blue-shifted, broad absorption maximum around 404 nm, whereas the emission maximum was found to be within the range of colors reported for other CFPs [90, 91]. Therefore, within its color class, psamFP488 appears to be one of only two CFPs known to exhibit a significantly extended Stokes shift. GFP-like proteins with similar excitation maxima include the

highly engineered tagBFP (λ_{ex} = 402 nm) with blue emission at 457 nm, and avGFP (*Aquorea victoria* GFP, λ_{ex} = 398 nm) with green emission at 508 nm [92]. CFPs with similar emission maxima include the engineered mTFP1 protein (λ_{em} = 492 nm), which has an absorption band centered on 462 nm. In addition, more blue-shifted CFPs have been developed that bear non-native chromophores derived from a tryptophan residue. These include the cerulean and turquoise line of variants [93-95], highly engineered proteins that absorb at ~433 nm and emit at ~475 nm.

CFPs with a large Stokes shift may prove useful in some types of live-cell imaging applications, such as dual color monitoring by excitation of two different FPs at the same wavelength [96]. In particular, an extended Stokes shift may be beneficial in FRET experiments frequently used to monitor macromolecular proximity on a subcellular level. To-date, the most common FP pairs used in FRET experiments involve CFPs and yellow fluorescent proteins (YFPs). PsamFP488 may prove advantageous as a donor fluorophore in combination with acceptors such as Venus or mOrange [97], as cross-excitation would be minimized due to the large separation of excitation and emission wavelengths. Notably, the sensitivity of multiparameter live cell imaging involving two FRET pairs with fine-tuned optical properties could be enhanced by the high quantum yield of psamFP488 when using an excitation wavelength provided by a 405 nm laser line [98].

GFP and many of its variants exhibit large Stokes shifts that find their origin in an ESPT process that results in deprotonation of the chromophore and subsequent fluorescence emission from the anionic chromophore [92, 99-103]. Recently, ESPT appears to be a frequently occurring feature in photoreceptor proteins [104-107],

sometimes coupled to electron transfer [108-115]. With its simple light-driven proton transfer reaction along a chain of a water molecule and two amino acids, GFP can be regarded as an attractive and compact model system to understand the basic principles of proton transfer in biological systems.

The origin of the large Stokes shift in psamCFP is not well understood. At 400 nm, the neutral form of the chromophore is excited, whereas emission appears to occur from the anionic form. Such behavior has not been described yet in CFPs, but has previously been observed in green and red homologs of GFP, where the mechanism has been attributed to excited-state deprotonation of the phenolic end of the chromophore. The origin of color tuning in CFPs by the protein matrix is also not understood. It is unknown why these proteins bear a GFP-like chromophore but emit in the cyan region of the spectrum. Although blue-shifting is thought to result from a quadrupolar electric field set up by positive and negative charges on surrounding residues, this mechanism has been contradicted by more recent structural work (Malo et al, 2008).

To investigate the mechanistic basis of psamFP488 fluorescence, the protein was characterized by homology modeling, fluorescence quantum yield and dynamic light scattering measurements, while collaborators applied ultrafast transient absorption and pump-dump-probe spectroscopy.

MATERIALS AND METHODS

Cloning, Expression and Purification of PsamFP488

The gene coding for full-length psamFP488 was PCR-amplified from a pGEM-T expression plasmid. PCR amplification, directional cloning of the PCR product into a linear pET151/DTOPO vector (Invitrogen), and transformation into *Escherichia coli*

BL21(DE3) competent cells (Invitrogen) were carried out according to the manufacturer's instructions. Plasmid was prepared from individual transformant colonies using the QIAprep kit (Qiagen). Single colonies were cultured overnight at 37°C in 25 mL of Luria-Bertani (LB) media with 100 mg/L carbenicillin, used to inoculate 1 liter of LB/carbenicillin, and cultured at 37°C until the OD_{600} reached 0.8. The cultures were cooled to 25°C. Protein expression was induced by the addition of 1 mM IPTG and allowed to proceed for 4 hours at 25°C. Cells were harvested by centrifugation and frozen at -80°C.

Cell paste was suspended in 50 mL of 25 mM HEPES pH 7.9, 300 mM NaCl, 10% glycerol, 3 mM BME and 0.1 mM PMSF, then disrupted by sonication. The lysate was centrifuged, and the supernatant was passed through a 0.2-μm syringe filter before loading onto a nickel-nitrilotriacetic acid Superflow column (Qiagen). N-terminally 6His-tagged protein was purified using an imidazole step gradient in 50 mM HEPES pH 7.9 and 300 mM NaCl. Fractions containing the His-tagged protein were pooled, 1.2 mg of tobacco etch virus (TEV) protease was added, and the sample was dialyzed overnight at 4°C against 1 L of 50 mM HEPES pH 7.9, 300 mM NaCl. The dialysate was reapplied to a nickel-nitrilotriacetic acid column, and purified psamFP488 was collected in the early fractions. Protein was concentrated and buffer-exchanged into 50 mM HEPES pH 7.0, 300 mM NaCl. Aliquots of purified protein were flash frozen in liquid nitrogen and stored at -80°C in buffer containing 50 mM HEPES pH 7.9 and 300 mM NaCl. Protein concentration was determined by absorbance at 280 nm using a theoretical extinction coefficient equal to $\varepsilon = 22{,}920\ M^{-1}\ cm^{-1}$. Steady-state absorbance and fluorescence spectra were collected on psamFP488 in 50 mM HEPES pH 7.9 and

300 mM NaCl, using a Shimadzu UV-2401 Spectrophotometer and a Jobin Yvon Fluoromax-3 fluorimeter. Fluorescence scans were collected at 1.0 nm increments utilizing an integration time of 1.0 second and a slit width of 1.0 nm for both excitation and emission.

Determination of the Quantum Yield of Fluorescence

The fluorescence quantum yield of psamFP488 (0.16 mg/mL) was determined using fluorescein as a standard (1 μM in 0.1 M NaOH) according to published procedures [116]. Fluorescence emission intensity was integrated upon excitation at 465 nm and 417 nm. The buffer for all protein preparations was 20 mM HEPES pH 7.9, 20 mM NaCl. The data were fit to the following equation: $\Phi = \Phi_R[I/I_R]\ [OD_R/OD]$, where Φ is the quantum yield, I is the integrated intensity, and OD is the optical density at 465 nm or 417 nm. R refers to the reference fluorophore with quantum yield 0.95.

Dynamic Light Scattering

Dynamic light scattering (DLS) experiments were performed using a DynaPro NanoStar instrument (Wyatt Technology Corp., Santa Barbara, CA,) and analyzed using the software Dynamics 7.0.3.12 (Wyatt Technology Corp.). Briefly, 80 μL aliquots of 0.5 – 5.0 mg/mL psamFP488 in 20 mM HEPES pH 7.9, 137 mM NaCl were spin filtered for 3 min at 3000 *g*, using 0.1 μm spin filters (Millipore). Filtrates were transferred to disposable UVette cuvettes (Eppendorf, Hauppauge, NY) for data collection at 20°C. Scattered light intensity fluctuations were averaged from forty acquisitions (5 seconds each) and the resulting autocorrelation functions fit via the regularization method. The hydrodynamic radius was estimated assuming a spherical particle shape.

Crystallization

Preliminary screening was performed using the Phoenix crystallization robot. The following Hampton Research screens were set up: Crystal Screen HT, Index HT, PEG/Ion Screen HT and Cryo Screen HT. Two sitting well drops were set up for each condition, containing 0.1 µL reservoir solution and either 0.1 µL protein or 0.2 µL protein. Hanging drop vapor diffusion was used to set up crystallography trials using the Hampton Cryo Screen 1 and 2, and optimizations of initial hits using 1.6 µL drops containing a 1:1 protein:reservoir solution ratio. Protein used in crystal trials was 32.64 mg/mL psamFP488 in buffer containing 20 mM HEPES pH 7.9 and 20 mM NaCl.

RESULTS

Absorption and Fluorescence Spectra, Quantum Yield and Quaternary Structure

Figure 49 shows the fluorescence excitation and fluorescence spectra of psamFP488. The absorption spectrum (figure 50) was essentially identical to the

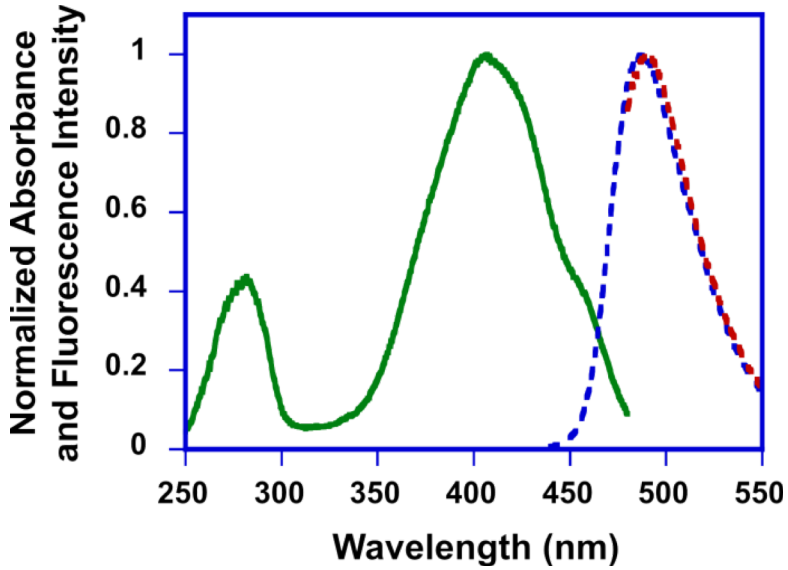

Figure 49. Normalized fluorescence and fluorescence excitation spectra of psamFP488. For the excitation scan (green solid line), the emission was monitored at 488 nm. For the emission scans (dotted lines), the excitation wavelength was set to 415 nm (blue) or 460 nm (red).

fluorescence excitation spectrum. The absorption spectrum shows a main band with maximum at 407 nm and a shoulder at 460 nm, and agrees with that published earlier [90]. The psamFP488 chromophore does not appear to titrate with pH, as the absorbance spectra remain unmodified between pH 4 and 10. The fluorescence has a single broad band with a flat maximum from 485 to 490 nm, corresponding to a Stokes shift of 4500 cm^{-1}, and is slightly blue-shifted from that published earlier [90]. As compared to GFP [92], the absorption and fluorescence bands are broader and less resolved. In particular, the fluorescence spectrum has a width of 60 nm (2500 cm^{-1}), compared to 30 nm (1000 cm^{-1}) for GFP.

The quantum yield of psamFP488 fluorescence (figure 50) measured on three independently prepared protein preparations was determined to be 0.850 ± 0.038 (n = 3)

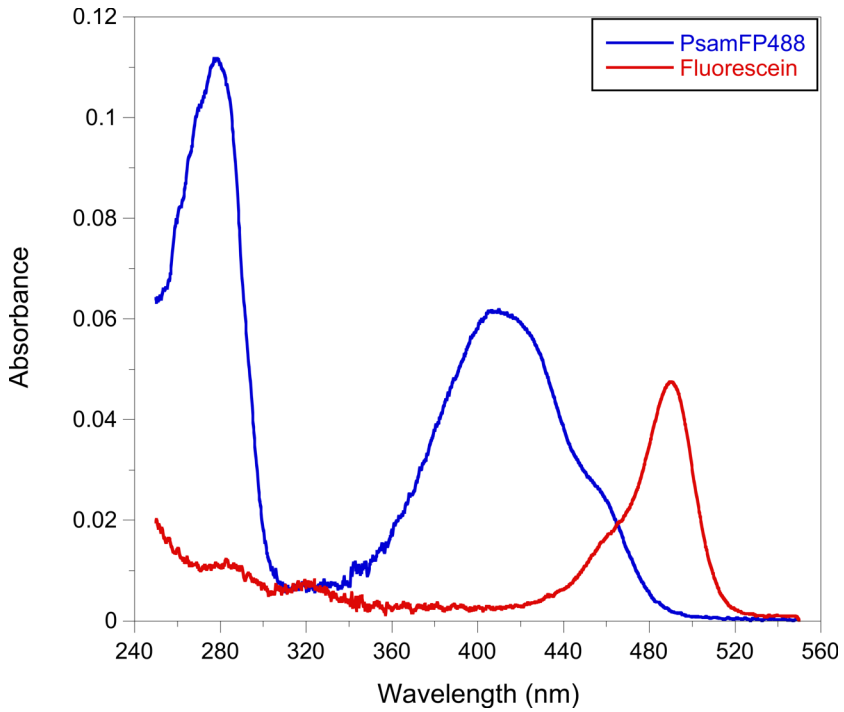

Figure 50. Absorbance spectra of psamFP488 and fluorescein. The absorbance was used to calculate quantum yield of psamFP488, with excitation at both 415 nm and 465 nm as described in the Methods.

with 465 nm excitation (anionic chromophore) and 0.876 ± 0.007 (n = 3) with 417 nm excitation (neutral chromophore), slightly lower than the published value of 0.96 [90].

Based on DLS measurements, the quaternary structure of psamFP488 was determined to be a homotetramer, as supported by sequence homology to other *Anthozoa* FPs known to be tetrameric [117]. DLS spectra collected at 20°C on samples containing 0.5 – 5.0 mg/mL protein appeared monodisperse, and the calculated hydrodynamic radius was consistent with 4.1 ± 0.2 (n = 6) protein chains per particle (figure 51).

	% Mass	MW (kDa)	Oligomeric State
Peak 1	100.0	108	4
Peak 2	0.0	43787	1652

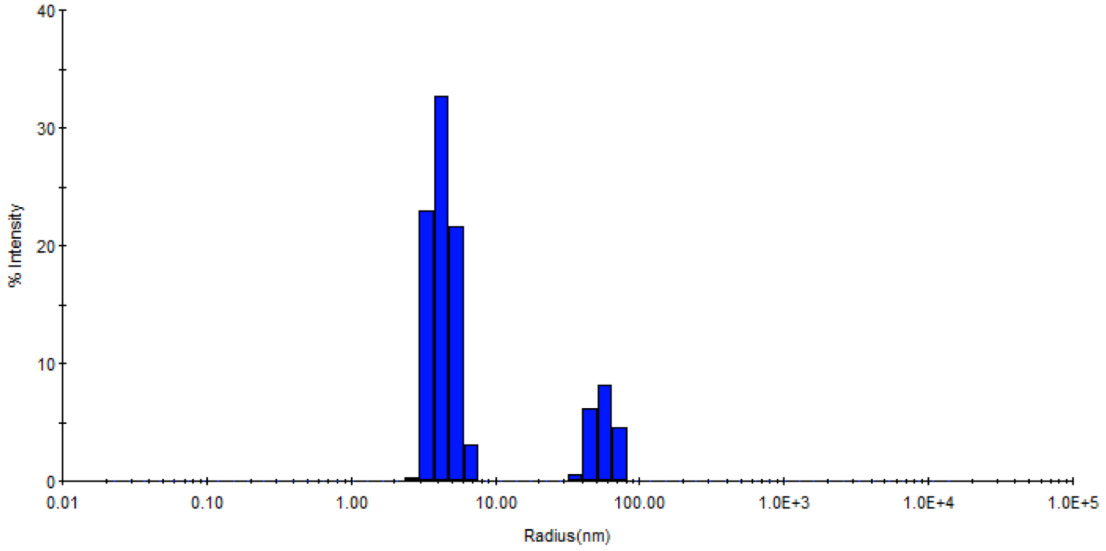

Figure 51. Dynamic light scattering spectrum of 2.0 mg/mL psamFP488 at 20ºC. The species with a 4.4 nm radius having 80.5% of the intensity, suggesting a monodisperse protein solution. 100% of the mass gave a molecular weight of 108 kDa, representing an oligomeric state of a tetramer.

Characterization of the Chromophore Environment Based on Close Homologs

A standard BLAST protein data base search indicates that the closest sequence homolog to psamFP488 is a CFP derived from *Montipora efflorescens* (71% sequence

identity) (figure 52); however, a three-dimensional structure is not available for this protein. A structural database search indicates that seven high-resolution X-ray structures are available for FPs exhibiting 59 – 61% sequence identity to psamFP488. All of these proteins were originally isolated from the button polyp *Zoanthus sp.,* including the yellow fluorescent protein zFP538 (61% identity) [117], the red fluorescent zRFP574, and the green fluorescent zGFP506 [118]. Previous works have demonstrated that the chromophore environment of many naturally occurring CFPs, such as amFP486 and dsFP483, closely resembles that of the yellow and red fluorescent proteins zFP538 and DsRed, and their immediate homologs [116, 119]. Therefore, we expect that psamFP488 bears the typical GFP-like two-ring chromophore consisting of the benzylidene imidazolinone group derived from a QYG tripeptide sequence (residues 66 to 68). Due to the high quantum yield for fluorescence, the chromophore π-system is likely held in a rigidly planar conformation by the surrounding protein matrix. On the basis of the high

```
PsamFP488       MASTKNVLPNMMTLTYHMEGSVNGHNFEIIGEGTGNPKEGKHTITLQVVKGGPLPFSVDI 60
CMonteff        MALSKQSLPSDMKLIYHMDGNVNGHSFVIKGEGEGKPYEGTHTIKLQVVEGSPLPFSADI 60
zFP538K66M      MAHSKHGLKEEMTMKYHMEGCVNGHKFVITGEGIGYPFKGKQTINLCVIEGGPLPFSEDI 60
                ** :*: * . *.: ***:* ****.* * *** * * :*.:**.* *::*.***** **

PsamFP488       LSTVFQYGNRCFTKYPPNTVDYFKNSCPPG-YTFERSFLYEDGAVCTASGDITLSDDKAS 119
CMonteff        LSTVFQYGNRCFTKYPPNIVDYFKNSCSGGGYKFGRSFLYEDGAVCTASGDITLSADKKS 120
zFP538K66M      LSAGFMD--RIFTEYPQDIVDYFKNSCPAG-YTWGRSFLFEDGAVCICNVDITVSVKENC 117
                **: *    * **:** : ********. * *.: ****:****** .. ***:* .: .

PsamFP488       FHHKSKFFGVNFPDDGPVMKKKTTDWEPSCEKMTPSGK--TLKGDVIEFLLLEGGGRYKC 177
CMonteff        FEHKSKFLGVNFPADGPVMKKETTNWEPSCEKMTPNGM--TLIGDVTGFLLKEDGKRYKC 178
zFP538K66M      IYHKSIFNGMNFPADGPVMKKMTTNWEASCEKIMPVPKQGILKGDVSMYLLLKDGGRYRC 177
                : *** * *:*** ******* **:**.****: *      * ***  :** :.* **:*

PsamFP488       QFHTVYRAKTEPK--RMPEFHFVQHKLTRTDVSDPLKQQWQLTEDAAACESCFHK 230
CMonteff        QFHTFHDAKDKSKKMPMPDFHFVQHKIERKDLPG-SMQTWRLTEHAAACKTCFTE 232
zFP538K66M      QFDTVYKAKSVPS--KMPEWHFIQHKLLREDRSDAKNQKWQLTEHAIAFPSALA- 229
                **.*.: **  ..   **::**:***: * * ..   * *:***.* *  :.:
```

Figure 52. Sequence alignment of psamFP488 and homologs. Alignment of psamFP488 with its closest sequence homolog, *Montipora efflorescens* (71% seq id), and closest sequence homolog with known structure: zFP538-K66M (61% seq id). Most residues are fully conserved (*), strongly similar (:), or weakly similar (.). The alignment was created using ClustlW2.

level of conservation of buried residues, the structural features of the chromophore environment are expected to be similar to zFP538 (figure 53). When comparing residue positions immediately surrounding the chromophore, zFP538 and psamFP488 contain identical residues with the sole exception of position 167 (residue numbering according to avGFP), where zFP538 bears a methionine (Met-167) and psamFP488 a glutamic acid (Glu-165 according to psamFP488 residue numbering) (figures 52, 53). Following convention, avGFP numbering will be used throughout the text. A structural model of psamFP488 was generated by introducing the in-silico mutation M167E, followed by selection of a common glutamic acid side chain rotamer with miminal steric interference

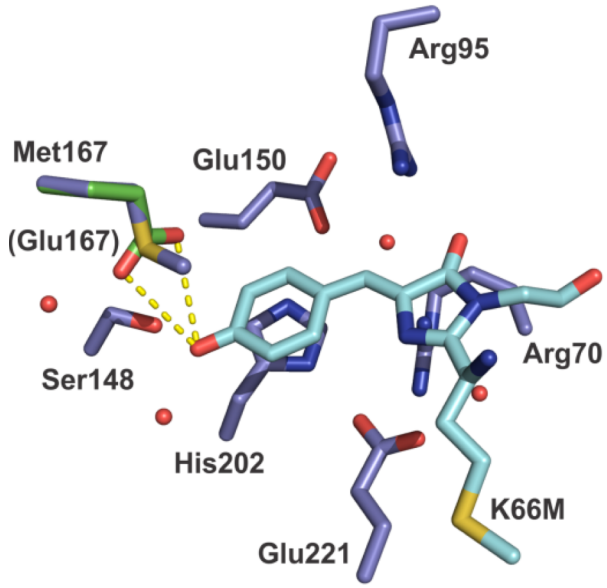

Figure 53. Active site structure of the psamFP488 homolog zFP538-K66M (PDB ID: 1XA9) bearing the standard green-fluorescent chromophore found in GFP (blue and cyan). In psamFP488, the position equivalent to Met167 is occupied by a glutamic acid (green), computer-modeled in a rotamer conformation that provides minimal steric clash. Suggested hydrogen bonding interactions with the chromophore are indicated as dashed yellow lines (3.3 and 3.4 Å in the model). Arg95, Glu150, Ser148, His202, Glu221 and Arg70 are conserved in psamFP488. Residue 66 is occupied by Gln in psamFP488 (not shown).

(figure 53). The model suggests that the two Glu-167 carboxy oxygen atoms are positioned within hydrogen bonding distance to the chromophore's phenolic hydroxyl group (3.3 and 3.4 Å without energy minimization). This scenario would provide a hydrogen bonded pathway for rapid proton transfer to Glu-167 upon chromophore excitation.

In dsFP483, a hydrogen-bonded network leading from Ser-148 to Glu-150 has been identified, and involves two crystallographically ordered water molecules [116]. A similar network involving Glu-167 and Glu-150 could also exist in psamFP488 (figure 53), suggesting that, at least in principle, either Glu-167 or Glu-150 could serve as a proton sink for ESPT.

It has been noted previously that the replacement of a positively charged residue with a polar one in position 167 may be coupled to cyan light emission in a DsRed-like protein environment [116]. This idea seems to hold true for psamFP488 as well, as Glu-167 may become protonated neutral upon ESPT, thus providing a similar electrostatic environment as a histidine residue in dsFP483 or a solvent molecule in amFP486 [119]. In support of this notion, position 167 was identified previously as an important determinant of cyan color based on statistical sequence analysis [120].

Ser-148 is conserved among many Anthozoa FPs, including dsFP483, amFP486, zFP538, and DsRed [116]. In addition, the quadrupole arrangement of charges consisting of Glu-150, Arg-70, His-202 and Glu-221 is highly conserved among many coral FPs including amFP486, zFP538, and psamFP488. However, not all cyan proteins bear this particular charge network, as dsFP483 contains a threonine residue in position 202 [116].

Crystallography

The DLS results showing monodispersity of psamFP488 suggests that this protein is a good target for crystallization. Considering GFP-like proteins have usually been relatively easy to crystallize, crystallography of PsamFP488 proved to be more difficult than expected. After extensive crystallization screening using commercially available kits and optimization, several crystal forms that exhibit cyan color were obtained in various conditions similar to ~0.5 M Ammonium Sulfate, 0.1 M HEPES ~pH 8, 30% 2-methyl-2,4-pentanediol (MPD) (figure 54). These crystals were brought to a synchrotron source and no diffraction data could be obtained. Unfortunately, for all twelve crystals, the data either showed the diffraction pattern of salt or no diffraction at all.

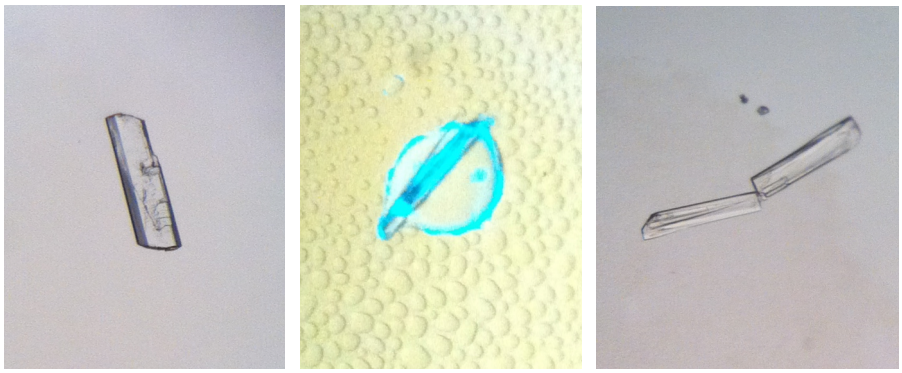

Figure 54. Crystals of psamFP488. Crystals were grown in ~0.5 M Ammonium Sulfate, 0.1 M HEPES ~pH 8, 30% MPD. Large, 3-dimensional plate-like crystals were observed in several of these optimization trials. An optical filter with a 450 nm cut-off was used to verify cyan color in the crystals.

SUMMARY

The novel excitation wavelength of psamFP488 (λ_{ex} = 404 nm) suggests that this clone could serve as a donor molecule with superior optical features in FRET applications, because direct excitation of YFP upon CFP excitation would likely be minimal, leading to a much-improved signal-to-noise ratio. The quantum yield of

psamFP488 was determined to be 0.876 ± 0.007 (n = 3) with 417 nm excitation and 0.850 ± 0.038 (n = 3) with 465 nm excitation. PsamFP488 was found to have a monodisperse, tetrameric quaternary structure based on DLS suggesting that this protein is a good target for crystallization. However, extensive crystallization screening and optimization was performed with no promising results. Twelve crystals were brought to a synchrotron source, but no usable diffraction data could be obtained.

PsamFP488 demonstrates a novel mechanism of cyan color generation that involves a glutamic acid residue in position 167. This position has been shown to exhibit strong statistical correlation with the biological evolution of cyan color from a common green ancestor [120]. However, ESPT has not previously been observed to be the underlying mechanism of cyan fluorescence in any GFP-like protein. By ultrafast transient absorption and pump-dump-probe spectroscopy performed by collaborators, it was determined that excited state proton transfer lies at the basis of the large Stokes shift. The data suggests Glu167 may act as the proton acceptor from the chromophore, since the distance between the two may be short enough to allow for hydrogen bonding and energy transfer. PsamFP488 represents an attractive model system that poses an ultrafast proton transfer regime in discrete steps. It constitutes a valuable model system in addition to wild type GFP, where proton transfer is relatively slow, and the S65T/H148D GFP mutant, where the effects of low-barrier hydrogen bonds dominate.

APPENDIX B

COPYRIGHT CLEARANCE

Chapter 3

Figure 48

This Agreement between Dayna Forbrook ("You") and Nature Publishing Group ("Nature Publishing Group") consists of your license details and the terms and conditions provided by Nature Publishing Group and Copyright Clearance Center.

Your confirmation email will contain your order number for future reference.

Printable details.

License Number	4062670046426
License date	Mar 05, 2017
Licensed Content Publisher	Nature Publishing Group
Licensed Content Publication	Nature Structural and Molecular Biology
Licensed Content Title	Substrate-translocating loops regulate mechanochemical coupling and power production in AAA+ protease ClpXP
Licensed Content Author	Piere Rodriguez-Aliaga, Luis Ramirez, Frank Kim, Carlos Bustamante, Andreas Martin
Licensed Content Date	Sep 26, 2016
Licensed Content Volume	23
Licensed Content Issue	11
Type of Use	reuse in a dissertation / thesis
Requestor type	academic/educational
Format	print and electronic
Portion	figures/tables/illustrations
Number of figures/tables/illustrations	1
High-res required	no
Figures	Figure 2a
Author of this NPG article	no
Your reference number	
Title of your thesis / dissertation	Understanding Rubisco Activase Subunit Exchange and Interaction with Rubisco Using FRET-based Assays
Expected completion date	Apr 2017
Estimated size (number of pages)	130
Requestor Location	Dayna Forbrook 2401 E Rio Salado Pkwy Unit 1157 TEMPE, AZ 85281 United States Attn: Dayna Forbrook
Billing Type	Invoice
Billing address	Dayna Forbrook 2401 E Rio Salado Pkwy Unit 1157 TEMPE, AZ 85281 United States Attn: Dayna Forbrook
Total	0.00 USD

Appendix A

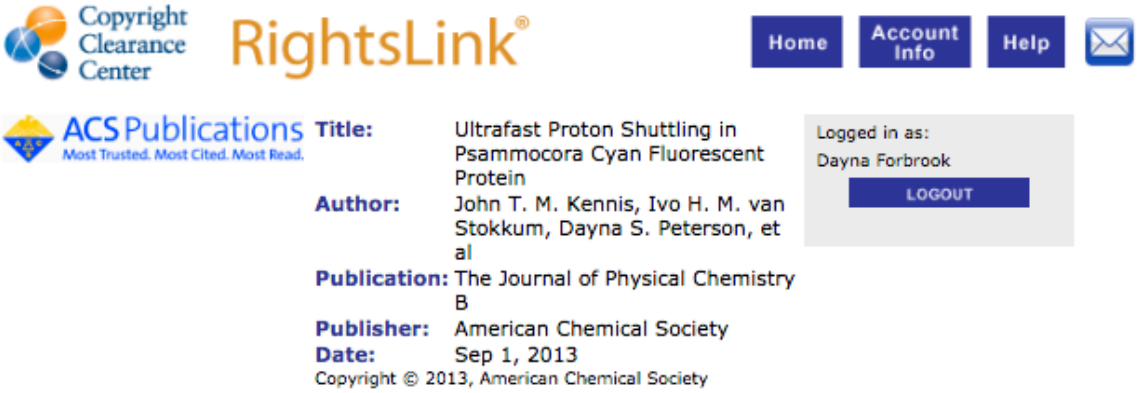

Copyright Clearance Center RightsLink®

Home | Account Info | Help

ACS Publications
Most Trusted. Most Cited. Most Read.

Title:	Ultrafast Proton Shuttling in Psammocora Cyan Fluorescent Protein
Author:	John T. M. Kennis, Ivo H. M. van Stokkum, Dayna S. Peterson, et al
Publication:	The Journal of Physical Chemistry B
Publisher:	American Chemical Society
Date:	Sep 1, 2013

Copyright © 2013, American Chemical Society

Logged in as:
Dayna Forbrook
LOGOUT

PERMISSION/LICENSE IS GRANTED FOR YOUR ORDER AT NO CHARGE

This type of permission/license, instead of the standard Terms & Conditions, is sent to you because no fee is being charged for your order. Please note the following:

- Permission is granted for your request in both print and electronic formats, and translations.
- If figures and/or tables were requested, they may be adapted or used in part.
- Please print this page for your records and send a copy of it to your publisher/graduate school.
- Appropriate credit for the requested material should be given as follows: "Reprinted (adapted) with permission from (COMPLETE REFERENCE CITATION). Copyright (YEAR) American Chemical Society." Insert appropriate information in place of the capitalized words.
- One-time permission is granted only for the use specified in your request. No additional uses are granted (such as derivative works or other editions). For any other uses, please submit a new request.

BACK | CLOSE WINDOW